Cell reactions to the degradation of Mg-based materials: chondrogenic differentiation

Dissertation with the aim of achieving a doctoral degree at the Faculty of Mathematics, Informatics and Natural Sciences

Department of Chemistry
University of Hamburg

Submitted by

Adela Helvia Martínez Sánchez

2017, Hamburg

Thesis defended and approved for publication on the 17th of Mach, 2017

The following evaluators recommend the admission of the dissertation:

Prof. Dr. Regine Willumeit-Römer

Prof. Dr. Ulrich Hahn

This dissertation was performed from January 2013 to November 2016 at the Institute of Materials Research, Helmholtz Zentrum-Geesthacht (Geesthacht, Germany). Part of the research was carried out at the Center for Medical Research, Medical University of Graz (Graz, Austria) over a three months stay.

1. LIST OF PUBLICATIONS

Publications in peer-reviewed journal articles

Related to doctoral work

1. AH Martinez-Sanchez*, F Feyerabend, D Laipple, R Willumeit-Römer, A Weinberg, BJC Luthringer (2016): Chondrogenic differentiation of ATDC5-cells under the influence of Mg and Mg alloy degradation. Materials Science and Engineering:C 72: 378–388. (*corresponding author).
2. AH Martinez Sanchez*, BJC Luthringer, F Feyerabend, R Willumeit-Römer (2015): Mg and Mg alloys: How comparable are in vitro and in vivo corrosión rates? - A review. Acta Biomaterialia 13, 16-31. (*corresponding author).
3. F Cecchinato, NA Agha, AH Martinez-Sanchez, BJC Luthringer, F Feyerabend, R Jimbo, et al. (2015): Influence of Magnesium Alloy Degradation on Undifferentiated Human Cells. PLoS ONE 10(11): e0142117.

Independent from doctoral work

1. C Sanjurjo-Rodriguez, AH Martínez-Sánchez, T Hermida-Gómez, I Fuentes-Boquete, S Díaz-Prado, FJ Blanco (2016): Differentiation of Human Mesenchymal Stromal Cells cultured on Collagen Sponges for Cartilage Repair. Histol Histopathol 11:11754.
2. AH Martínez Sánchez, C Sanjurjo Rodríguez, T Hermida Gómez, E Muiños Lopez, IM Fuentes Boquete, FJ de Toro, J Buján, S Díaz Prado, FJ Blanco (2013): Tissue Engineering for Cartilage Repair: Growth and Proliferation of HBM-MSCS on Scaffolds Composed of Collagen I and Heparan Sulphate. Osteoarthritis & Cartilage 21:S310-S311.

2. LIST OF ABBREVIATIONS

A: absorbance
ACAA2: gene encoding 3 ketoacyl CoA thiolase
ACAN: aggrecan
ACTN4: gene encoding alpha actinin 4
AGC: automatic gain control
αMEM: alpha minimum essential media
AMV: avian myeloblastosis virus
ANGPTL4: gene encoding angiopoietin related protein 4
APEP: gene encoding aminopeptidase N
APOD: gene encoding apolipoprotein D
ASNS: gene encoding asparagine synthetase
ATP: adenosin tri-phosphate
ATP5B: gene encoding ATP synthase subunit beta
B2m: actin, beta
BLMH: gene encoding bleomycin hydrolase
bp: base pairs
BSA: bovine serum albumin
C1QBP: gene encoding complement component 1 Q subcomponent binding protein
Ca: Calcium
cAMP: cyclic adenosine monophosphate
cDNA: complementary DNA
Cl: chloride
cm: centimeters
CO_2: carbon dioxide
COL1A1: alpha-1 type I collagen
COL2A1: alpha-1 type II collage
COL4A2: gene encoding collagen alpha 2(IV) chain
COL6A3: gene encoding collagen alpha 3(VI) chain
COLI: type I collagen
CPAMD1: gene encoding complement C3
Cq: quantification cycle
CRYAB: gene encoding Alpha crystallin B chain
CTNNA1: gene encoding catenin alpha 1
DDA: data-dependent acquisition
ddH_2O: double distilled water
DNA: deoxyribonucleic acid
dNTP: deoxynucleotide
DPP: digital pulse processing
ECM: extracellular matrix
EDTA: ethylenediaminetetraacetic acid

EDX: energy dispersive X-ray
ERO1A: gene encoding ERO1 like protein alpha
ESI: electrospray ionization
FA: fusidic acid
FAM129B: gene encoding niban like protein 1
FAP: gene encoding prolyl endopeptidase FAP
FBS: fetal bovine serum
FDR: false discovery rate
FIB: focus ion vean
FITC: fluorescein isothiocyan
FLNA: gene encoding Filamin A
FN1: gene encoding Fibronectin
FWHM: full width at half maximum
g: grams
GAG: glycosamynoglycans
GSN: gene encoding Gesolin
H: Hydrogen
HCD: higher energy collision dissociation
HCO_3^-: Bicarbonate ion
HEXB : gene encoding Beta hexosaminidase subunit beta
HEXB: gene encoding Beta hexosaminidase subunit beta
HIV: human immunodeficiency virus
HLAA: gene encoding HLA class I histocompatibility antigen
HPLC: high-performance liquid chromatography
HSP60: gene encoding 60 kDa heat shock protein
HSPE1: gene encoding 10 kDa heat shock protein
HSPG2: gene encoding basement membrane-specific heparan sulfate proteoglycan core protein
HUCPV: human umbilical cord perivascular cells
I ICAM1: gene encoding intercellular adhesion molecule 1
IL-1: interleukin-1
ISO: international organization for standardization
ITGA2: gene encoding integrin alpha 2
ITGA5: gene encoding integrin alpha 5
ITGAV: gene encoding integrin alpha V
K: potasium
KNG1: gene encoding kininogen 1
KRT18: gene encoding keratin. type I cytoskeletal 18
KRT8: gene encoding keratin type II cytoskeletal 8
LAMP1: gene encoding lysosome associated membrane glycoprotein 1
LC-MS/MS: liquid chromatography-tandem mass spectrometry
LMIS: liquid metal ion source

M-MulV: moloney murine leukemia virus
m/z: mass/charge
MC: mechanosensitive channels
Mg-10Gd: magnesium with 10% gadolinium
Mg-2Ag: magnesium with 2% silver
Mg: magnesium
$MgCl_2$: magnesium chloride
$MgCO_3$: magnesium carbonate
MgO: magnesium oxide
$MgSO_4$: magnesium sulfate
MHz: megahertz
min: minutes
mM: millimolar
MRI: magnetic resonance imaging
MSCs: mesenchymal stem cells
mTOR: mammalian target of rapamycin
N-CAM: neural cell adhesion molecule
N: number of replicates
Na: sodium
NaCl: sodium chloride
NAFT5: nuclear factor of activated T cells 5
ng: nanograms
nm: nanometer
NONO: gene encoding Non POU domain containing octamer binding protein
O: oxygen
ºC: degrees Celsius
OC: osteocalcin
OPN: osteopontin
P: phosphorus
Pa: pascals
PAIRBP1: gene encoding plasminogen activator inhibitor 1 RNA binding protein
PARK7: gene encoding protein deglycase DJ1
PBS: phosphate-buffered saline
PDCD5: gene encoding Programmed cell death protein 5
PHB: gene encoding prohibitin
PHB2: gene encoding prohibitin 2
PIGPLD1: gene encoding phosphatidylinositol glycan specific phospholipase D
PLCγ1: phospholipase Cγ1
PLOD2: gene encoding gene encoding oxoglutarate 5-dioxygenase 2
PLS3: gene encoding plastin 3
pmol: picomol
PO_4^-: hydrogen phosphate

PON1: gene encoding serum paraoxonase/arylesterase 1
PSM: peptide spectrum match
PTGS2: gene encoding prostaglandin G/H synthase 2
qPCR: real time polymerase chain reaction
REEs: rare earth elements
RLP10: ribosomal protein L10
RNA: ribonucleic acid
RNase H: hybrid-dependent exoribonuclease
RNH1: gene encoding ribonuclease inhibitor
rpm: revolutions per minute
RT-PCR: reverse transcription polymerase chain reaction
RTN4: gene encoding reticulon 4
RUNX2: runt-related transcription factor 2
S: Sulfur
S100A9: gene encoding Protein S100 A9
S18: 40S ribosomal protein S18
SEM: electron scanning microscopy
SO_4^{2-}: sulfate ion
SOD2: gene encoding superoxide dismutase
SOX9
SOX9: (Sex Determining Region Y)-Box 9
SP: substance P
TARDBP: gene encoding TAR DNA binding protein 43
TFA: trifluoroacetic acid
TGFBI: gene encoding transforming growth factor beta induced protein igh3
TGFβ: transcription growth factor beta
TNC: gene encoding tenascin
TNF: tumor necrosis facto
TSP1: gene encoding thrombospondin 1
U: units
UDG: uracil-DNA glycosylase
UPLC: ultra performance liquid chromatography
VCP: valosin containing protein
VDAC1: gene encoding voltage dependent anion selective channel protein1
VTN: gene encoding vitronectin
YBX3: gene encoding Y box binding protein 3
YWHAB: gene encoding 14+3+3 protein beta/alpha
µL: microliter

3. ZUSAMMENFASSUNG

Das Knochenwachstum bei Kindern wird in knorpeligen Bereichen reguliert, die als Wachstumsplatten bezeichnet werden und anfällig für Schäden sind. Das Einfügen und Entfernen von Implantaten kann zu Schäden und irreversible Knochenfehlbildungen in diesen Bereichen führen. Biologisch abbaubare Magnesium (Mg)-basierte Materialien sind eine potentielle Alternative zu permanenten Implantaten, um eine Implantatentfernung zu umgehen. Allerdings müssen dafür zunächst mögliche negative Effekte dieser Materialien auf den Wachstumsplattenknorpel bewertet werden.

Die chondrogene Differenzierung von perivaskulären Stammzellen der menschlichen Nabelschnur (HUCPV) und von einer chondrogenen Zelllinie (ATDC5) wurde *in vitro* unter dem Einfluss von Extrakten aus reinem Mg (Mg), Mg mit 10 % Gadolinium (Mg-10Gd) und Mg mit 2 % Silber (Mg-2Ag) - untersucht. Nach 7, 14 und 21 Tagen wurde die Genexpression, das Zellwachstum, die Morphologie und die extrazelluläre Matrix (EZM)-Produktion bewertet. Zusätzlich erlaubten Massenspektrometrie Studien die Identifizierung von Proteinen, die unter dem Einfluss der Extrakte reguliert wurden. Bei der direkter Kultur auf den Materialien wurden nach 7 Tagen das Zellwachstum, die Verteilung der Zellen und die EZM-Synthese zusammen mit der Zusammensetzung der Abbauprodukte auf der Oberflächenschicht der Materialien untersucht.

Die Ergebnisse zeigten, dass die drei Mg-Materialien ein chondrogenes Potential aufweisen. Bei Mg-10Gd ist dieses am stärksten, da eine Chondrozytenreifung oder Hypertrophie induziert wurde. Die Zellabdeckung und die EZM-Produktion in direktem Kontakt mit den Proben wurde durch die Homogenität der Degradationsschicht beeinflusst, die bei Mg-10Gd und Mg-2Ag höher war als bei Mg-Proben. Weiterhin wurde durch direkten Kontakt mit den Materialien sowohl bei HUCPV als auch ATDC5-Zellen die Chondrogenese der Zellen verstärkt.
Diese Studie bestätigt die Toleranz der am Knochenwachstum beteiligten Zellenfür Mg-basierte Materialien was ein mögliches Potenzial für die Behandlung von Frakturen bei Kindern zeigt.

4. ABSTRACT

Bone growth in children is regulated by cartilaginous areas named growth plates, which are vulnerable to damage. Implant application and removal can cause damage of those areas and generate irreversible bone malformations. Biodegradable magnesium (Mg)-based materials are a potential alternative to permanent implants, avoiding implant removal. Nevertheless effects of those materials on growth plate cartilage need to be evaluated.

In vitro chondrogenic differentiation of human umbilical cord perivascular (HUCPV) stem cells and ATDC5 chondrogenic cell line was evaluated under the influence of pure Mg (Mg), Mg with 10 wt% of gadolinium (Mg-10Gd) and Mg with 2 wt% of silver (Mg-2Ag) extracts. Specifically, gene expression, cell growth, morphology and extracellular matrix (ECM) production were studied after seven, 14 and 21 days. Additionally, proteomic studies allowed the identification of proteins regulated under the influence of the extracts. After seven days of direct culture on the materials, cell growth, distribution and ECM synthesis were investigated, together with the composition of the resulting degradation layer on the materials.

Results indicated that the three materials have chondrogenic potential, being stronger in Mg-10Gd, which induced chondrocyte maturation or hypertrophy. Cell coverage and ECM production in direct contact with the samples was influenced by the homogeneity of the degradation layer, being higher in Mg-10Gd and Mg-2Ag than in Mg samples. Furthermore, chondrogenesis of cells in direct contact with the materials was enhanced with both HUCPV and ATDC5 cells.

This study confirmed the tolerance of cells involved in bone growth to Mg-based materials, which shows its possible potential for treating children´s fractures.

5. STATE OF THE ART

5.1. Magnesium as implant

Magnesium (Mg) and its alloys have been progressively investigated in recent decades as promising candidates for medical applications as implants. These materials exhibit biocompatibility and appropriate mechanical properties for use, for example, as orthopaedic implants [1-4]. Furthermore, Mg and Mg alloys are biodegradable materials and can degrade and disappear completely during exposure to physiological conditions, avoiding the need for a second surgical intervention to remove the implant after tissue healing. The main discussed application in this section will be orthopaedic.

5.1.1. Advantages of Mg-based materials regarding other implants

Biological implant materials can be divided in three main groups: metals, ceramics and polymers. Metal materials have been widely used in many medical fields, especially in orthopaedics. They have a crystal structure and strong metallic bonds with a superior mechanical property. Furthermore, metallic materials show high degradation resistance, biocompatibility, high wear resistance and good ductility and strength. Therefore, metals have been preferred practically completely to other materials for load-bearing application, as joint arthroplasties and fracture fixation (wires, pins, screws and plates). The main implantable medical materials commonly used nowadays are stainless steel, titanium alloy and cobalt-chromium alloy. Other metals include nitinol, tantalum and Mg.

Among the metals, Mg is well known for its light weight. Additionally, in the 1930s, Mg alloy has been found biodegradable in the human body. The biodegradability avoids the need of a second surgery for implant removal (when implants are required only temporary) and other complications associated with permanent implants. Among such complications, the mechanical wear and corrosion associated with the long-term implantation in the body can result in the release of toxic metal ions (e.g. chromium, nickel and cobalt) in the body, which can trigger the undesirable immune responses, thereby reducing the biocompatibility of metallic implants [5]

Compared with the polymers, Mg has better mechanical compatibility, and can provide higher initial stability and support. Therefore, Mg alloys become the study hotspot in the field of medical implant materials.

The mechanical properties of Mg are especially suitable for orthopaedic application. Its specific strength is 133GPa/(g/cm^3), and the specific strength of Mg alloy with super strength is 480GPa/(g/cm^3), nearly double than that of Ti6Al4V (260GPa/(g/cm^3)). Its modulus of elasticity (45GPa) and density (1.74 g/cm^3) is closer to human body skeleton (20GPa, 1.75 g/cm^3) than that of traditional biomedical metals (stainless steel, cobalt chromium alloy and titanium alloy). Thus, Mg can effectively reduce the effect of the stress shielding once implanted in the body. Additionally, Mg is lighter than other medical metal, being suitable for hard tissue implant and tissue engineering scaffold material [6].

5.1.2. Mg properties for orthopaedic application

Magnesium-based materials were first introduced for orthopaedic applications in the beginning of twentieth century. Lambotte [7, 8] was the first author reporting the use of a pure Mg plate along with gold plated steel nails to secure lower leg bone fracture. Since then, studies have shown that Mg materials achieve enhanced bone response, stimulating bone growth and healing and excellent interfacial strength when implanted [9]. Magnesium materials have been used for different types of fixation devices for orthopaedic surgery, such as screws, plates, and fasteners. Degradation of Mg leads to the formation of harmless corrosion products, which are excreted through urine [10] and show minimal changes to blood composition without causing damage to excretory organs like the liver or the kidneys [11].

Besides all the positive properties exhibited, the main problem associated with Mg-based materials is a fast or undesirable degradation rate. Thus, already in the first reported use of Mg as implant, Lambotte reported that the *in vivo* corrosion was too rapid as the implant degraded completely in just 8 days [8]. As a biodegradable implant for bone application, Mg-based materials should degrade slowly, reducing the local changes in the surrounding tissues. Its low degradation resistance leads to the rapid production of hydrogen gas and as consequence, gas bubbles can appear. The formation of hydrogen gas can increase the pH around the implant, which alters

pH-dependent physiological process in the proximity of the implant [12]. Furthermore, the bubbles can accumulate around the implant and delay the healing of the tissue [7].

A low degradation rate is especially necessary directly after implantation in order to allow tissue repair before losing mechanical stability. Afterwards the degradation should be gradual and homogeneous, allowing a complete tissue healing, and finally the implant should disappear totally. From a cellular point of view, this means that initially the material should allow cells to attach and synthesize proteins that constitute the extracellular matrix (ECM) before its structural integrity gets affected. The ECM will serve as a support for the cells and will enhance normal cell functions. Once cells are supported by the surrounding ECM, a gradual degradation of the material will leave behind newly synthesized ECM [13].

5.1.3. Tailoring the degradation rate of Mg-based materials

In order to avoid deleterious effects on human physiology, a controlled degradation rate is preferable. This is the main challenge in the development and utilization of Mg-based materials. Alloy composition, sample surface condition, and composition of the immersion media significantly affect the degradation rate of the materials, not only independently but as factors interacting with each other.

The degradation reaction of Mg-materials in water involves the following anodic dissolution of metals and cathodic reduction reactions:

$$Mg + 2H_2O \rightarrow Mg^{2+} + 2OH^- + H_2\uparrow \qquad \text{Equation-1}$$

$$Mg^{2+} + 2OH^- \leftrightarrow Mg(OH)_2\downarrow \qquad \text{Equation-2}$$

In general, immediately after contact with moisture/ body fluids, Mg is oxidized to form cations following an anodic reaction. As a result, electrons are generated, that will be consumed for reduction of water corresponding to cathodic reactions (Equation-1). These reactions occur randomly over its entire surface.

Under physiological conditions, accelerated degradation can occur due for example, to the adsorption of organic molecules on the surface of the material, which enhances galvanic degradation. Additionally, dissolved oxygen, proteins and

electrolyte ions (*i.e.* chloride and hydroxide ions) present in physiological fluids provide a highly corrosive environment to Mg and its alloys resulting in the formation of an hydroxide layer (Mg $(OH)_2$) on their surface (Equation-2). This hydroxide layer acts as a passive layer or kinetic barrier. However, in the presence of chloride ions this layer is slightly soluble and susceptible to breakdown, which subsequently leads to the pitting corrosion [14].

In order to improve the degradation resistance, a better understanding of the mechanisms involved in Mg degradation *in vitro* and *in vivo* is necessary. The main impediment to analyze Mg degradation *in vitro* is the difficulty to mimic physiological conditions, including the presence of buffer, proteins, all the ions present in body fluids (*e.g.* Na^+, K^+, Ca^{2+}, Mg^{2+}, HCO_3^-, Cl^-, HPO_4^{2-} and SO_4^{2-}), temperature and oxygen tension among others. Any change in those parameters *in vitro* regarding *in vivo* conditions can lead to variations in Mg or Mg-alloy degradation kinetics and influence not only the degradation rate but also the morphology. As a consequence, the degradation behavior *in vivo* is still very hard to predict or define [15].
One of the approaches employed to control degradation behavior is tailoring the composition and microstructure, including the grain size and texture of the base material. Such tailoring can also be achieved by using post-processing techniques such as heat-treatment and the use of alloying elements. The application of surface coatings helps to decrease mainly the initial degradation rate and furthermore increases the biocompatibility of medical devices [16, 17].

5.2. Selection of alloying elements

The main reason for using alloying elements is the reduction of the degradation rate while keeping or improving the mechanical properties of the materials. The Rare Earth Element (REE) Gadolinium (Gd) with a concentration up to 10% [18] and Silver (Ag) after heat treatment [19], both improve the mechanical properties and degradation resistance of Mg materials. From a medical point of view, Gd is widely used as contrast agent for Magnetic Resonance Imaging (MRI) in clinics. REEs are present in human serum in really low concentrations [20] and accumulate in human bones in a age-related manner [21]. Even though the toxic limits of REEs are still under discussion, evidence of its anti-cancerogenic properties has grown in the last years. Specifically, it has been reported that Gd-containing nanoparticles could be

used not only for identifying but also for treating tumours [22]. In addition, previous evaluations of $GdCl_3$ effects on cell behavior have shown that Gd^{3+} increases cell viability and decreases apoptosis [23]. Silver is well known for its antibacterial properties, reducing risk of infection around the implant [19].

Nevertheless, the degradation of Mg-alloys gives rise to more complex degradation products (more than the Ag and Gd salts generally used in the literature as model test compounds) since Mg, Gd and Ag can react with elements present in the surrounding fluids (culture medium *in vitro* and blood *in vivo*). Thus, the use of extracts containing the products of the degradation (Mg and the alloying elements) seems more reliable than the use of salts, although a comparison between both is still necessary in order to confirm their different effects. Therefore, a better understanding of the mechanisms underlying cell reactions to those elements is necessary in order to confirm the suitability of the materials for medical application.

5.3. Function and importance of Magnesium, Gadolinium, Silver and their derivates in the organism

5.3.1. Magnesium

Magneium is the fourth most abundant cation found naturally in vertebrate organisms, and the second intracellular one (after potassium, K). The adult human body contains about 1 mole (24g) of Mg.

Magnesium is in nature forming part of salts (*e.g.* $MgCl_2$, MgO, $MgSO_4$ and $MgCO_3$) that dissolve very easily making Mg available for the organisms. This metal shows often antagonist behavior to calcium in the cells. This is due to the fact that dissolved Mg binds hydration water, forming a hydrated Mg that is not able to pass through narrow channels in the biological membranes, therefore using Ca channels [24, 25].

- ***Mg distribution in the organism***

The organism owns mechanisms to keep Mg concentrations in serum constant. Three organs are responsible for maintaining Mg homeostasis in the body: the bone, the kidney and the intestine. Magnesium is absorbed mainly in the small intestine and in some extent also by the large intestine. Bone acts as the main reservoir of

Mg, followed by muscle and other soft tissues [26, 27]. A constant interchange of Mg occurs between the bone and the blood plasma (Figure 1). Around one third of the skeletal Mg is available to keep physiological extracellular Mg levels [28].

The kidney plays a key role in Mg homeostasis in the blood plasma, reabsorbing about 95% of the filtered Mg under physiological conditions. When there is an excess of Mg in plasma, it can be stored in bone (when necessary) and the remaining Mg is excreted via the urine (together with 5% not reabsorbed in the kidney) and feces.

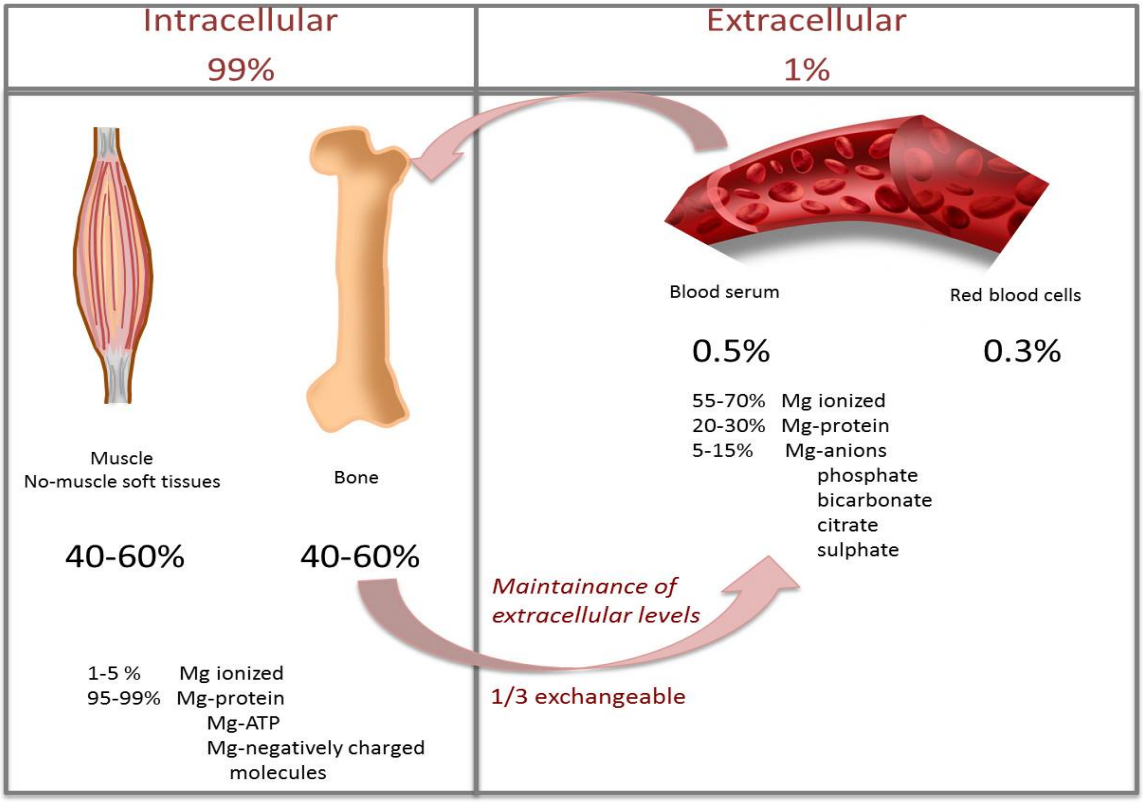

Figure 1. Magnesium storage and homeostasis in blood plasma. Bone and muscle provide the most important Mg^{2+} stores. One third of the Mg is exchangeable between the stores and blood serum, in order to maintain the extracellular levels in blood serum.

- ***Cell functions***

The majority of Mg in the organism can be found within the cells (99%), where it plays a role in most cellular processes. It acts as an activator of at least 200 enzymes and as cofactor of 600 enzymes [29]. Table 1 summarizes some of the most relevant functions in the cells.

Table1. List of cell functions in which Mg is involved. Table compiled according to references [29, 30]

CELL FUNCTIONS	TARGET
Enzymatic Activity	
DNA replication, RNA transcription, amino acid synthesis, protein formation ➢ proper structure and activity of DNA and RNA polymerases ➢ enzymes involved in DNA repair mechanisms	Topisomerases Helicases Exonucleases Protein kinases Cyclases ATP-ases
Glycolysis	Adenine nucleotides hexokinase Phosphofructokinase Aldolase Phosphoglycerate kinase Pyruvate kinase
Nucleotide binding	
Stabilization of RNA tertiary structure **Stabilization of DNA secondary structure** **Stabilization of DNA tertiary structure (natural DNA conformation)** **DNA protection against oxidants**	
Cell Signaling	
Mg as antagonist of Ca within the cell can modify Ca signaling ➢ Variation in Mg^{2+}/Ca^{2+} ratio ➢ Induction of Mg^{2+} influx and reduction of Ca^{2+} influx	Ca^{2+}-ATPases Ca^{2+} transporting proteins Activation of phospholipase Cγ1 (PLCγ1), in T-cells
Regulation of cell cycle progression and proliferation	
Activation of mammalian target of rapamycin (mTOR) complex (main regulator of cell proliferation) **Induction of Ca^{2+} release from endoplasmatic reticulum** **Increase in ribosomal activity and protein synthesis giving rise to DNA replication and mitosis**	
Cell adhesion	
Transmembrane electrolyte efflux (Ca^{2+} and K^{+})	
Apoptosis	
Antagonizes calcium-overload apoptotic effect **Anti-apoptotic in mitochondrial permeability transition**	

Mg increases cell proliferation and differentiation. High extracellular Mg stimulates protein synthesis and energy metabolism, thus allowing initiation of cell division [31, 32], probably by modifying the intracellular concentration of Mg. It has been shown to enhance migration of capillary endothelial cells, showing its role in angiogenesis [33].

- ***Physiological functions***

Regarding the physiological functions of Mg in the organism, regulation of vascular tone, muscle contraction and relaxation, and normal neurological function are some relevant examples. Moreover, in bone Mg stimulates osteoblasts proliferation and inhibits the release of pro-inflammatory molecules, such as interleukin-1 (IL-1), tumor necrosis factor (TNF), and substance P (SP), therefore inhibiting osteoclasts activity [34].

In cartilage, Mg induces (Sex Determining Region Y)-Box 9 (Sox9) expression, a transcription factor that plays a key role in chondrogenesis [34]. As a result, Mg allows appropriate chondrocyte column formation in growth plate cartilage and chondrocyte density in articular cartilage (Figure 2).

As indicated in Table 1, Mg is necessary for cell adhesion, which is an essential cellular process involved in chondrogenesis and cell-material interaction after implantation. It has been shown that stem cells adhesion and synthesis of cartilage is induced with Mg both *in vitro* and *in vivo* [35]. Those findings suggest a role of Mg inducing chondrogenic differentiation, but the discussion is still open [36].

5.3.1. Gadolinium

Gadolinium is a lanthanide compound not present naturally in the body. Gadolinium compounds are used as contrast agents in MRI [37]. Toxic effects are not found in cells until doses higher than 1 mM [23, 38-40] and have been mainly associated with kidney inflammation.

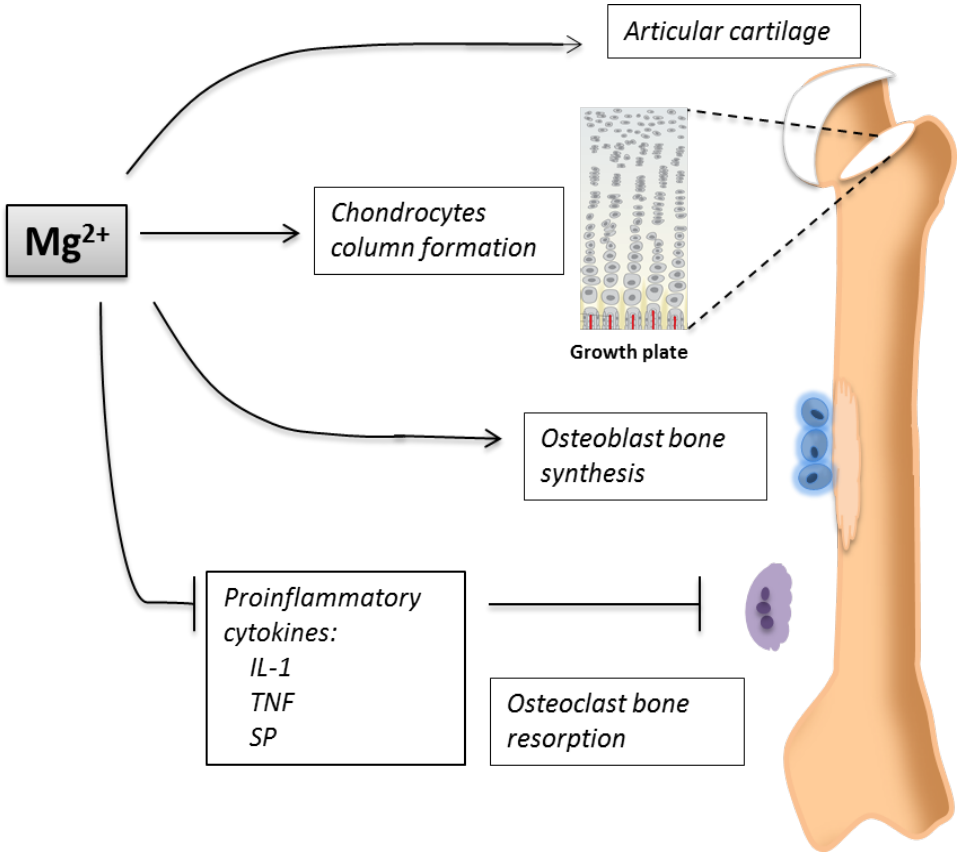

Figure 2. Role of Mg in bone and cartilage development. Arrows indicate stimulation whereas blunt arrow inhibition. IL-1: interleukin-1; TNF: tumor necrosis factor; SP: substance P. This image has been inspired by reference [26].

Gadolinium ion can inhibit cell response to mechanical forces and osmotic stress. Such inhibition is a result of a decrease in Ca^{+2} influx due to Gd^{+3} capability for 1) blocking most of mechanosensitive channels (MC) at low concentrations (lower than 0.1 mM) [41, 42]; 2) blocking L-type Ca^{2+} voltage channels present in chondrocytes, when undergoing mechanical pressure [43].

It has been proposed that Gd can enhance cell cycle progression, by the up-regulation of proteins involved in the G1/S transition [44, 45]. Gadolinium action starts extracellularly, activating a signal-regulated kinase (ERK) member of MAOK and P13K signaling cascade [46]. It was suggested that this effect is enhanced by the formation of Gd^{3+}- precipitates (formed with phosphates, citrates and hydroxides), which occurs in blood stream [47] and under physiological conditions *in vitro* [44].

5.3.2. Silver

Ag-containing materials are widely used as implants in order to diminish infections after surgery. Additionally, Ag is incorporated in some antibiotics, cosmetics and wound dressings. Chronic absorption of Ag^+ ion has been associated with a blue discoloration of the epidermis, known as Argyrya. Information about toxic effects of Ag on mammalian cells as well as on chondrogenesis is limited in the literature. Most of the attention has been given to Ag-nanoparticles, but since Ag^+ ions are released from their surface in physiological fluids, the real cause of cell changes is difficult to determine [48]. Silver-nanoparticles are taken up by endocytosis into the cell, and can then release Ag^+ ions in acidic environments (as in lysosomes and endosomes). Additionally, it is known that extracellular ions are transported intracellularly through copper transporter 1 (Ctr1) and divalent metal transporter (Dmt1), which are also responsible for copper (Cu) homeostasis. Since Cu is a cofactor for enzymes involved in growth, development, oxidative stress resistance, energy generation and connective tissue maturation, high extracellular Ag ion concentration could give rise to notable changes on cell metabolism. The limit defining Ag toxicity is variable in literature. While some authors determined levels of free ions above 5 µg/mL [49, 50], the majority of authors found a much higher non-cytotoxic limit for a variety of cell types [51].

5.4. Mg-based implants for application in children orthopedics

Children bones deserve special attention due to their high probability of suffering injuries. Magnesium-based implants have been extensively studied in adult bone tissue, showing osteoinductive potential (stimulating bone healing and growth), biocompatibility, appropriated strength and interface material-surrounding tissue. Nevertheless, the reaction of growing bone to those materials has not been evaluated yet [52].

Conservative fracture treatment in children (used before the 1980s) required immobilization and casting, which apart from being undesirable for a child also involves high economical cost to the health care service and big efforts for the family. Those treatments were later substituted by other methods, as elastic stable intramedullary nails (ESIN), developed by French surgeons (Figure 3). Advantages of ESIN include an easy application, avoidance of a cast and early load bearing [53].

They are made of non-biodegradable materials, as stainless steel or titanium [54], making still necessary an additional surgery for implant removal [52, 55]. Therefore, Mg-based biodegradable ESIN would be potential substitutes for application in pediatric orthopedics.

Figure 3. Radiographs of a fracture of the mid-shaft of the femur, showing a lateral view, in a boy aged six years A) before surgery; B) after intramedullary fixation with intramedullary stabilization with two flexible nails [56].

Fractures of growing bones are similar to the ones in adult bones. The healing process is also similar, going through inflammation, reparation and remodeling. Nevertheless growing bones heal faster than adult bones and can correct any defect on fracture alignment or angulation after healing. Hence, implants should mainly help the bone to support the loading forces, while stabilizing the fracture. One of the reasons for the fast healing is that growing bones have a greater subperiosteal hematoma and a stronger periosteum, contributing to a more rapid formation of a callus. Therefore, growing bones require less initial stability and callus formation than adult bones to achieve a clinically stable or healed fracture. Another reason is the

osteogenic environment present in growing bone. Thus, osteogenic factors are already ongoing at the time of fracture, while in adults those factors have to be re-activated [57].

Growing long bones present two cartilaginous areas located in both ends, which constitute functional systems responsible for the appropriate development and elongation of the bones. Any damage in those areas (which furthermore show higher susceptibility to injuries than the rest of the bone) can give rise to malformations during further bone development [58, 59]. This can result in different lengths between both bones of the child.

Implantation and removal of permanent implants increase the risk of damage of the growth plates. Therefore, the use of biodegradable implants would diminish such a risk avoiding the second surgery and thus, the undesirable immobilization when the bone is completely healed. Nevertheless, it is necessary to tailor any possible effect of the degradation products on the cartilaginous growth plate, and to determine if such effect will influence bone growth with both, direct contact with that tissue or due to the diffusion of the degradation products.

5.5. Development of cartilage and growth plate

Hyaline cartilage is a type of connective tissue formed by a specialized type of cells, the chondrocytes, and by ECM. The ECM is mainly composed of water, collagen fibers, proteoglycans and other matrix proteins (Figure 4).

Hyaline cartilage arises from mesenchymal stem cells (MSCs) condensation during fetal development. In most of the condensation areas, cells will become chondrocytes, throughout a process named chondrogenesis, giving rise to cartilaginous tissue. Part of the hyaline cartilage will specialize and cover the surfaces of synovial joint (articular cartilage). Hyaline cartilage will furthermore develop in epiphyseal cartilage, which will be limited to disk-shaped areas located in the epiphysis of long bones, which constitute the growth plates.

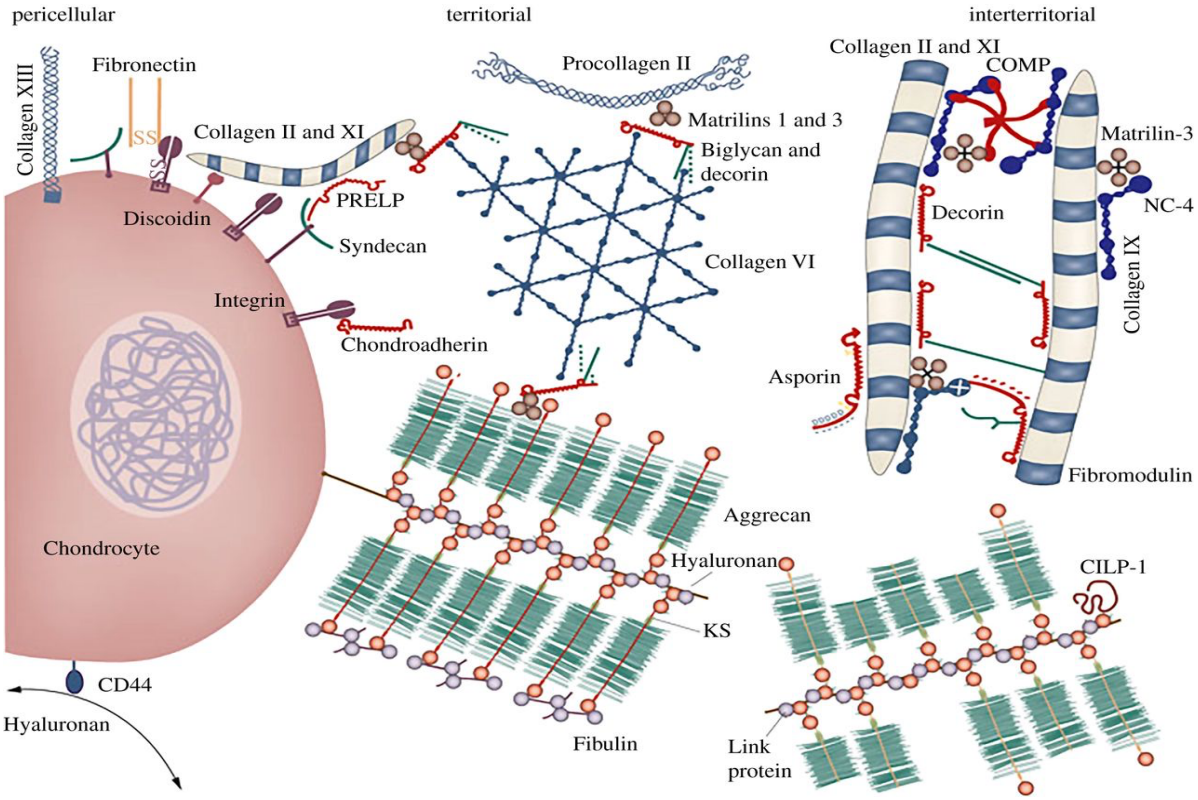

Figure 4. Molecular composition and organization of hyaline cartilage [60]. Chondrocytes are the cells responsible for the biosynthesis and maintenance of the ECM. Most of the collagens found in hyaline cartilage are type II, with certain contribution of types VI, IX, XI, XII, and XIV. Type I and X collagens gradually substitute type II collagen as chondrocyte maturation occurs. PRELP: Proline and Arginine Rich End Leucine rich repeat Protein; KS: Keratan Sulfate; COMP: Cartilage Oligomeric Matrix Protein; NC-4: Non Collagenous domain 4; CILP-1: Cartilage Intermediate Layer Protein [60, 61].

Apart from a same origin, articular and growth plate cartilages also exhibit a similar spatial organization (Figure 5), being divided in three zones depending on chondrocyte size, shape and organization, with similar qualitative composition [62].

Nevertheless, those tissues show important differences. Growth plate cartilage is characterized by a quantitative prevalence of cell mass over the matrix mass, while in the articular cartilage the opposite occurs. Furthermore, both tissues have clear functional differences and therefore, the differentiation program that chondrocytes undergo will have variations in the regulation mechanisms.

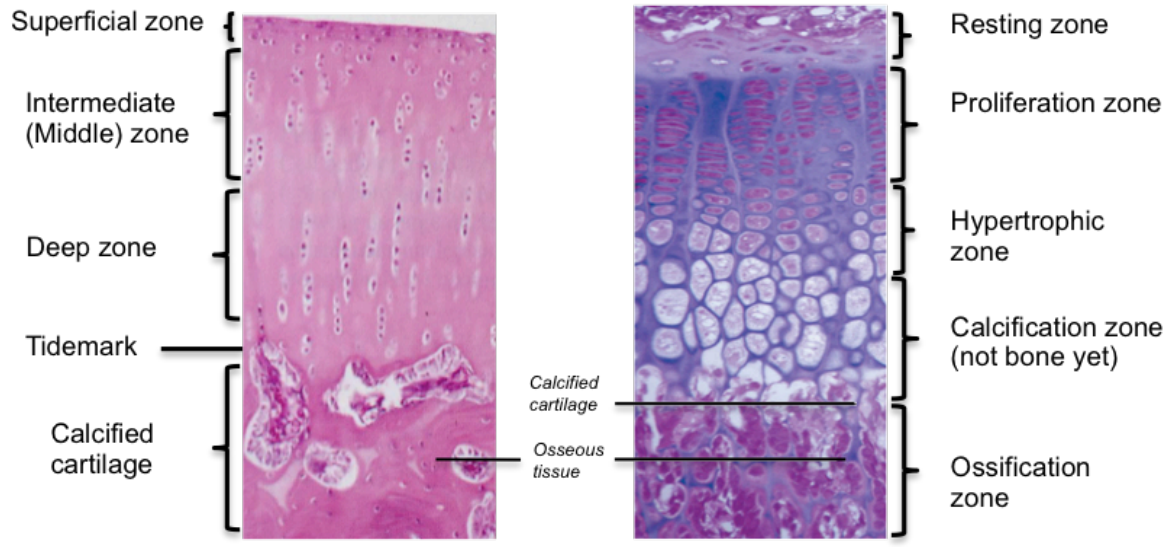

Figure 5. Structural zones of articular cartilage (left image) and growth plate cartilage (right image). The main differences are the amount and distribution of chondrocytes throughout the tissue.

On one side, articular cartilage provides a low-friction gliding surface, with increased compressive strength and is known to be wear-resistant under normal circumstances [63]. On the other side, the function of the growth plate is to generate new bone during bone growth (Figure 6). This process is named endochondral ossification, and occurs until adult status is reached [64]. Subsequently bones stop growing and the growth plate is replaced by an epiphyseal line.

In the cartilage tissue of the growth plates, the resting zone is located directly beneath the secondary ossification center and contains progenitor cells that continuously infiltrate and renew the proliferative and hypertrophic zones.

The underlying proliferative zone contains chondrocytes that replicate at a high rate and line up along the long axis of the bone, forming columns of cells. In the zones far from the resting zone, proliferative chondrocytes stop replicating and start enlarging to form the hypertrophic zone, which consists of chondrocytes undergoing terminal maturation.

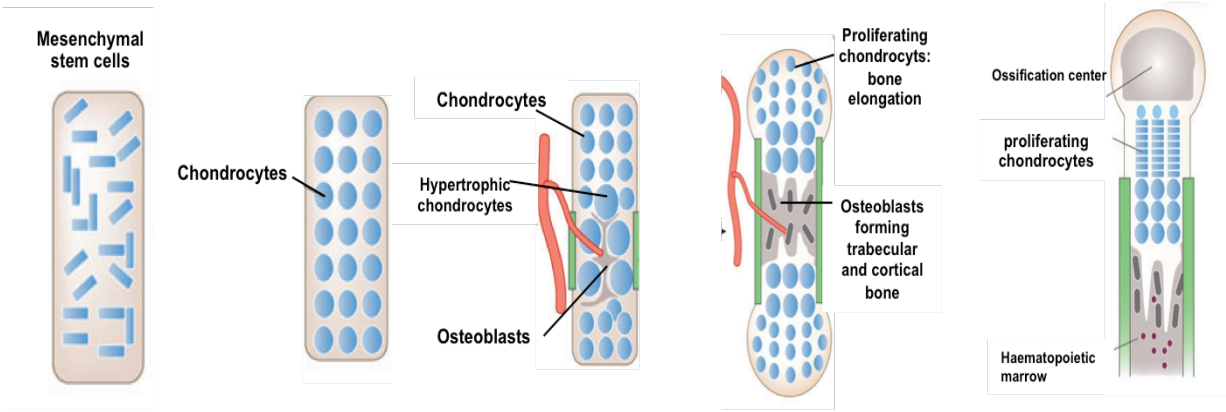

Figure 6. Bone development and elongation. MSCs condense and become chondrocytes. Chondrocytes at the center of condensation stop proliferating and undergo hypertrophy. Cells adjacent to hypertrophic chondrocytes become osteoblasts. Hypertrophic chondrocytes direct the mineralization of ECM, attract blood vessels, and undergo apoptosis. Chondrocytes proliferation generates bone lengthening. Osteoblasts of primary spongiosa are precursors of eventual trabecular bone. At the end of the bone the secondary ossification center is formed. Below the secondary center of ossification proliferating chondrocytes are organized forming columns, constituting the growth plate. Image modified from Kronenberg et al. [64].

Cell proliferation, hypertrophy and apoptosis contribute to the formation of a cartilage scaffold that will allow osteoblast mineralization and bone elongation. [64]. The hypertrophic chondrocytes are responsible for the calcification of the extracellular matrix. They furthermore produce growth factors, which attract bone cells and endothelial cells to form vessels and remodel the newly formed cartilage into bone [65-67].

5.6. Chondrogenesis and chondrocyte maturation in growth plate cartilage

All the events that constitute the chondrogenic differentiation are regulated by complex molecular pathways that vary during developmental phases and involve changes in chondrocyte proliferation, morphology and spatial organization among others [64]. The nature and amount of ECM also varies during the different stages, leading to a variation in the expression of different markers (Figure 7). Synthesis of cyclic adenosine monophosphate (cAMP), transcription growth factor beta (TGFβ), fibronectin, neural cell adhesion molecule (N-CAM) and N-cadherin is involved and necessary in the induction of chondrogenesis. Proliferating and maturing chondrocytes mainly synthesize collagen type II, IX and the proteoglycan aggrecan (ACAN). When chondrocytes reach hypertrophy, type X collagen will be the main component before mineralization of the ECM [68, 69].

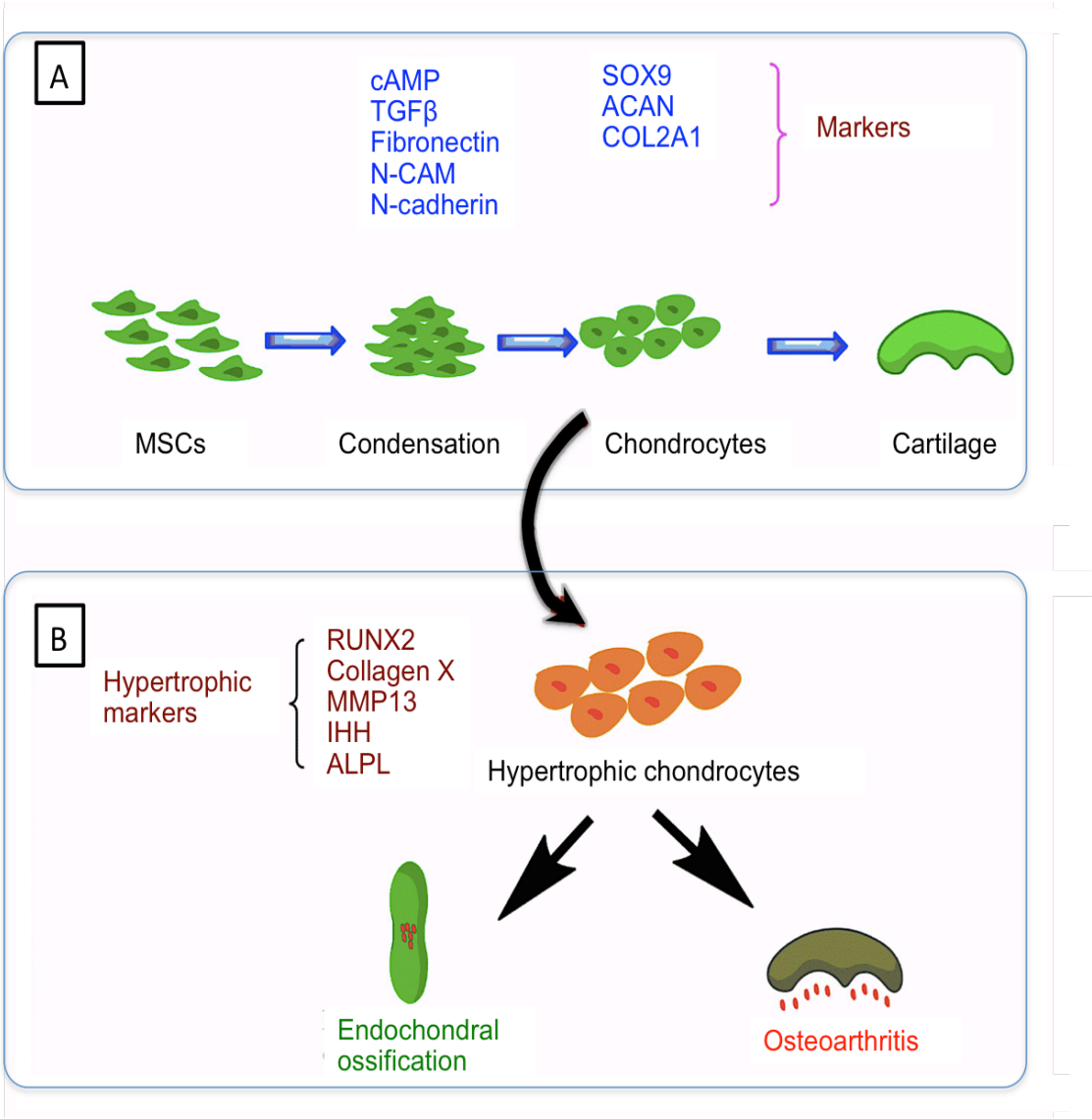

Figure 7. Chondrogenesis and hypertrophy of MSCs. **A)** MSCs condensation and cell-cell interaction is accompanied by the production of cAMP, TGFβ, Fibronectin, N-CAM and N-cadherin and the expression of chondrogenic genes: SOX9, ACAN and COL2A1. Mature chondrocytes produce cartilage extracellular matrix, secreting Collagen II and GAG. **B)** Mature chondrocytes can undergo hypertrophic differentiation, characterized by the expression of RUNX2, Collagen X, MMP13, IHH and ALPL. Finally, hypertrophic chondrocytes could undergo mineralization of the ECM and apoptosis, involved in endochondral ossification and pathological osteoarthritis *in vivo* [70].

It is noteworthy that type II collagen cleavage occurs at a time when type X collagen is synthesized and secreted in the hypertrophic zone [3, 4, 48] and interacts with fibrils of type II collagen [14, 15]. Extensive damage to the fibrillary organization of type II collagen and appearance of type X collagen is a unique feature observed prior to calcification. Some markers involved in osteogenesis also appear prior to mineralization, as type I collagen (COLI), osteopontin (OPN), osteocalcin (OC) and runt-related transcription factor 2 (RUNX2) [71]. RUNX2 is a transcription factor that

has been associated with the regulation of chondrocytes maturation and apoptosis. The expression of those markers will increase as ossification takes place [72].

Cell morphology changes also take place among the different zones. Thus, chondrocytes exhibit a rounded morphology in the maturation zone, and acquire an enlarged size, as they become hypertrophic chondrocytes [70].

In order to understand the molecular and biochemical mechanisms that underlie the changes in chondrocyte phenotype during chondrogenesis, proteomic approaches have been used in the last years. The proteome is the entire complement of proteins produced by an organism under specific conditions (which could be variable). The evaluation of the chondrogenic differentiation of MSCs revealed valuable information in this regard. Even though existing controversy about some regulated proteins during chondrogenesis, results agreed that the majority of the regulated proteins are metabolic enzymes and stress response proteins. Others are proteins that constitute the cytoskeleton and ECM (or involved in their organization), as well as proteins involved in protein synthesis and degradation [73-76].

5.7. Cell models for evaluating chondrogenesis *in vitro*

Cell lines are considered as standards *in vitro* cell types, due to the homogeneity and constancy that those cultures guarantee since they are not influenced by cell passage or source [77]. Thus, cell lines reduce the requirements needed to perform a multitude of replicative experiments and allow comparison between results obtained with the same cells under different conditions. Nevertheless, primary cells are a superior model of the *in vivo* situation, allowing the translation of *in vitro* results to *in vivo* conditions [78, 79]. The combination of both, human primary stem cells and mouse chondrogenic cell line which are used in the present work, allowed a wider evaluation of the whole chondrogenic process. Combination of both is required to guarantee the reliability of the results.

5.7.1. Human umbilical cord perivascular cells (HUCPV)

Stem cells are widely used to obtain neo-tissue or cartilage constructs *in vitro* for cell therapy and tissue engineering applications (in combination with biomaterials). They

allow a detailed evaluation of the differentiation process into different cell lineages, using specific culture conditions to direct the cell development.

Mesenchymal stem cells can differentiate into the musculoskeletal lineages (adipocytes, osteoblasts, tendons muscle, skin and chondrocytes) among others. Furthermore they own the capability of self-renewing while maintaining their multipotency.

A specific type of MSCs, the HUCPV, were first isolated by Sarugaser et al. [80]. He proposed that there should be a mesenchymal precursor population of cells that would give rise to the connective tissue of Warton´s Jelly during gestation. Those cells are located in the region surrounding the blood vessels (perivascular) within the human umbilical cord (Figure 8). HUCPV cells are a potential alternative to another cell sources for cell therapy. They exhibit stronger potential for self-renewing and multilineage differentiation than other established MSCs, both *in vitro* and *in vivo* [81]. Furthermore, since those cells are obtained from umbilical cord, they can overcome some problems due to donor age (usually associated with MSCs) or the use of invasive techniques.

The chondrogenic differentiation of MSCs is enabled through high-density pellets formation, which in turn produces a round morphology (mimicking mesenchymal condensation in the limb bud) [82].

Additionally, MSCs must be treated with specific developmental clues to stimulate chondrogenesis and cartilage phenotype. The chondrogenic biofactors include growth factors (Insulin-like growth factor-I, TGFβ superfamily members), ascorbic acid and aminoacids (L-Cysteine, L-Proline) among others [81].

A special characteristic of HUCPV cells is their intrinsic potential to differentiate into the osteogenic lineage without stimulus, forming bone nodules when cells are cultured at high confluence in monolayer under normal culture conditions [80]. In contrast, hypoxic conditions were used to suppress osteogenic differentiation while increasing cell proliferation and colony-forming efficiency, as well as maintaining the same chondrogenic potential [83]. Hence, HUCPV cells were cultured at 5% oxygen tension.

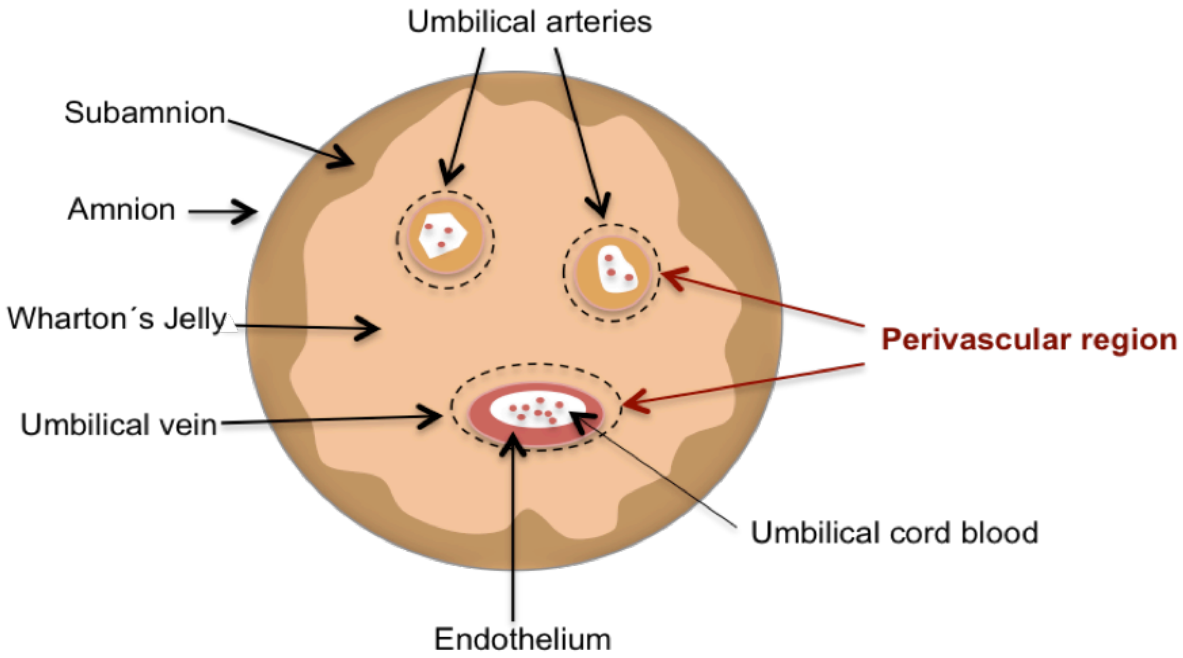

Figure 8. Schematic representation of the cross-section of a human umbilical cord, with the different anatomical areas. Wharton´s Jelly, vein, blood and perivascular region are sources of different types of MSCs.

5.7.2. ATDC5 cells

ATDC5 cells are derived from mouse teratocarcinoma and characterized as a chondrogenic cell line, which goes through a sequential process analog to chondrocyte differentiation. Thus, those cells are a well-established *in vitro* model of endochondral ossification [84].

ATDC5 cells proliferate fast and easily, leading to vast amount of cells in short time periods and as a result, a fast set up of the *in vitro* culture system. Furthermore, they maintain the undifferentiated state during expansion, unless re-differentiation is stimulated with chondrogenic factors. When inducing chondrogenesis of ATDC5 cells in monolayer, cartilaginous nodules can be formed through cellular condensation (when high cell concentration is reached in the culture surface). These cells exhibit the phenotype of chondrocytes, going through all the phases of differentiation [85]. Hence, a three dimensional (3D) culture model and low oxygen tension are not necessary for inducing the chondrogenic differentiation of ATDC5 cells. Those cells are well characterized and considered as an excellent model to investigate molecular mechanisms of chondrogenesis *in vitro*.

6. MOTIVATION

High concentrations of Mg have shown good cell tolerance [52] and chondrogenic potential *in vitro*, and an increased cell adhesion *in vivo*, enhancing chondrogenesis in endochondral injuries.
In this work it is hypothesized that pure Mg (Mg) and two binary Mg-alloys (Mg-10Gd and Mg-2Ag) are well tolerated by the cells involved in bone elongation (stem cells and chondrocytes) and enhance chondrogenic differentiation. Furthermore, we believe that the alloying elements could give rise to small differences in cell reaction.

The main aim of this study is the characterization of cell response to Mg, Mg-2Ag and Mg-10Gd materials, focusing on the progression of chondrogenesis, in order to predict possible influences in the growth plate cartilage when applied as implants *in vivo*. HUCPV primary cells and ATDC5 cell line were used as model to mimic chondrogenesis in combination with the materials in direct contact and with the degradation products (extracts).
With this purpose, this work was divided in the next sections:

- Evaluation of cell viability and proliferation of both cell types under the influence of the extracts and in direct contact with the materials, in order to exclude cytotoxic effects.

- Identification of variations in the chondrogenic differentiation of HUCPV and ATDC5 cells under the influence of the materials (both in direct contact and under the influence of the extracts), evaluating chondrogenic gene and protein markers, as well as cell morphology, distribution and ECM production.

- Determination of differentially expressed proteins during chondrogenesis under the influence of Mg-materials extracts with the aim of identifying relevant proteins involved in chondrogenesis affected by those biodegradable metallic materials.

7. MATERIAL AND METHODS

7.1. Material production and sample preparation

Pure Mg (Mg, 99.95%) and Mg with 10 wt% gadolinium (Mg-10Gd) alloys were prepared by permanent mold gravity casting, while Mg with 2 wt% silver (Mg-2Ag) alloy was produced via permanent mold direct chill casting (Helmholtz Zentrum Geesthacht, Geesthacht, Germany). Subsequently, the alloys were homogenized with T4 treatment. Heat treatment is applied to Mg alloys in order to alter their mechanical properties. Three basic types of thermal treating processes for Mg alloys are commonly applied: solution heat treatment (T4), precipitation or aging, and annealing. T4 treatment consists in heating the alloy material to a temperature at which certain constituents go into solution, and are kept into solution while cooling. Therefore the resulting alloy shows a homogenize microstructure and improved degradation resistance.

Afterwards, ingots were extruded into rods of 1.2 cm diameter, and finally machined to obtain a diameter of 1 cm. Discs of 1.5 mm thickness were then cut and gamma sterilized with a total dosage of 29 kGy (BBF Sterilisationsservice GmbH, Kernen-Rommelshausen, Germany). Detailed parameters are already published [86].

7.2. Degradation rate of the materials

The degradation rate was calculated from the mass loss of the samples (six samples of each material) following Equation-3, after immersion during seven days in culture medium containing alpha minimum essential media (αMEM; Fisher Scientific GmbH, Schwerte, Germany) with 15% fetal bovine serum (FBS; Stem Cell Technologies, Vancouver, Canada) and 1% antibiotics penicilin / streptomicin (Pen strep; Invitrogen, Bremen, Germany) and under cell culture conditions (21% CO_2, 5% O_2, 37 °C).

$$DR=(8.76 \times 10^{4} \times \Delta w)/(d \times A \times t) \qquad \text{Equation-3,}$$

where Δw: weight loss; d: density; A: area; t: time.

Each sample was culture in 12-well plates coated to avoid cell adhesion, and with 3 mL of medium. Change of medium was done after two-two-three days. After seven

days, the medium was removed and the samples where soaked in chromic acid (180 g/L in distilled water, VWR international, Darmstadt, Germany) for 20 min at room temperature, turning the samples after 10 min to expose both surfaces of every disk. Subsequently the samples were removed from the chromic acid solution, immersed in distilled water and shacked to enhance the removal of the degradation products. Finally, the samples where washed with ethanol to remove rests of water and thus, avoiding further degradation until the samples were weighted.

7.3. Extract preparation and characterization

Sample disks, with an average weight of 0.2 g and 1.5 mm thickness were immersed in αMEM (Fisher Scientific GmbH) with 10% FBS for mesenchymal stem cells (SC-FBS; Stem Cell Technologies, Vancouver, Canada) and 1% antibiotics Pen strep (Invitrogen) for 72 hours at 37°C, according to EN ISO standards 10993:5 [87] and 10993:12 [88]. Afterwards, the culture medium was filtered with a 0.2 µm filter (Merck KGaA, Darmstadt, Germany). Then, pure elutes were diluted in Dulbecco's Modified Eagle's Medium/Nutrient Mixture F-12 Ham (DMEM / F-12 Ham; Sigma-Aldrich, Vienna, Austria) with 5% fetal bovine serum (FBS; Fisher Scientific GmbH, Vienna, Austria) Sodium Selenite (30 nM, Sigma-Aldrich GmbH) and Human transferrin (10 µg/mL, Sigma-Adrich GmbH).

Table 2. pH and elemental characterization of the initial extracts (pure) and after dilution (diluted) measured via ICP_MS, compared with the element composition of the culture medium. All units are given in millimolar (mM).

Element / ***Extract***		**Mg**	**Ca**	**P**	**Gd**	**Ag**	**pH**
Mg	*Pure*	51.43	0.7	0.3	——	——	8.68
	Diluted	6.08	1.79	1.26	——	——	8.15
Mg-10Gd	*Pure*	80.64	0.32	0.32	2.16×10^{-3}	——	8.51
	Diluted	6.08	1.77	1.26	1.27×10^{-3}	——	8.15
Mg-2Ag	*Pure*	50.60	0.54	0.54	——	71×10^{-3}	8.68
	Diluted	6.08	1.72	1.16	——	11×10^{-3}	8.25
αMEM	*Pure*	0.814	1.80	1.014 + proteins /FBS	——	____	7.34
	Diluted						

In order to allow the highest cell proliferation 10% dilution of Mg extract was prepared. This dilution corresponded to a Mg concentration of 6.08 mM (detailed information about how this concentration was determined is shown in section 2.5.1). This value was used with Mg-10Gd and Mg-2Ag extracts in order to keep a common Mg concentration that allows the determination of cell reaction to the alloying elements. Such a specific Mg concentration was obtained diluting the initial pure extracts with culture medium. Then the element content of elutes (both, initial concentrated and diluted) was measured via inductively coupled plasma mass spectrometry (ICP-MS; Agilent 7700x ICP-MS, Waldbronn, Germany). pH was measured with a pH-meter HI 111 Hanna (Hanna Instruments, Ulm, Germany). Results are shown in Table 2.

7.4. HUCPV isolation

HUCPV cells are human primary cells located in the perivascular area of umbilical cords. Umbilical cord samples were provided by Asklepios Klinik Altona (Hamburg, Germany) after approval of consent donors. Fragments of approximately 5 cm length were cut and transported in αMEM (Fisher Scientific GmbH) containing 15% stem cells FBS (Stem Cell Technologies) and 5% antibiotics Pen strep (Invitrogen) (Figure 9 A). The use of antibiotics is necessary in the case of primary cells due to their susceptibility to contamination *in vitro*. The isolation of the MSCs consisted of removing the epithelium and part of Warton´s Jelly with the help of a scalpel and tweezers, until the three vessels (two arterial and one vein) present in the umbilical cord were completely separated from the rest of the sample (Figure 9 B). Using a thread, both ends in each vessel were then tied together forming a loop (Figure 9 C).

Vessels were transferred to cell culture flasks containing culture medium and kept for one week without disturbances under cell culture conditions. Culture medium was changed every week until cells appeared in the culture flask (mainly close to the vessel) (Figure 9 D). Then the medium was changed every two-trhee days. When cells reached approximately 60% confluence, they were trypsinized and transferred to T75 flasks.

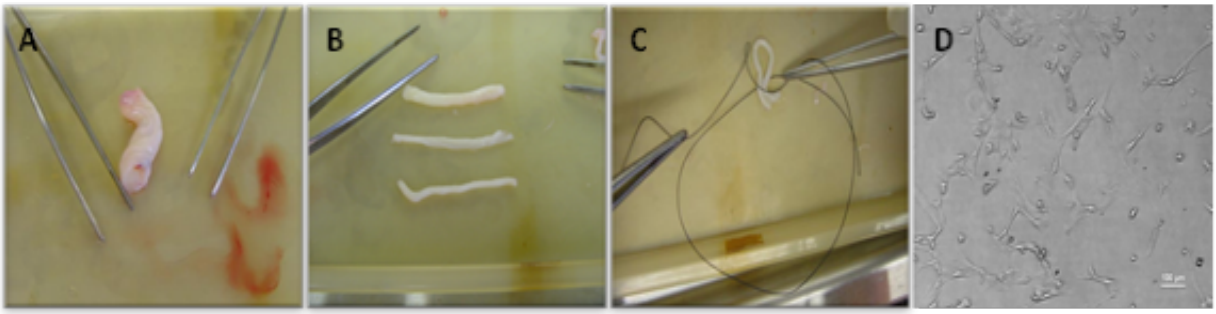

Figure 9. HUCPV isolation from human umbilical cord samples. A) fragment of umbilical cord samples, 5 cm length. B) Vein and two arteries isolated from the umbilical cord after removing the epithelium and Warton´s Jelly with the help of tweezers and a scalpel. C) Opposite ends of the vessel tied together with a thread to avoid the release of cells from the inner part. D) HUCPV attached to the culture flask after 10 days of culture of the vessels.

7.5. Direct and indirect test of cell reaction to Mg material

In order to evaluate the cellular reaction to material degradation, both HUCPV and ATDC5 cells were cultured using indirect and direct test. The indirect test allowed the evaluation of the degradation products or extracts (previously described) on cells. It consisted of cell culture in monolayer in presence of the extracts. Tables 3 and 4 show the composition of the different conditions used with HUCPV and ATDC5 respectively. In the case of HUCPV cells, furthermore a 3D culture in the extracts was necessary to induce and evaluate genesis (see section 2.4.1.).

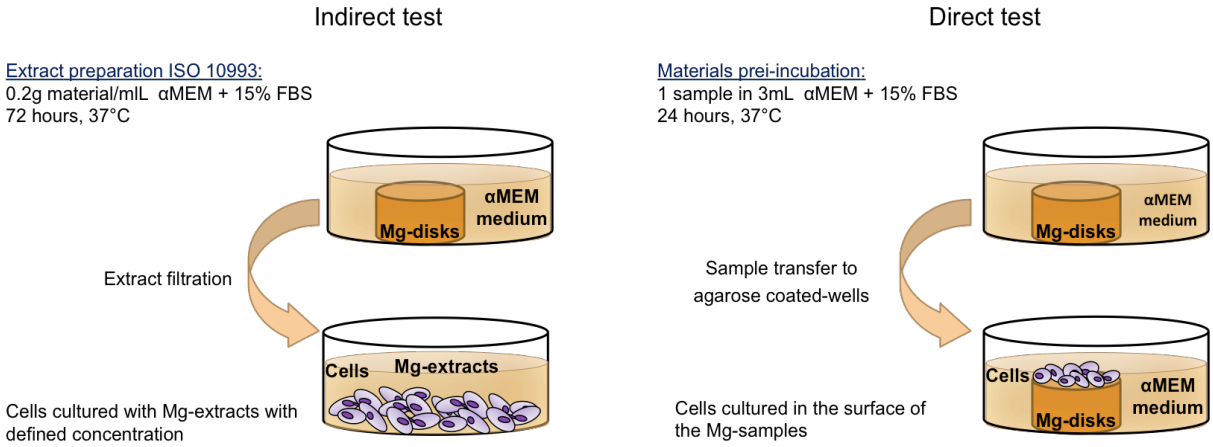

Figure 10. Scheme of the testing methods for evaluating cell reactions to the Mg-materials. Indirect test (left part of the figure) consisted of preparing extracts, filtering them and adding to cultured cells. In the direct test, disks are pre-incubated and cells seeded directly in the surface of the material (right part of the figure).

The direct test was used to evaluate the cell reaction when seeded directly on the surface of the sample discs. A pre-incubation period of the materials was necessary before cell seeding. This test was performed in monolayer with both cell types (Figure 10).

7.5.1. Indirect test

Trypsinized cell pellets were washed with phosphate-buffered saline (PBS; Scientific GmbH, Schwerte, Germany), re-suspended in growth medium and transferred to well-plates (with the necessary cell density depending on the experiment performed). Then cells were allowed to attach to the plastic wells for 1 hour under culture conditions. Subsequently, growth medium was replaced by the extracts. Controls were kept in growth medium. Change of medium was made every two-two-three days.

The indirect test was performed with HUCPV cells to evaluate cell proliferation (after one, two and three days), viability with Life/dead staining (after seven days) and expression of chondrogenic antibodies with fluorescence staining. ATDC5 indirect test was performed for seven, 14 and 21 days to evaluate cell growth and ECM production by optical microscopy.

In order to induce chodrogenic differentiation of HUCPV cells, high density pellets (micromasses) were formed and chondrogenic factors were added to stimulate the differentiation.

After cell detachment with trypsin, 300 000 HUCPV cells were seeded in 15 mL polypropylene conical falcon tubes (Greiner Bio-One, Frickenhausen, Germany) and centrifuged for 10 min at 1 000 rpm. Then supernatants were removed, and replaced by 1.5 mL of growth medium. Tubes were centrifuged again for 10 min at 1 000 rpm, and transferred to the incubator with loosened caps in order to allow oxygen transfer to the samples. Tubes were incubated during 3 days without disturbance under a humidified atmosphere, 37° C, 5% CO_2, and low oxygen content (5% O_2).

After three days of culture, spherical cell aggregates (micromasses) were formed at the bottom of the tubes (Figure 11). Subsequently, growth medium was replaced with 1.5 mL of chondrogenic medium or chondrogenic medium with the addition of

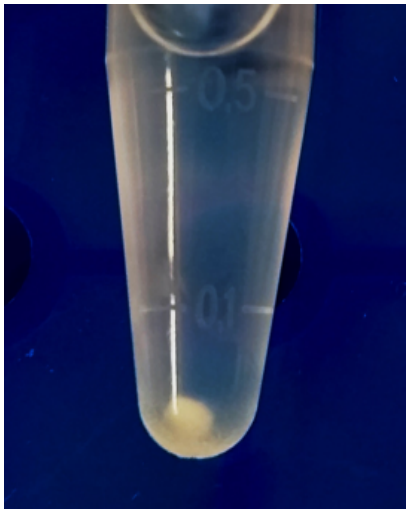

the extracts. Chondrogenic medium consisted of αMEM with 10% FBS, 1% pen strep, 0.28 nM L-Ascorbic acid 2-phosphate (Sigma-Aldrich, Munich, Germany), 1 mM L-Cystein (Merck, Darmstadt, Germany), 100 ng/mL Insulin like growth factor I, IGF-I (Peprotech, Hamburg, Germany), 20 ng/mL Transforming growth factor β_1, TGF- β_1 (Peprotech) and 10 ng/mL, IL-1 (Peprotech).

Figure 11. Micromass formed after three days of culture of high-density HUCPV pellets.

Culture medium was changed every two-two-three days. Micromasses were collected after 11 days for proteomic analysis, and after 21 days for evaluating the gene expression, cell growth and synthesis of GAG.

Table 3. Medium composition in the different conditions for HUCPV cells culture.

Condition	**Composition**
Differentiation medium (control)	αMEM + 10% SC-FBS + 1% antibiotics Penicillin / Streptomycin + 0.28 nm L-Ascorbic acid 2-phosphate + 1 mM L-Cystein + 100 ng/mL IGF-I + 20 ng/mL TGF- β_1 + 10 ng/mL IL-4
Mg extract	Differentiation medium + pure extract
Mg-10Gd extract	Differentiation medium + pure extract
Mg-2Ag extract	Differentiation medium + pure extract

Table 4. Medium composition in the different conditions for ATDC5 cells culture.

Condition	**Composition**
Growth medium	DMEM + 5% FBS+ 10 µg/mL human transferrin + 30 nM sodium selenite
Differentiation medium	Growth medium + 10 µg/mL insulin + 37.5 µg/mL ascorbic acid
Mg extract	Growth medium + pure extract
Mg-10Gd extract	Growth medium + pure extract
Mg-2Ag extract	Growth medium + pure extract

7.5.2. Direct test: Preincubation of samples and cell seeding

Samples were pre-incubated in 12 well-plates, with 3 mL of αMEM medium (Fisher Scientific GmbH) supplemented with 15% FBS (Stem Cell Technologies) for 24 hours at 37ºC. Pre-incubation under cell culture conditions is used to create a natural degradation layer on the samples, which improves cell adhesion and proliferation and therefore enhance *in vitro* experimentation [89]. The longer the pre-incubation time, the better the cell adhesion and proliferation. Nevertheless, also an increased risk of contamination is observed with longer experiment periods. Therefore, 24 h was established as standardized pre-incubation period [90].

Samples were transferred to 12 well-plates coated with agarose (2%). The coating avoids cell attachment to the plates. Then cells were washed with PBS (Scientific GmbH, Schwerte, Germany) and detached from the culture flasks with accutase (Stem Pro Accutase Cell Dissociation Reagent, Life Technologies). The ATDC5 and HUCPV cells were seeded on the surface of the materials (40 000 cells in 50 µL of medium) and allowed to attach to the surface of the material during 30 min at 37ºC. Subsequently 2 mL of αMEM (Fisher Scientific GmbH) medium were added to the wells. Change of medium was performed every two days.

The direct contact test with HUCPV cells was carried out for seven days, and subsequently, Life/dead staining and fluorescence staining of chondrogenic antibodies was performed. Regarding ATDC5 cells, after seven days of culture samples were analyzed by Life/dead staining and SEM.

7.6. Evaluation of cell reactions to the materials

7.6.1. Use of $MgCl_2$ solution or Mg-extracts

Firstly the effects of Mg as salt ($MgCl_2$) and as Mg extract were compared to determine if both could be used interchangeably. This means, if the use of Mg as salt is appropriated for further experiments and the results could be translate to the same concentration of Mg in the extracts. Otherwise, if differences are appreciated, the use of the extract will be necessary. For this purpose, a proliferation assay was made, using a label-free cell counter (CASY Model TT 150 µm, Roche Applied Science, Penzberg Germany), which allows the quantification of live cells in

suspension, after exposure to any of both, the $MgCl_2$ or the Mg extract solutions, after three different time points. The principle of CASY technology for cell analysis combines digital pulse processing (DPP) with a high scanning rate and a highly-standardized method of analysing cell signals. This combination ensures maximum resolution and reproducibility for all measuring parameters and facilitates measuring range dynamics.

In brief, cells are suspended in an electrolyte solution developed for cell counting, and the suspension is aspirated through a precision measuring pore. A voltage field with 1 MHz is applied to the measuring pore, which exhibits a defined electrical resistance when filled with electrolyte suspension. It is a requirement that the cells are aligned in the suspension for individually analysis. Cells displace electrolyte when passing through the measuring pore, in a quantity corresponding to their volume. Since cell membrane acts as an electrical barrier, an increase in the resistance is achieved when intact cells pass, while dead cells are detected from the size of their nucleus.

Three different concentrations were used of $MgCl_2$ (5, 10 and 15 mM) and four with Mg extract (3.04, 6.08 and 12.16 mM and 60.8 mM) corresponding with a dilution 1:5, 1:10, 1:15 (in αMEM) and the pure extract without diluting respectively. 1 mL of growth medium containing 10 000 HUCPV was added per well in 12 well-plates. Cells were allowed to attach for 1 hour under cell culture conditions. Then, controls were kept in growth medium (αMEM), and the different concentrations of $MgCl_2$ and Mg extracts were added to the remaining wells. After 24, 48 and 72 hours, HUCPV were trypsinized from the wells and quantified with CASY. 100 µL of cell suspension from the sample were transferred into a cup containing 10 mL of CASYton (Roche Applied Science). Four measurements were performed for any of the 6 biological replicates. From the data obtained with CASY counter (viable cells/mL), the total number of viable cells in the biological samples was calculated as indicated:

Viable cells/mL (from CASY counter) x Total mL of the sample = viable cells in the sample.

7.6.2. Selection of appropriate concentration of Mg in Pure Mg extracts

The most suitable concentration of Mg in the extracts for cell growth and chondrogenesis was determined, using pure Mg extract, prior to the evaluation of the selected Mg-alloys (Mg-10Gd and Mg-2Ag). The obtained concentration (6.08 mM) was used in all the experiments described in this work (unless indicated). The selection criteria consisted of the evaluation of gene expression of chondrogenic gene markers (SOX9, COL2A1 and ACAN) and the hypertrophic marker OPN. Furthermore, GAG production was studied by quantifying its content in the ECM and in the supernatants.

7.6.3. Gene expression

- ***RNA extraction and isolation***

The RNA extraction and purification was performed using the RNeasy mini Kit (Qiagen GmbH, Hilden, Germany). The RNeasy technology consists of the selective binding of RNA to a silica-based membrane, while contaminants are washed away using microspin technology.

The binding of the RNA to the silica membrane is enhanced by the use of a specialized high-salt buffer system and ethanol, and the centrifugation forces the solution to pass through the membrane. After washing the membrane for removing any kind of impurities, the RNA is eluted from the column by using low-ionic salt buffers or water (Figure 12).

Due to the differences in the culture model for HUCPV and ATDC5 cells, the procedure for isolating RNA were different regarding some steps. Micromasses from HUCPV cells contain low amount of differentiate chondrocyte cells and are constituted mainly by cartilaginous ECM, which requires a homogenization or mechanical breakage process previously to RNA isolation.

Furthermore, the use of a trizol-containing agent is necessary (Tri Reagent, Qiagen GmbH, Hilden, Germany) during the homogenization in order to break the cells and allow the access to RNA.

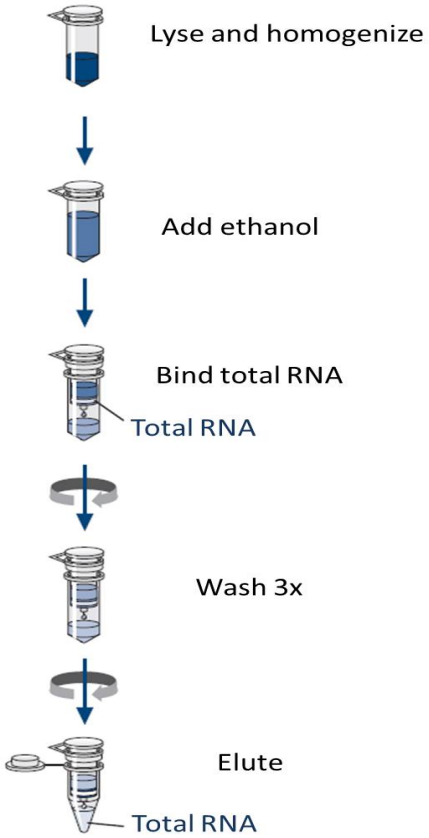

Figure 12. Procedure for RNA isolation with RNeasy Mini Kit assay. Qiagen. RNeasy® Mini Handbook. 2012. Available from: http://www.bea.ki.se/documents/EN-RNeasy%20handbook.pdf

Procedure with HUCPV cells

The RNA extraction of HUCPV cells was performed after 21 days of culture. In order to homogenize the micromasses and enhance the breakage of the cells, micromasses were transferred into ceramic bead tubes 1.4 mL (Dianova, Hamburg, Germany) with the help of a spoon. Then the tubes were frozen in liquid nitrogen, placed in the vortex adapter for vortex Genie® (Qiagen, Dusseldorf, Germany) and vortexed until the pellets were fragmented or not visible among the ceramic beads (10-15 min). Subsequently, 200 µL of Tri Reagent was added, as indicated in the protocol for 300 000 cells. Then the tubes with the beads were vortexed again for 5 min. The supernatants were mixed thoroughly and transferred into RNease-free tubes.

Procedure with ATDC5 cells

After seven, 14 and 21 days of ATDC5 culture (in monolayer) in 12 well plates, culture medium was removed and 200 µL of buffer RLT was added (which contains high concentration of guanidine isothiocyanate). This buffer not only lysates the cell membrane and denaturalizes proteins, but furthermore enhances RNA binding to the silica membrane due to its high content of salts. Subsequently, cells were scratched

from the surface of the well with the help of a pipette. Then, cells were transferred to Eppendorf tubes (Eppendorf AG, Hamburg, Germany) and homogenized with a vortex for 20 seconds.

Common procedure for HUCPV and ATDC5 cells

200 µL of ethanol (95%) were added to every lysate and mixed thoroughly to enhance RNA separation in the column. The mixture was then transferred into the Zymo-Spin™ IIC Column (Figure 13 a) placed in a Collection Tube (Figure 13 b) and centrifuged. The column was transferred into a new collection tube to continue with the prewash (using 400 µL Direct-zol™ RNA PreWash and centrifuging for 10 seconds) and wash steps (700 µL RNA Wash Buffer to the column and centrifuge for 2 minutes). To elute the RNA from the membrane of the column into a collection tube, RNAse free water was added. RNA was concentrated in a final volume of 50 µL water for all the samples.

Figure 13. Spin column containing a silica membrane (a) and collection tubes (b). The spin column can be placed in the collection tubes and removed, allowing to discard repeatedly the elute and continue using the spin column.

The concentration of RNA was determined by measuring the absorbance at 260 nm (A_{260}) in a spectrophotometer (NanoDrop 2000, Thermo Fisher Scientific, Bremen, Germany). Spectrophotometry is a technique that allows the quantification of molecules in a solution. The principle of this method is the capability of colored solutions to absorb light of specific wavelength. The measure of the degree of absorption is named absorbance (A), and is expressed as the logarithm of the radio between the intensity of the light entering the solution (incident light) and the intensity of the light leaving it. The intensity of the incident light is obtained using water or a reagent blank, which has no color. In the colorimetric quantification a

chemical substance (reagent) reacts with the substance to be determined, generating a colored and detectable product. A standard curve is generated using specific amounts of the molecule of interest. Using a wavelength appropriated for the color of the solution it is possible to read the absorbance of the unknown samples and determine their concentrations extrapolating on the standard curve [91].

Nevertheless, NanoDrop 2000 spectrophotometer is designed to measure specifically nucleic acids concentrations in really reduced volumes (approximately 1 μL). Since RNA together with nucleotides, ssDNA, and dsDNA all absorb at 260 nm, it is possible to determine the concentration of those molecules without the need of reagent that generates a colored solution. A specific feature of NanoDrop 2000 regarding other spectrophotometers is its retention system, which consists of surface tension to hold the sample. Thus, samples with a very high concentration (up to 200 times higher than with regular cuvettes) can be measured without the need for dilutions and additional containment devices. Samples 0.5-2 μL are enough to measure with NanoDrop technology (available from: http://www.mlz-garching.de/files/nanodrop_2000_user_manual.pdf).

Even though the samples analyzed were previously purified to isolate only RNA, their purity was evaluated. To ensure significance, A_{260} readings should be greater than 0.15. The ratio of the readings at 260 nm and 280 nm (A_{260}/A_{280}) provides an estimate of the purity of RNA. Pure RNA has an A_{260}/A_{280} ratio of 1.9–2.1. Different values indicate the presence of contaminants as phenols or nucleic acids. Samples with values out of this interval were discarded.

Purified RNA was stored at –80°C, industry standard method used for preserving RNA integrity for at least one year [92].

- ***RNA transcription***

The isolated RNA (three replicates/condition) was transcribed into complementary DNA (cDNA) by quantitative reverse transcription polymerase chain reaction (RT-PCR) in order to serve as template for real time PCR (qPCR).

Reverse transcriptase enzymes are generally derived from RNA-containing retroviruses such as avian myeloblastosis virus (AMV), Moloney murine leukemia virus (M-MulV), or human immunodeficiency virus (HIV). Reverse transcriptase is a multifunctional enzyme with three distinct enzymatic activities: an RNA-dependent DNA polymerase, a hybrid-dependent exoribonuclease (RNase H), and a DNA-dependent DNA polymerase.

The main differences regarding the two kits used for RNA transcription from HUCPV micromases and ATDC5 consisted of a different reverse transcriptase and concentration of the reagents. Also the concentration of the RNA template was higher in the case of the ATDC5 samples (200 ng) than the HUCPV micromasses (100 ng), due to the limited cell growth and difficulties to extract the RNA from the micromasses. For micromasses RNA transcription, Qiagen kit was used, which includes Omniscript reverse transcriptase, a recombinant heterodimeric enzyme expressed in E. coli. For ATDC5 chondrocytes, First Strand Synthesis Kit (Fisher Scientific, GmbH, Vienna, Austria) was used, which includes M-MuLV Reverse Transcriptase (with a lower RNase H activity). All chemicals and samples were kept on ice. To avoid contamination, tubes, pipettes and working areas were sterile and nuclease free.

Procedure with HUCPV cells

Template RNA was thawed on ice. A master mix solution was prepared for all the reactions that were performed (Table 5).

The solution was thoroughly and carefully mixed by vortexing. Then, 8 µL of the master mix solution were transferred to as many tubes as reactions were performed, and RNA template was added to the individual tubes. The minimum advised RNA amount per reaction is 100 ng. Therefore, 12 µL of each RNA template were individually added to the tubes containing the master mix (maximum amount allowed in the reaction).

Reverse transcription reaction was performed incubating for 60 min at 37°C (Figure 14). cDNA was frozen at -20°C or immediately used for qPCR.

Table 5: Composition of the Master Mix used for reverse transcription of RNA isolated from HUCPV micromasses, using Qiagen Kit.

Master mix/reaction	Volume (µL)	Final concentration
10x Buffer RT	2	1x
dNTP Mix (5 mM each dNTP)	2	0.5 mM each dNTP
Oligo-dT primer (10 µM)	2	1 µM
RNase inhibitor (10 units/µL)	1	10 units (per 20 µL reaction)
Omniscript Reverse Transcriptase	1	4 units (per 20 µL reaction)
RNase-free water	Variable	
RNA template	Variable	200 ng
Total volume	**20**	

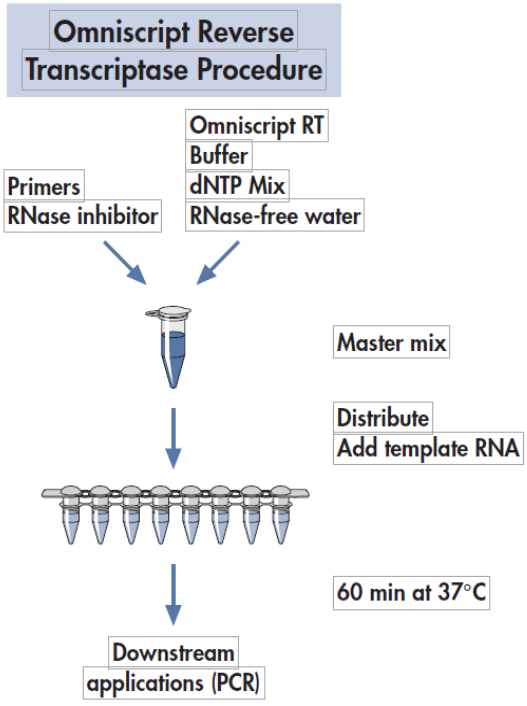

Figure 14. Procedure for RNA reverstranscription with Omniscript RT kit. Qiagen. Omniscript® Reverse Transcription Handbook. 2010. Available from: https://www.qiagen.com/us/shop/pcr/end-point-pcr-enzymes-and-kits/omniscript-rt-kit/#productdetails

Procedure with ATDC5 cells

First Strand Synthesis Kit (Fisher Scientific, GmbH, Vienna, Austria) was used with ATDC5 cells.

9 µL of the mix reaction (Table 6) were added in independent tubes. The volume of RNA template was calculated to have a final concentration of 2 µg per sample. Water was added to fill until 20 µL.

Table 6. Composition of the Master Mix used for reverse transcription of RNA isolated from ATDC5 cells, using First Stand Synthesis Kit.

Master mix/reaction	Volume (µL)	Final concentration
5x Reaction Buffer	4	1x
dNTP Mix (10 mM)	2	1 mM each dNTP
Oligo-dT primer (100 µM)	1	5 µM
RiboLock RNase inhibitor (20 U/µL)	2	40 units (per 20 µL reaction)
M-MulV Reverse Transcriptase (20 U/µL)	2	40 units (per 20 µL reaction)
RNase-free water	Variable	
RNA template	Variable	2 µg
Total volume	**20**	

With both samples (from HUCPV micromasses and ATDC5 cells) after mixing and centrifuging, the reverse transcription reaction was performed incubating for 60 min at 37°C. cDNA was frozen at -20°C or immediately used for qPCR.

- ***Real-time Polymerase chain reaction (qPCR)***

Real-time qPCR is a technique that allows to reliably and accurately calculating the initial amount of template DNA present in the samples. The principle of this technique consists of the amplification of specific sequences of the DNA templates by a DNA polymerase in combination with a fluorescent nucleic acid dye which binds to double strand DNA (new strand) sequences increasing its intensity. The DNA amplifies exponentially during several PCR cycles, each one consisting of: 1) cDNA template denaturalization, 2) hybridization primer-DNA template and 3) DNA elongation.

As double-stranded amplicons are produced, the fluorescence of the dye increases until reaching values detectable by qPCR thermocycler. The amplified DNA sequences are selected with the used of specific primers. As reference for calculating the relative quantification of the genes of study, genes whose expression is not influenced by the conditions of the experiment were used.
Furthermore, in order to evaluate variations in the gene expression under the influence of the extracts, relative quantification normalized to the control condition in differentiation medium was calculated. The same amount of DNA and 2 reference genes were used in all the cases to ensure accurate results.

> ***Note: Mg^{2+} is a cofactor needed to activate the enzyme DNA polymerase and helps in the addition of the right dNTPs during the synthesis of complementary strand of DNA. Therefore, $MgCl_2$ is one of the components of the qPCR reaction. Nevertheless interference from the Mg present in the extracts is not expected, due to the appropriate washing steps previous to RNA extraction, and the purity detected.***

The calculation of the relative gene expression is based on the cycle at which the fluorescence is detected by the thermocycler (quantification cycle, Cq). The method used was the $2^{-\Delta\Delta Cq}$ (Livak) Method, which assumes a 100% efficiency of both reference and target genes. The calculations performed with this method are:

1) normalization to reference gene
   $\Delta Cq(test) = Cq(target, test) – Cq(ref, test)$
2) normalization to control gene
   $\Delta Cq(calibrator) = Cq(target, calibrator) – Cq(ref, calibrator)$
3) normalization of ΔCq of the test sample to the ΔCq of the control condition
   $\Delta\Delta Cq = \Delta Cq(test) – \Delta Cq(calibrator)$
4) calculation of the expression ratio
   $2^{-\Delta\Delta Cq}$

Procedure

The qPCR was performed in a CFX96 Touch real-time PCR detection system (Bio Rad, Munich, Germany; version 3.1).

Variations in the procedure with HUCPV micromasses and ATDC5 mainly consisted of different target and reference genes due to the stages of differentiation expected when inducing chondrogenesis of stem cells or redifferentiation of chondrocytes and to the different nature of the cells (primary human cells and mice cell line). Furthermore, the fluorescence dyes used were different but both exhibit similar spectra properties (Table 7). The reference and target genes evaluated were selected from literature. Expression of some recognized markers of chondrogenic differentiation (aggrecan; alpha-1 type II collagen; SRY (Sex Determining Region Y)-Box 9), were evaluated in both cell types. Hypertrophy or pre-mineralization gene markers varied between both experiments. In HUCPV micromasses those target genes were alpha-1 type II collagen (COL1A1) and osteopontin (OPN) while in ATDC5 cells the evaluated genes were Runt-related transcription factor 2 (*Runx2*), alpha-1 type X collagen (*Col10a1*) and alpha-1 type I collagen (*Col1*). Two genes were used as internal reference to normalized targeted cDNA with every cell type. Primers were provided by MWG-Biotech AG (Ebersberg,Germany).

Results were calculated with CFX Manager™ Software 3.0 (Bio Rad) using the ΔΔCq method, expressed as a relative gene expression value normalized to the control samples in differentiation medium.

Reactions were performed in triplicate (3 reactions per experimental replicate). The primers, DNA and water were added to the Master Mix, in a final volume of 32.5 µL (for every reaction in triplicate) (Table7).

Table 7. Composition of the PCR Master Mix used for HUCPV (left) and ATDC5 cells (right)

SsoFast EvaGreen supermix with (2x)	Fast SybrGreen Master Mix
Sso7d-fusion polymerase	AmpliTaq® Fast DNA Polymerase
EvaGreen dye	SYBR® Green I dye
Deoxynucleotides (dNTPs)	Deoxynucleotides (dNTPs)
$MgCl_2$	$MgCl_2$
Sso-binding protein (stabilizer)	Uracil-DNA Glycosylase (UDG)
Buffer	Buffer

Procedure with HUCPV cells

SsoFast EvaGreen Supermix (Bio-Rad Laboratories GmbH, München, Germany) was used, together with the primers (100 pmol/µL), and cDNA template. Volumes and concentration for every reaction and technical replicates are shown in Table 8.

Human primer sequences are shown in Table 9.
The cDNA obtained after reverse-transcription was four times diluted in DNAse free water to obtain a concentration 100 pmol/µL. Primers were also added in a concentration of 100 pmol/µL.

The parameter used followed the standard protocol to ensure the activation of the polymerase and denaturalization of the DNA.

The protocol followed during the qPCR run consisted of the next steps:

		SsoEva	Sybr
Enzyme activation		95°C for 3 minutes (min)	95° for 10 min
40 cycles	DNA denaturalization	95°C for 0:20 min	95° for 0:15 min
	Primer annealing	62° for 0:20 min (should be primer dependent)	60° for 1:00 min
	Elongation	75° for 0:30 min	
		95° for 15 sec	1cycle 95° for 0:15 min
Melt curve		from 65° to 95°, increment 0.5 sec	Melt curve 65 to 95, increment 0.5 sec

Note: even if the Mg^{2+} is a cofactor of the reaction, the Mg present in the extracts should not interfere since the cells were properly washed with PBS, the RNA was isolated and purified and its purity was checked.

Procedure with ATDC5 cells

Fast SYBR® Green Master Mix (Fisher Scientific, GmbH, Vienna, Austria) was used in combination with DNA (10 times diluted) and primers. The volumes were the same as with EvaGreen (see Table 7). The sequence of the primers for the target genes is

specified in Table 10. The protocol followed for the PCR was also the same as with HUCPV cells

Table 8. Volume of the different components of the mastermix reactions, including the triplicates.

	µL/reaction	**µL/triplicates**
SsoFast EvaGreen supermix (2X) **Fast SYBRGreen master mix (2X)**	5 µL	16.25 µL
Forward primer	0.5 µL	1.63 µL
Reverse primer	0.5 µL	1.63 µL
cDNA template	0.125 µL	4.0 µL
ddH_2O	3.875 µL	9.0 µL
Total final volume	10	32.5 µL

Table 9. Human primer sequences used in the qPCR with HUCPV cells. bp: base pairs.

Group	Target name / NCBI RefSeq			
	Abbreviation	Forward	Reverse	Amplicon length (bp)
Reference genes	Ribosomal protein L10/NM_006013			
	RLP10	AGTGGATGAGTTTCCGCTTT	ATATGGAAGCCATCTTTGCC	135
	Valosin Containing Protein/NM_007126.3			
	VCP	AGTTTGGCATGACACCTTCC	TTTGGCCAACAAAGTTTTCC	74
Target genes	alpha-1 type II collage/NM_001844			
	COL2A1	AGACTTGCGTCTACCCCAATC	GCAGGCGTAGGAAGGTCATC	180
	Aggrecan / NM_001135.3			
	ACAN	TTCACCTCCAGGGAGAGCTA	ATACATTCAGCTGCGGTTCC	104
	SRY (Sex Determining Region Y)-Box 9/NM_000346			
	SOX9	AGACCTTTGGGCTGCCTTAT	TAGCCTCCCTCACTCCAAGA	121
	Osteopontin (or SPP1, secreted phosphoprotein 1)/NM_000582			
	OPN	CTCCATTGACTCGAACGACTC	CAGGTCTGCGAAACTTCTTAGAT	230
	alpha-1 type I collagen/NM_000088			
	COL1A1	AAGACATCCCACCAATCACC	GCAGTTCTTGGTCTCGTCAC	159

Table 10. Primer sequences and conditions used in the qPCR to amplify mouse chondrocyte-specific mRNA, and reference genes. bp: base pairs.

Group	Target name / NCBI RefSeq			
	Abbreviation	Forward	Reverse	Amplicon length (bp)
Reference genes	Actin, beta / NM_009735			
	B2m	AGAATGGGAAGCCGAACATA	CCGTTCTTCAGCATTTGGAT	82
	40S ribosomal protein S18 / NG_032038			
	s18	ATGCGGCGGCGTTATTCC	GCTATCAATCTGTCAATCCTGTCC	203
Target genes	SRY (Sex Determining Region Y)-Box 9 / NM_011448			
	Sox9	CAGTACCCGCATCTGCAC	TCTCTTCTCGCTCTCGTT	81
	alpha-1 type II collagen / NM_001844			
	Col2a1	ACCTTGGACGCCATGAAA	GTGGAAGTAGACGGAGGAA	230
	Aggrecan/ NM_007424			
	Acan	AGTGGATCGGTCTGAATGACAGG	AGAAGTTGTCAGGCTGGTTTGGA	105
	Runt-related transcription factor 2 / NM_001145920			
	Runx2	CCTGGGATCTGTAATCTGACTCT	TGTTCTCTGATCGCCTCAGTG	146
	alpha-1 type X collagen / NM_009925			
	Col10a1	TCTGGGATGCCGCTTGT	CGTAGGCGTGCCGTTCTT	261
	alpha-1 type I collagen / NM_007742			
	Col1a1	TGTGTGCGATGACGTGCAAT	GGGTCCCTCGACTCCTACA	133

7.6.1. GAG production

GAG quantification was performed in the ECM of HUCPV micromasses after 21 days of differentiation and under the influence of the extracts. Furthermore, GAG released to the supernatants was also quantified during this culture period. For calculating the GAG production in the ECM, the GAG quantified in every sample was normalized to the DNA content (as a indicative of cell number). For enabling the

quantification of both the GAG and DNA in the micromasses, a previous digestion of other proteins of the ECM was necessary.

- ***Papain digestion***

Papain is necessary to solubilize GAG and DNA in the micromasses. It is a cysteine hydrolase that is stable and active under a wide range of conditions, including wide range of pH (6.5-7.5) and elevated temperatures. It owns endopeptidase, amidase, and esterase activities. Papain is activated by cysteine, sulfide and sulfite, heavy metal chelating agents like ethylenediaminetetraacetic acid (EDTA) and N-bromosuccinimide. Combination of Papain with B-mercaptoethanol, which denaturalizes proteins by cleaving the disulfide bonds that may form between groups of cysteine residues, will ensure the appropriated solubility of the GAG and DNA.

Procedure

For papain digestion, fresh micromasses were washed with PBS (Scientific GmbH) and transferred to 24-well plates (one pellet/ well). Three samples per condition were used. A buffer solution consisting of 0.1 M Sodium phosphate monobasic (NaH_2PO_4; MM: 119.98 $g.mol^{-1}$, Sigma-Aldrich) and 5 mM EDTA (372.24 $g.mol^{-1}$; Merk), pH 6 adjusted with NaOH in ddH_2O was prepared. EDTA was added to activate the enzyme. Then 500 µL of buffer with 5 µL B-mercaptoethanol (Merck) and 2.5 µL of a papain (AppliChem, Hamburg, Germany) solution (10 µg/mL) were added in every micromass sample. Wells were covered with adhesive strip and incubated overnight under the hood on a shaker at 60ºC. For DNA and GAG quantification, the resulting papain digestion was split.

- ***DNA quantification***

Bisbenzimide (Hoechst 33258; Sigma-Aldrich) is a membrane-permeable DNA fluorochrome, which bind specifically to the AdenineThymidine (A-T) regions of DNA. The dye is weakly fluorescent itself, but when bound to A-T regions, the fluorescence becomes more intense and the emission maximum shifts from 500 to 460 nm. The DNA quantification is therefore based on the intensity of the fluorescence detected in every sample (Absorbance), and extrapolation in a standard curve made with control-DNA.

Procedure

After Papain-digestion, 100 µL from every sample were diluted in 400 µL of DNA Dilution Buffer (2.5 M NaCl, Merk; 19 mM tri-Sodium citrate dihydrate, pH 7, Merk). 100 µL of DNA Working Buffer (2 M NaCl, 15 mM tri-Sodium citrate dihydrate, pH 7) were added in every well of 94 well-plates. Serial dilutions of every digested sample were made in triplicate (100 µL/well in the first well) in every row of the plates. Then 100 µL of Bisbenzimide Solution (2 µg/mL Bisbenzimide Fluorochrome, diluted in DNA Working Buffer) were added in each well and incubated during 15 min in the dark. Wells were measured fluorometrically (Excitation: 355 nm, emission: 460 nm), in a spectrophotometer (VICTOR3 ™ multilabel reader; PerkinElmer, Baesweiler, Germany). The principle of spectrophotometry has been previously described in section 2.5.3. DNA content was calculated extrapolating the Abosarbance mean value for every sample in a standard curve done with Calf thymus DNA (Sigma-Aldrich).

- ***GAG quantification***

1,9-dimethyl-methylenblue is a thiazine chromotrope agent that binds to sulfated GAG (Figure 15). Due to its metachromatic nature, changes in the absorption spectrum are detected once bound to the GAG. Quantification of the GAG in solution can be performed with a control (*e.g.* Chondroitin Sulfate).

Procedure

A standard was prepared with Chondroitin sulfate C, sodium salt, from shark cartilage (Sigma-Aldrich), in a concentration 2 mg/mL in ddH_2O.
One liter of staining solution consisted of a mixture of:

- 27.2 mg of 1,9-dimethyl-methylenblue (78 mM, Serva, Amstetten, Austria) in 50 mL ddH2O.
- 5.168 g Glycine (69 mM) and 4.03 g NaCl (69 mM) in 800 mL ddH2O.
- 32.3 mL HCl (1M).

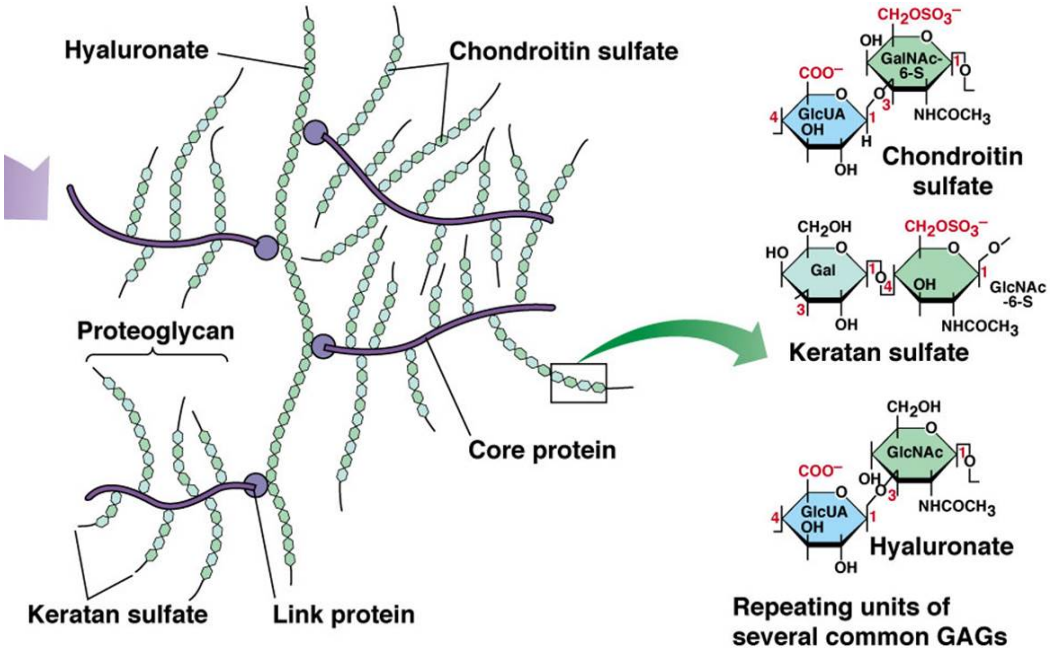

Figure 15. Scheme of the matrix of GAG from the ECM of chondrocytes. GAG consist of repeating disaccharide subunits. One of the two sugars in the disaccharide is often an amino sugar (N-acetylglucosamine or N-acetylgalactosamine; usually with an attached sulfate group) and the other is a sugar or sugar acid (galactose or glucuronate). GAG bind to proteins and constitute the mayor part of proteoglycans. Chondroitin sulfate, keratan sulfate and hyaluronate are the most common GAGs.

Next steps were performed in 96 well-plates. For every sample (three biological replicates) serial dilutions were made in duplicate from row A to H. The initial content in row A was 50 µL of the papain digestion previously prepared and 150 µL of ddH2O. Therefore all wells had a final volume of 100µL after serial dilution. Standard dilutions were also prepared, in triplicate, from a concentration 20 µg/mL to a concentration 0.3 µg/mL.

Subsequently, 150 µL of the staining solution was added to every well plate, and after 30 seconds resting, the absorbance at 530 nm was measured in a spectrophotometer (VICTOR3 ™ multilabel reader; PerkinElmer, Baesweiler, Germany). The principle of spectrophotometry has been previously described in section 2.5.3.

For the calculations, the average absorbance of the standard was represented in a table against the concentrations of chondroitin sulfate. The average absorbance for

every sample was calculated, and the values were extrapolated in the standard curve, to obtain the GAG concentration.

7.6.2. Life/dead staining

For evaluating the viability, morphology and distribution of the cells on the surface of the materials, LIVE/DEAD Viability/Cytotoxicity Kit, for mammalian cells (Fisher Scientific GmbH, Schwerte, Germany) was used after seven days of culture.
This kit contains two fluorescent dyes, calcein and ethidium homodimer. Live cells are permeable to calcein and impermeable to ethidium homodimer. Once in the cytoplams, the activity of esterases will convert the non-fluorescent calcein to intense fluorescent calcein observed in green (exitation ~495 nm/ emission ~515 nm). Simultaneously, ethidium homodimer will access only dead cells, which have damaged membranes. This dye binds to nuclei acids, and undergoes a 40-fold increase in fluorescence, emitting an intense red fluorescence (excitation ~495 nm/ emission ~635 nm).

Procedure
Life/dead viability kit (Fisher Scientific GmbH) was used with HUCPV cells cultured in well plates under the influence of the extracts (indirect test) and with HUCPV and aTDC5 cells cultured directly on the surface of the materials. In both cases, this viability assay was used after seven days of culture, and the procedure followed was the same.

First, samples and wells were carefully washed with PBS (Scientific GmbH) and subsequently immersed in the calcein and ethidium homodimer-1 staining solution consisting of 10 mL of PBS + 5 µL calcein and 20 µL of ethidium homodimer-1 stock solutions. The samples were incubated in the darkness at 37ºC during 20 min. Then samples were again washed carefully with PBS and transferred to new well plates with culture medium. Regarding the wells with HUCPV cells, after washing with PBS culture medium was added. Cells were visualized under a confocal fluorescent microscope, the Eclipse Ni-E (Nikon Corporation, Tokyo, Japan) with a resolution of 0.23 µm/pixel. Life cells are observed in green using a Semrock Inc filter block (FITC-3540C), which emits blue and detects green light. Dead cells are observed in red, using a TXRED-4040C filter block, which emits green and detects red light.

7.6.3. Scanning electron microscopy and energy dispersive X-ray

SEM images from cells and EDX- elemental mapping of degradation layer

Material samples with ATDC5 cells were processed for analysis by Scanning Electron Microscopy (SEM) of both the surface and the cross section of the samples. The analysis of the surface allowed the observation of cell morphology, distribution and adhesion structures when cells were in contact with the material. Cross section analysis of the materials was done by Focus Ion Bean (FIB) and allowed the evaluation of the degradation layer, including its size and its elemental composition by Energy Dispersive X-ray (EDX)- element mapping. Both the FIB cross-section and EDX analysis were performed by Dr. Danniel Leipple at HZG (Geesthacht, Germany), as part of a research collaboration.

- ***Sample processing for SEM***

Material disks seeded with ATDC5 cells were washed with PBS (Scientific GmbH) and fixed with a solution containing 2% paraformaldehyde, 2.5% glutaraldehyde in 0.1 M Sodium cacodylate buffer, pH=7.4 (Ladd Research, Macherio, Italy) during one hour at room temperature. Then, dehydration was performed with isopropanol and critical point drying: samples were immersed in isopropanol baths with increasing concentrations (20-40-60-80-100%), during periods of 30 minutes each. During critical point drying (EM CPD030, Leica Mikrosysteme Vertrieb GmbH, Wetzlar, Germany), the isopropanol contained in the cells was gradually substituted by CO_2 inside the cells, by repeated baths with CO_2 at 8°C. Then temperature was increased to 40°C and pressure rinsed to 75.5 Bar, so that critical point with CO_2 was reached at 31°C. After 31°C, CO_2 evaporated without change of density, allowing complete elimination of water without affecting cell structures.

- ***SEM, FIB and EDX***

Principle

A nanometer sized electron beam spot scans the surface of the specimens in SEM, producing a magnified image. For every single local spot of the scan region on the sample, different responses are generated. Those responses are measured by specific detectors, amplified and visualized by grey values on a screen. The resolution is determined by the spot size of the electron beam focus [93].

The FIB is used to mill a sample to desired micro scaled shapes, or to process a small structure out of a region of interest from the original sample for further investigations. The functional principle of FIB is the same as SEM but using ions, commonly gallium, instead of electrons. The ions are released from the gallium by evaporation. First a liquid metal ion source (LMIS) heats the metal to liquid state. Then a emission current is generated in a Taylor cone by an extractor tension [94]. The choice of gallium as ion is due to its low melting point, vapor pressure and reactivity. From the emitted ions, some are implanted into the substrate material after collision (a minimum penetration depth of the ion into the substrate of approximately 1 nm/kV[7] is generally necessary) and some are sputtered. The first step for excavating the sample is performed with its surface perpendicular to the ion beam and with relative high current (in the nA[8] range). Then the thinning is performed by modifying the position of the sample with a micro-manipulator and applying lower currents in the pA[9] range at over- and under- tilted positions regarding the perpendicular orientation to the FIB [95, 96].

In the EDX, secondary electrons generated by SEM irradiation, beat and kick out the electron from its shell in the atoms of the specimen. In lower energetic shells, the empty electron place is filled with an electron from a higher energetic shell. The energetic difference between the atom shells determines the characteristic X-ray photon. The energy of the X-ray photons can be measured by a detector. This technique is named energy dispersive X-ray spectroscopy or EDX and allows the detection of the elementary composition of the specimen with an energetic resolution of up to 100 eV [93].

Procedure

The SEM and FIB crossbeam workstation Auriga (Zeiss, Oberkochen, Germany) equipped with the Canion column from Orsay physics (Fuveau, France) had been used. At 15 kV of electron high tension a resolutions of about 1 nm are possible.

The Auriga is operated by the SmartSEM software (version V05.0403.00), from Zeiss. By SEM, a detailed magnified image of the sample surface is provided, enabling a precise alignment of the sample for cutting by the subsequent FIB milling. The regions of interest were excavated by a FIB current of about 10 nA or higher to

achieve the desired cross section. A subsequent fine milling was performed successively with 2 nA and 200 pA.

The non conductive samples were coated with a Gold-Palladium alloy to allow SEM investigations. Coating was done by the sputter device SCD 030 (Balzers Union, Balzer, Liechtenstein). To equal the deposit thickness of the sputtered coating, each pair was exposed to 30 mA for a time of 60s.

EDX measurements were done by the Apollo XP device from EDAX (Ametek GmbH, Wiesbaden, Germany) attached to the Auriga. The Silicon drift detector (SDD) of Apollo XP enables an energy resolution of 127 eV. EDX at the Auriga is calibrated to a working distance of 8.5 mm. EDX measurement and analysis was runned by the software Genesis Spectrum (Version 6.255) from EDAX.

7.6.4. Detection of chondrogenic markers with antibodies and fluorescence

To investigate the possible chondrogenic potential of the materials, HUCPV cells were cultured directly on its surface for seven days, without chondrogenic stimulation (in growth medium). HUCPV cells cultured in well plates were used as controls.
Immunofluorescence was used to visualize chondrogenic marker proteins in the ECM (type II collagen, type X collagen and aggrecan) and intracellulary (transcription factors Sox9 and NAFT5). The chondrogenic proteins and Sox9 have been described in the introduction. NAFT5 (Nuclear factor of activated T cells 5) is a transcription factor that forms complex on the DNA to regulate the expression of cytokines in T cells. Therefore it is an indicator of inflammatory response. Nevertheless, NAFT5 is detected in immune and non-immune cells. NAFT proteins are activated by increases in intracellular Ca. Then the proteins suffer a conformational change and tend to go to the nucleus.

The used immunofluorescent technique relies on the use of antibodies that label specific target (proteins), and which are conjugated to fluorescent dyes, that allow the detection of the targets under a fluorescent microscope. To allow the visualization of two targets simultaneously in the same sample, indirect method was used, consisting of two antibodies, an unconjugated primary and a fluorophore-conjugated secondary (Figure 16). The fluorophores selected were

fluorescein isothiocyanate (FITC), seen in green and Texas Red, seen in red. The secondary and corresponding primary antibodies need to be raised in different animals, to allow reaction. Furthermore, cell nucleus was visualized by staining with DAPI (4′,6-diamidino-2-phenylindole), a blue fluorescent compound that binds to DNA regions rich in AT, which produces a ~20-fold fluorescence enhancement.

Procedure

After seven days of cell culture, samples with cells on its surface were carefully washed with PBS (Scientific GmbH) by immersion for some seconds. Samples were then fixed in 500 µL of 2% paraformaldehyde in PBS, during 20 min. Two washes in PBS were then performed. Since the fixation method used was not organic, it was necessary a permeabilization step that makes intracellular structures accessible to antibodies which otherwise would not pass through the lipid membrane of the cell. Therefore, 3% of Triton X-100 detergent (Bio-Rad Laboratories, Munich, Germany) in PBS was applied for 20 min to the samples. In order to avoid unspecific binding of the primary antibody within the cells, blocking solution consisting of Bovine Serum Albumin (BSA; 3% in PBS) was also added to the samples, and incubated for 20 min.

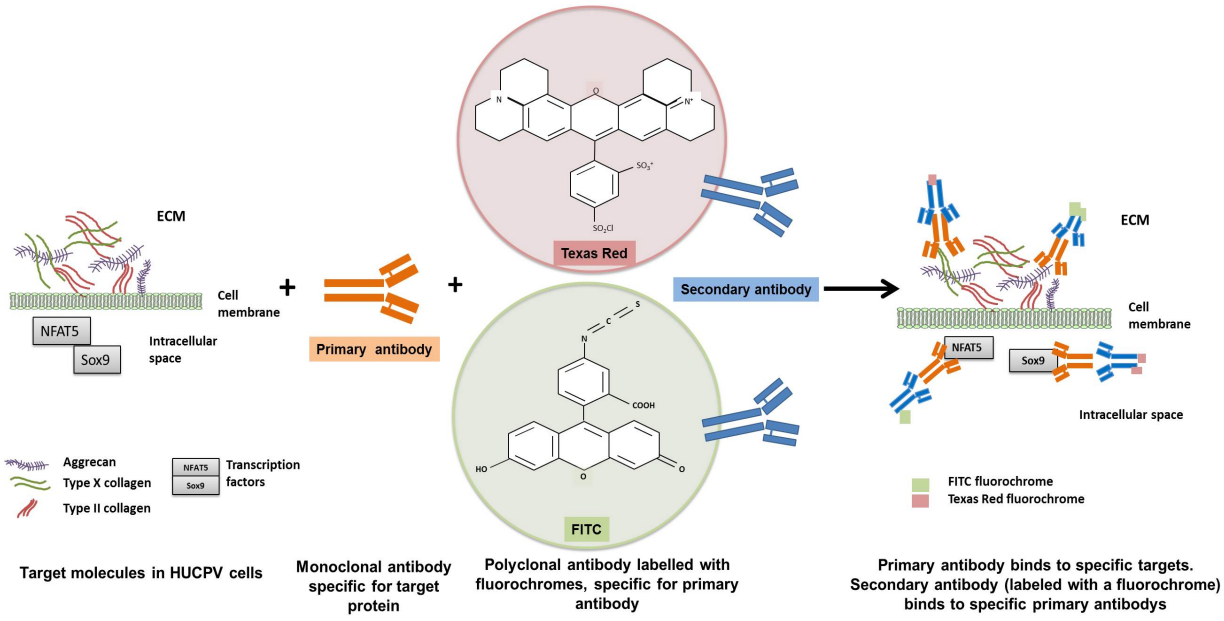

Figure 16. Scheme of the indirect method for immunofluorescence detection of chondrogenic markers in cells. Fluorochromes used: FITC and Texas Red.

Samples were washed again, and subsequently, incubation with one or two primary antibodies, referred as antibody A and antibody B (Table 11 shows the specific antibodies used in each replicate) for 45 min was carried out (all the antibodies used were provided by Santa Cruz Biotechnology, Heidelberg, Germany). The dilution containing the primary antibody (concentration 5 µg/mL) consisted of (for every sample):

- 25 µL of primary antibody A
- 25 µL of primary antibody B
- 950 µL of PBS

Samples were rinsed twice with PBS and incubated during 45 min with the secondary antibody complementary to the primary antibodies previously added (see Table 11 for specific antibodies used in each replicate). Each secondary antibody was conjugated with a fluorochrome (Texas Red or FITC), therefore absolute darkness was necessary. The solution with the secondary antibody, in a concentration 5 µg/mL for every sample consisted of:

- 12.5 µL of antibody secondary-Texas Red
- 12.5 µL of antibody secondary- FITC
- 985 µL of PBS

The antibodies and combinations used for different sample-replicates are indicated in Table 11.
Finally, samples were stained with 4´,6-diamidino-2-phenylindole (DAPI) solution. For this purpose, during the last 15 min of incubation with the secondary antibody, DAPI was added in a concentration of 5 µg/mL.

Unspecific binding of the secondary antibody or the fluorochrome to the cells could occur as a result of *e.g.* electrostatic interactions, glycolipid interaction in the cell membrane, protein-protein interactions or DNA binding. In order to confirm the lack of such unspecificity, a negative control was used in which the primary antibody was omitted.

Table 11. Combination of antibodies and fluorochromes. For every condition, three replicates were stained. Two of the replicates were stained with two different primary antibodies and two secondary antibodies, one bound to Texas Red and the other one bound to FIT. The other replicate was stained only with Aggrecan primary antibody and Texas Red fluorophore.

	Replicate 1		Replicate 2		Replicate 3
Primary antibody	**NAFT5** rabbit	**Sox9** mouse	**ColII** rabbit	**ColX** goat	**Aggrecan** rabbit
Secondary antibody/ Conjugated fluorophore	Donkey anti-rabbit/ **Texas Red**	Donkey anti-mouse/ **FITC**	Donkey anti-rabbit/ **Texas Red**	Donkey anti-goat/ **FITC**	Donkey anti-rabbit/ **Texas Red**

Furthermore, interaction of the antibodies with the surface of the materials could give rise to artifacts. For this reason an additional control was included consisting of the materials without cells, incubated with primary antibody and secondary antibody-fluorochrome.

After incubation, samples where immersed in PBS and evaluated under fluorescence microscopy, the Eclipse Ni-E (Nikon Corporation, Tokyo, Japan) with a resolution of 0.23 μm/pixel.

Fluorescence occurs when the fluorescent dye is excited by a light with a specific wavelength. Therefore, the location of the proteins in the cell is observed as shining spots or areas. Two different fluorophore were used, Texas Red (red) and fluorescein isothiocyanate (FITC, green). Two filter blocks from Semrock Inc (Roche, USA) were used to visualize the fluorescent markers. The fluorochrome FITC binds to the IgG of the secondary antibody by the isothiocyanate group (Figure 16). The isothiocyanate group (-N=C=S) replaces a hydrogen atom in the bottom ring of the FITC structure and is reactive with amine groups of proteins inside cells.

Its fluorescence is very high; excitation occurs at 494 nm, while emission occurs at 525 nm. The filter used was FITC-3540C, which emits blue and detects green light. Texas Red conjugates with proteins and antibodies via the sulfonyl chloride (SO_2Cl). Excitation occurs at 561 or 594 nm and emission at 615 nm.

7.6.5. Proteomic analysis

Proteomics is defined like the large-scale characterization of the entire protein complement of a cell line, tissue, or organism, considering that the proteome is dynamic and dependent on the protein environment at a given time [97]. Apart from identifying all the proteins in a cell, the aim of proteomics is also to create a 3D map of proteins locations within the cells. Some steps of the proteomic analysis (protein extraction, tryptic in-solution digestion and desalting, liquid chromatography-tandem mass spectrometry (LC-MS/MS) analysis and data analysis) were performed at UKE, Hamburg, by the PhD student Maryam Omidi as part of a research collaboration.

Immediately after the 11 days of culture, micromasses were processed using a protease inhibitor cocktail (cOmplete ULTRA tablests, Roche Diagnostics GmbH, Mannheim, Germany) to avoid protein degradation. The protease inhibitor Tablet was diluted in 50 mL PBS. Micromasses were washed with this cocktail. Then media was completely removed and samples were frozen in liquid nitrogen and stored at -80ºC until further analysis.

- ***Protein extraction***

For protein extraction a lysis buffer consisting of 8M Urea (Merck, Darmstadt, Germany), one mM phenylmethylsulfonyl fluoride (PMSF) (Sigma-Aldrich, Munich, Germany), protease inhibitor (cOmplete™, Mini, EDTA-free Protease Inhibitor Cocktail), and 375 U Benzonase (Sigma-Aldrich) was added to all the samples.

Due to the presence of compact ECM, it was necessary to perform a homogenization of the samples using TissueLyzer II (QIAGEN) at a frequency of 25.0/s in 3.5 minutes followed by one-hour incubation in ice. Then cell lysates were centrifuged at 12 000 g for 30 minutes to precipitate cell debris. The supernatants were collected.

- ***Protein digestion and desalting procedure***

6 M Urea was added to the supernatants to decrease the hydrophobicity of the proteins, followed by a centrifugation at 14 000 g for 30 minutes (twice). Then, the cysteine residues were reduced by 10 min incubation at 56 °C with 10 mM

dithiothreitol (Sigma-Aldrich Chemie, Taufkirchen, Germany) and alkylated by incubation in the dark at room temperature for 20 minutes with 300 mM iodoacetamide (IAA) solution (Sigma-Aldrich Chemie). Finally, 2 µg of sequencing grade modified trypsin (Promega Corporation, Madison, USA), with a final concentration 0.25 µg/µL, was added to each vial followed by overnight incubation at 37 °C. Then, the supernatants were transferred to new collection vials and the extracted digests were entirely dried in a speed vac.

PorosOligo R3 (PorosOligo R3 Bulk Medium (Applied Biosystems, Darmstadt, Germany) (4 mg/mL, dissolved in 50% acetonitrile, ACN) reversed phase packing material and (PerSeptiveBiosystems 1-1339-06 Empore™) C18 disk were used for desalting procedure. The suspended samples in 60 µL of 0.1 % trifluoroacetic acid (TFA) (Sigma-Aldrich, Steinheim, Germany) in High-performance liquid chromatography (HPLC) grade water (Merck Millipore, Darmstadt, Germany) were loaded on the Oligo3 column, which was conditioned and equilibrated respectively with 50% acetonitrile and 0.1 % TFA in HPLC grade water. Then, the samples were eluted in 25 µL of 50% acetonitrile, 0.1 % TFA. The elutes have been fully dried in a speed vac.

- ***Liquid Chromatography-tandem Mass Spectrometry (LC-MS/MS) analysis***

Principle

Chromatography is used to separate proteins, nucleic acids, or small molecules in complex mixtures. Liquid chromatography (LC) separates molecules in a liquid mobile phase using a solid stationary phase. In this study, in column LC was used. In column LC, the liquid mobile phase containing the proteins passes through the column, components (stationary phase). Molecules of interest in the mobile phase are separated based on their differing physicochemical interactions with the stationary and mobile phases. Those interactions can be based in its charge, molecular size or hydrophobicity among others. The elutes can be collected and protein concentration measured using spectrophotometry or dye-base assays. Nevertheless, the chromatograph obtained does not allow to differentiate all the

proteins present in the elute and it is used as molecular fractionation prior to mass spectrometry (MS).

Mass spectrometry converts proteins, peptides or molecules in ions and provides qualitative (structure) and quantitative (molecular mass or concentration) information. The ionization source of the mass spectrometer, ionize the molecules to acquire positive or negative charges. Subsequently, the ions travel through the mass analyzer and, depending on their mass/charge (m/z) ratio, arrive at different parts of the detector. The detection of the molecules leads to the generation and recording of signals by a computer system. A mass spectrum is then generated, which shows the relative abundance of the signals according to their m/z ratio. The electrospray ionization (ESI) is a type of ionization source that uses electrical energy to assist the transfer of ions from solution into the gaseous phase before they are subjected to mass spectrometric analysis. Charged droplets are generated at the exit of the electrospray tip and pass down a pressure gradient and potential gradient toward the analyzer region of the mass spectrometer. The ions at the surface of the droplets are ejected into the gaseous phase when the electric field strength within the charged droplet reaches a kinetically critical point [98].

Procedure

20 µL of formic acid (0.1%) was added to all the desalted samples followed by 5 minutes centrifugation at 15 000 rpm at 4°C. Then, LC-MS/MS measurement was performed with a nano-flow ultra-performance liquid chromatography (UPLC)-column (DionexUltiMate 3000 RSLCnano, Thermo Fisher Scientific, Bremen, Germany) via ESI to an Orbitrap mass spectrometer (Orbitrap-Fusion, Thermo Fisher Scientific). Samples were injected into a C18 trapping column, 180 µm × 20 mm, five µm, and 100 Å using an auto sample. The flow rate was 200 nL/min during the whole chromatographic run. The ratio of buffer A (0.1% fusidic acid, FA in HPLC-H2O): B (0.1% FA in ACN) was 98:2 throughout column equilibration, application of the samples and the washing phase.

A gradient elution phase was initiated by increasing the concentration of buffer B to 30% in 30 minutes and then rising to 70% for 5 minutes followed by a holding phase for two minutes. Then, the ratio of buffer B was decreased to 2% for 25 minutes for column equilibration. Peptides were eluted and then ionized by electrospray

ionization with an Orbitrap MS. Data-dependent acquisition (DDA) mass analysis was operated using top speed mode in the positive ionisation mode, and the following parameters: the m/z scan range was 400 to 1300, with a resolution of 12 000 FWHM, higher energy collision dissociation (HCD) collision energy of 30%, automatic gain control (AGC) target of 2.0e5, maximum injection time of 50 ms, including charge states 2-5, mass tolerance of 10 ppm, a minimum intensity of 2.0e5, an isolation width of 1.6 m/z. The MS/MS spectra were recorded by using Ion trap as a detector in rapid mode by a maximum injection time of 200 ms and an AGC target of 1.0e4.

- ***Data analysis***

To compare the relative protein abundance, raw data files obtained from the Orbitrap-Fusion were processed by MaxQuant 1.5.2.8. For identification and label-free quantification, the parameters used were: identification of the proteins against SwissProt database downloaded from UniProt in July 2015 and internal contaminants database of MaxQuant, precursor mass of 20 ppm and fragment mass tolerance of 0.5 Da. Peptide spectrum match (PSM) and protein false discovery rate (FDR) was set to 0.01, with the minimum peptide length of 6 amino acids for identification and using match between runs. For protein quantification at least two ratio counts were considered. Specific digestion mode and trypsin as an enzyme with one missed cleavage allowed for peptide identification. Carbamidomethylation on cysteine residues was set as a static modification and oxidation of methionine residues as variable modifications. Perseus 1.5.2.8 (http://www.perseus-framework.org/), Excel 2010 (Zoschke Data GmbH, Schleswig-Holstein, Germany), and Mathematica 10.0 (Wolfram, Oxfordshire, United Kingdom) were used for bioinformatics analysis. Tables 13-17 show the list of proteins regulated, and the fold change of HUCPV cells incubated for 11 days with Mg-alloys (Mg-10Gd, Mg-2Ag, and Pure Mg) compared to control cells after 11 days incubation without Mg-alloys (permutation-based FDR of 0.01, s0 = 0.1).

- ***Data interpretation***

Up-regulated and down-regulated proteins under the influence of the three extracts were searched individually in UniProt [99] and further investigation of their functions was carried out from literature.

7.7. Statistical analysis

Statistics were performed using Origin 9 software (OriginLAb, Friedrichsdorf, Germany). Normal distribution was calculated based on the standard deviation. Statistical analysis was conducted using a one-way ANOVA followed by Bonferroni's multiple comparison test. The one-way ANOVA or one-way analysis of variance is used to compare the means of more than two independent groups with an only treatment and test if there are significant differences among them. Specifically, it tests the null hypothesis (H_0):

$$H_0 : \mu_1 = \mu_2 = \mu_3 = \ldots = \mu_k \quad ,$$

where μ = group mean and k = number of groups. When statistically significant differences are observed, the alternative hypothesis (H_A) is accepted, which indicates that there are at least two group means that are statistically significantly different from each other. In order to determine between which specific groups exist the differences, a post hoc test as Bonferroni is necessary. When increasing the number of mean comparison, the probability that significant differences exist just due to chance (or alpha value) also increases. The Bonferroni´s correction simply calculates a new pairwise alpha to keep the familywise alpha value at .05 (or another specified value). This is achieved dividing the alpha value by the number comparisons.

Analysis of the differences in gene expression was performed with CFX Manager Software 3.1 (Bio-Rad Laboratories, Munich, Germany), using the t-test method which also compares two group means independently to calculate statistical variations. Significant differences were accepted at significance levels $P < 0.05$.

8. RESULTS

8.1. Comparison of cell reactions to $MgCl_2$ and Mg-extracts and determination of the most suitable Mg concentration for cell culture

With the aim of establishing an appropriate *in vitro* set-up, the use of $MgCl_2$ and Mg-extracts was compared to determine if they could be used equally or Mg-extract were more suitable than $MgCl_2$ for evaluating the degradation products of the materials. Furthermore, high cell proliferation and enhanced differentiation would be appropriated for further evaluation of cell reactions to the extracts. Hence, the effects of different content of Mg in the extracts on cell proliferation, gene expression and GAG productions were analysed. Since primary cells are more sensitive than cell lines and better resemble in vivo conditions, HUCPV were used for this purpose.

8.1.1. Cell proliferation

Proliferation assay with HUCPV cells was performed by counting viable cells with CASY (n=12 for each time and condition), after culturing with $MgCl_2$ (Figure 17) and with Mg-extracts (Figure 18) for one, two and three days.

The cell proliferation under the influence of $MgCl_2$ showed not significant effects on cell growth with any of the three concentrations used (5, 10 and 15 mM) after one day. After two and three days the reduction of proliferation was significant at concentrations of 10 and 15 mM $MgCl_2$.

When cultured with Mg-extracts at different concentrations (3.04, 6.08, 12.16 and 60.8 mM), that correspond with a dilution 20x, 10x, 5x and the pure extract respectively, a significant reduction in cell proliferation compared to the control was observed with extracts containing 12.16 mM and 60.8 mM Mg after the three time points, inhibiting completely cell proliferation with a concentration 60.8 mM.

The pure extract, with a 60.8 mM, is used to mimic the worst situation that could be found in vivo, if the degradation products are not diluted in body fluids.

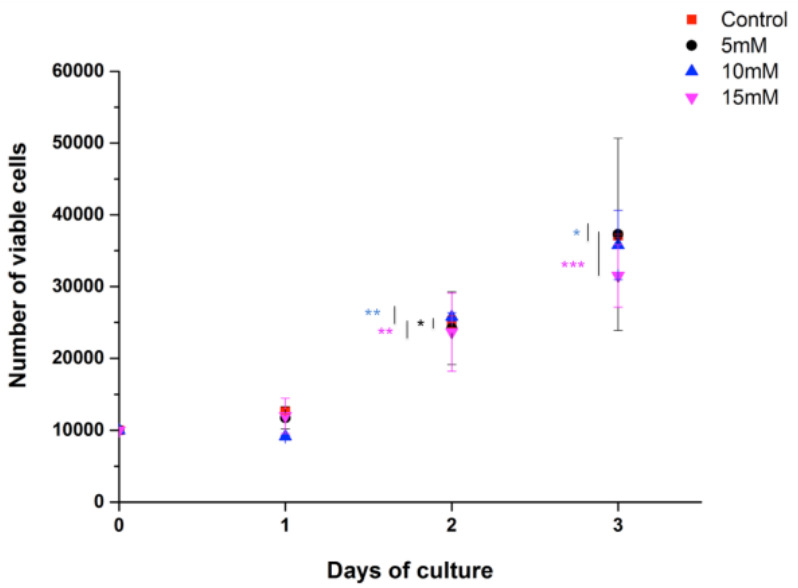

Figure 17. HUCPV cells viability after one, two and three days of culture in alpha-MEM (control) and alpha-MEM with the addition of 5 mM, 10 mM and 15 mM of $MgCl_2$. N=9 (per condition and time point). Stars indicate statistically significant differences regarding the control ($p < 0.05$ = *; $p < 0.01$ = **; $p < 0.001$ = ***) calculated with Origin 9 software using one-way ANOVA and applying Bonferroni´s correction post t-test.

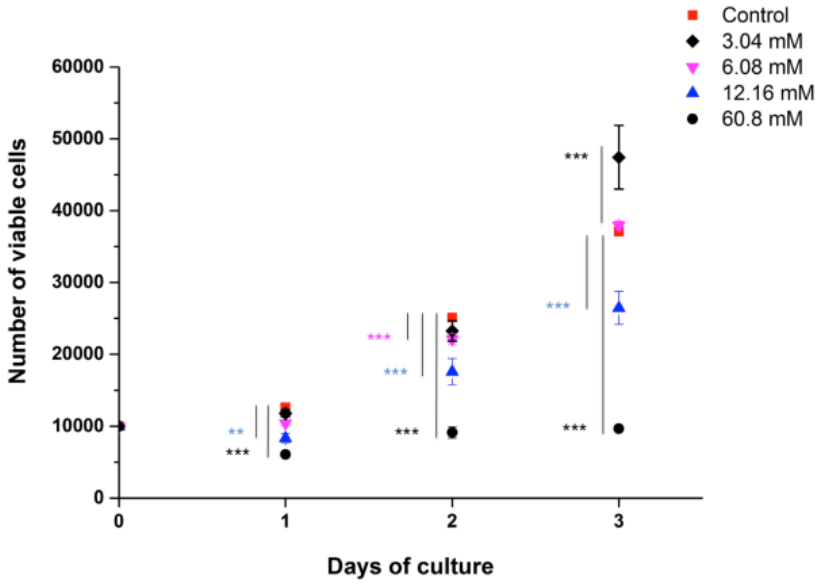

Figure 18. HUCPV cells viability after one, two and thee days of culture in alpha-MEM (control) and Mg extracts (dilutions 20x, 10x and 5x, and pure extract) with a Mg concentration 3.04 mM, 6.08 mM, 12.16 mM and 60.8 mM. N=9 (per condition and time point). Stars indicate statistically significant differences regarding the control ($p < 0.05$ = *; $p < 0.01$ = **; $p < 0.001$ = ***) calculated with Origin 9 software using one-way ANOVA and applying Bonferroni´s correction post t-test.

Nevertheless, the degradation rate *in vivo* is lower than *in vitro* [100]and this situation is not likely to take place. After two days, a decrease cell proliferation was detected with all the extracts. Differently, after three days of culture, Mg-extracts with a concentration 3.04 mM Mg induced a significant increase in cell proliferation, and with a concentration 6.08 mM showed not effects on cell proliferation compared to the control.

Those results confirm that the effects of $MgCl_2$ are not comparable to those of Mg extracts with about the same determined Mg concentration. Therefore, Mg extracts were exclusively used in further analysis.

8.1.2. Gene expression

Gene expression after inducing chondrogenic differentiation in HUCPV cells for 21 days under the influence of Mg-extracts (concentrations 3.04, 6.08 and 12.16 mM, respectively) is shown in Figure 19. The expression was normalized to control conditions with differentiation medium.

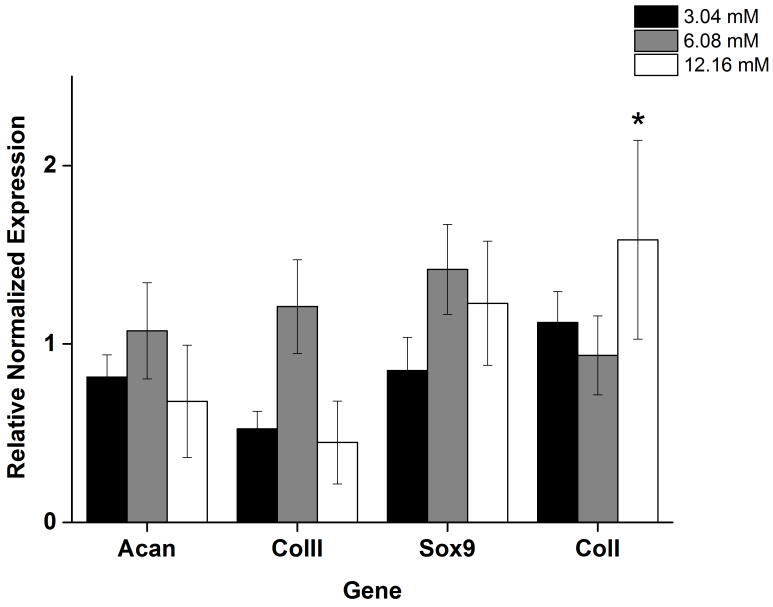

Figure 19. Relative normalized gene expression in HUCPV micromasses after 21 days of culture. The graph shows means ± standard deviation (N=9). Data normalized to two reference genes and to control in differentiation medium. Stars indicate statistically significant differences regarding control in growth medium ($p < 0.05$ = *) calculated with FCX manager software 3.1 using t-test method.

Cells cultured in extracts with a concentration 12.16 mM of Mg showed an increase in the expression of SOX9 and OPN and a decrease in the expression of COL2A1 and ACAN. When cultured in extracts with a concentration 6.08 mM, a slight increase was observed in the expression of all the genes, as well as a notable increase of OPN. Finally, with a concentration 3.04 mM of Mg, cells showed a slight decrease of SOX9 and ACAN expression, a notable decrease of COL2A1 and an up-regulation of OPN.

8.1.3. GAG production: content in ECM and release into supernatants

The chondrogenic differentiation of HUCPV cells during 21 days of culture under the influence of the three different concentrations of Mg extracts (3.04, 6.08 and 12.16 mM of Mg) was evaluated by quantifying the GAG production by the cells, and comparing to control conditions (differentiation medium). This involved the total emount of GAG released into the supernatants during the 21 days of culture of the micromasses and the GAG content in the ECM after 21 days.

The total GAG released into the supernatants during the 21 days of culture of the micromasses showed no significant differences regarding control conditions, but a slight increase in those cultured in Mg extracts with 6.08 mM of Mg (Figure 20.A.).

In Figure 20.B. it is possible to appreciate that GAG content in the ECM was not altered when cells were cultured in extracts containing 3.04 mM of Mg. A significant increase was observed in micromasses cultured in 6.08 mM Mg-extracts. A concentration 12.16 mM of Mg in the extract induced a decrease in GAG content in the ECM.

Cell proliferation, gene expression and GAG results indicated that the concentration of Mg in the extracts that allowed the highest cell proliferation and differentiation was 6.08 mM, being therefore the most suitable for continuing evaluating the effects of pure Mg, Mg-10Gd and Mg-2Ag. Therefore this concentration was kept in further investigations.

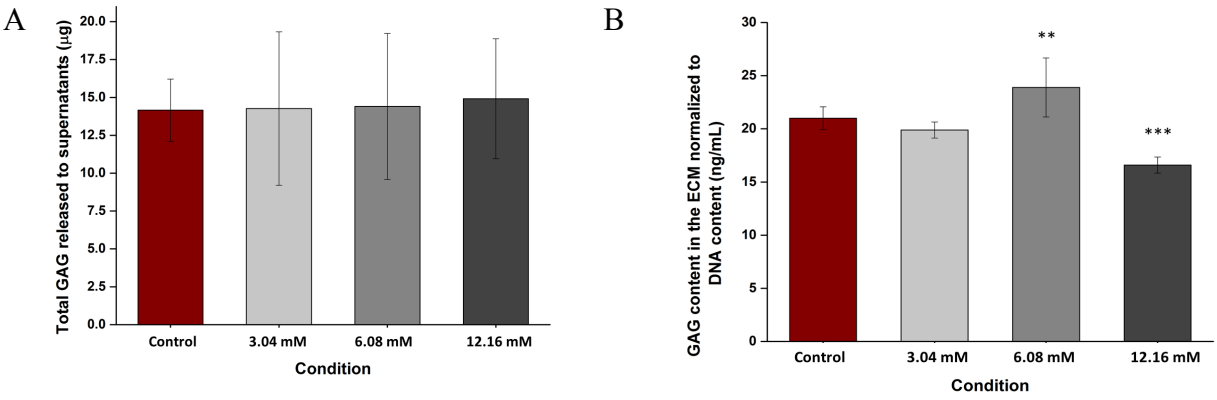

Figure 20. GAG content corresponding to: A) the total GAG released into supernatants (µg). Average value of the absolut quantifications of the GAG contained in the supernatants everytime media was changed. B) GAG content in the ECM of the micromasses (ng/mL) normalized to DNA content (ng/mL) after 21 days of chondrogenic differentiation.
Control was performed in differentiation medium. N=9. Stars indicate statistically significant differences regarding the control ($p < 0.01$ = **; $p < 0.001$ = ***) calculated with Origin 9 software using one-way ANOVA and applying Bonferroni´s correction post t-test.

8.2. ATDC5 cell reaction to pure Mg, Mg-10Gd and Mg-2Ag extracts and in direct contact

Cell viability and chondrogenic differentiation of ATDC5 cells under the influence of Mg, Mg-10Gd and Mg-2Ag extracts was evaluated, keeping a concentration 6.08 mM of Mg in all of them, to avoid different concentrations of Mg due to different degradation rates and thus, distinguishing the effects caused by the alloying elements. Furthermore, cell reaction in direct contact to the materials was analysed and related with changes in the composition of the degradation layer in order to better understanding the causes of such reactions.

8.2.1. Cell viability and growth in extracts

Living cells were quantified with CASY cell counter. Significant differences in ATDC5 cells viability were not detected after seven days of culture (Figure 21). Cells grown in control conditions showed 80% of viability. Mg-10Gd and Mg-2Ag exhibited a slight increase in the % of viable cells, with a value of 81.7% and 80.2% respectively. Finally, 76.8% viability was detected in cells cultured with Mg (which corresponds to 96% viability regarding the control).

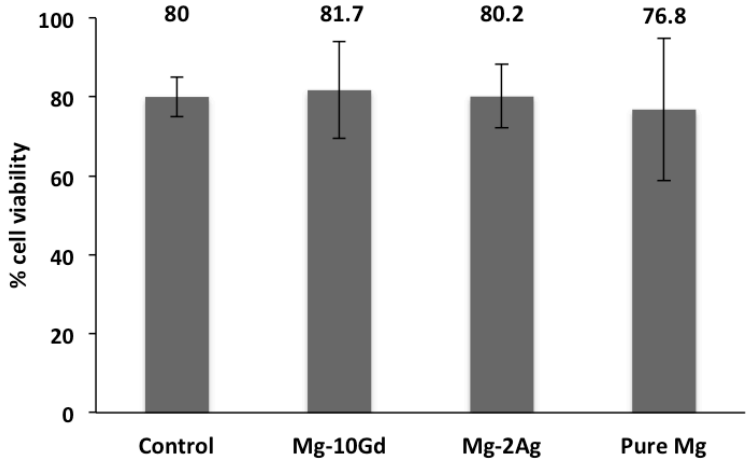

Figure 21. Percentage (%) of viable cells after seven days of culture in control conditions (maintenance medium) and in extracts. N=6.

Cell growth was also evaluated by microscopy. Optical images of ATDC5 cells under influence of the extracts and in control conditions are shown in Figure 22. After six days, cells were more confluent when cultured in the extracts. In differentiation medium some areas of cell condensation and synthesis of ECM can be already observed (white areas).

After 12 days of culture, the highest cell confluence was observed in differentiation medium, which furthermore exhibited higher cell condensation and ECM than after days days. In Mg-10Gd extract, some zones showed an increase in cell size and round-shaped morphology as well as lower density than in the other conditions, all characteristic of chondrocytes maturation and hypertrophy. Nevertheless, in other areas cell condensation is also observed. Cells cultured in Mg-2Ag and Mg extracts showed a slightly higher cell confluence than in growth medium. Cell condensation is also recognized in located areas.

Finally, after 18 days ATDC5 chondrocytes showed similar confluence and cell size in growth medium, Mg-2Ag and Mg extracts. In differentiation medium the formation of cartilage nodules is noticeable (areas with high cell density and enhanced production of ECM). When cultured with Mg-10Gd, nodule formation is also observed, but some cells show hypertrophic and apoptotic phenotypes.

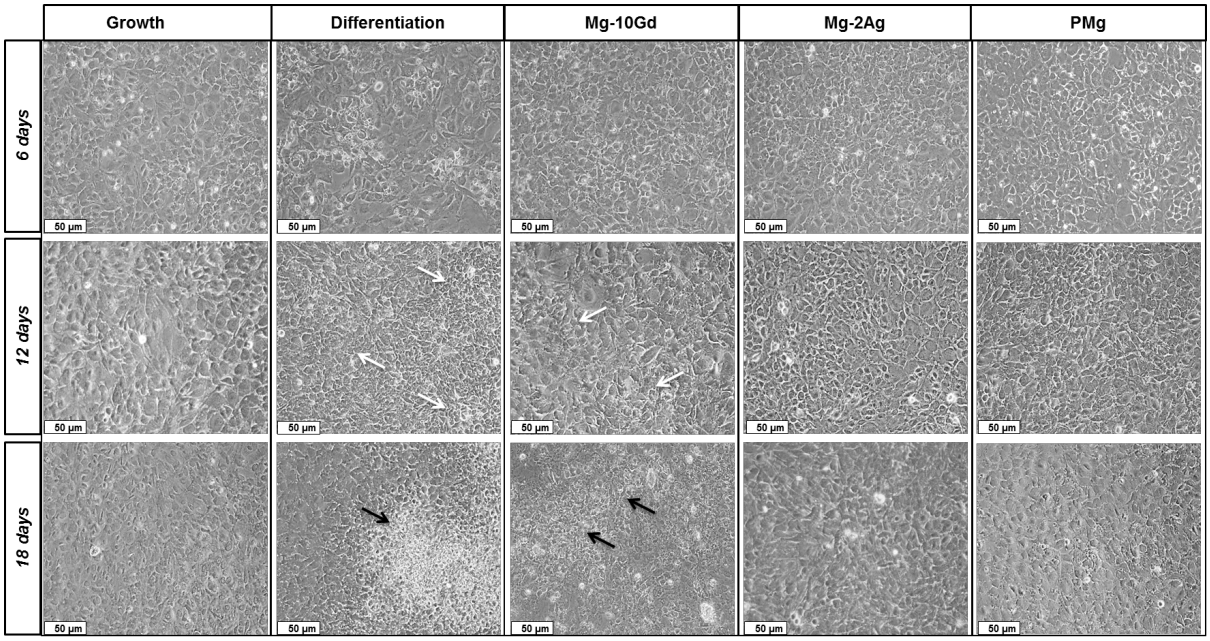

Figure 22. Optical images of ATDC5 chondrocytes cultured during 6, 12 and 18 days under the influence of growth medium, differentiation medium and Mg-10Gd, Mg-2Ag, Mg extracts. Condensation areas (white arrows); cartilage nodule formation (black arrows).

8.2.2. pH evolution

Strong differences in the color of the media were found already after three days of cells culture with ATDC5 cells in the extracts, mainly in Mg-10Gd, indicating a change in pH. Therefore, the pH was measured during the whole culture period (21 days) to obtain a complete profile of the pH fluctuations. This will give information about the capability of the cells to stabilize the pH values during the culture period, as well as about their metabolic activity (an acidic pH would indicate an increased metabolic activity).

pH was measured in the supernatants before the culture medium was changed. Both maintenance (control in growth medium) and differentiation conditions showed no significant differences between them, and only differentiation is represented in the Figure 23. Differentiation showed a slight increase from the initial pH 7.34 till 7.53 after 19 days of culture. The initial pH of the extracts (before cell culture) was higher than in the control (8.15 in Mg-10Gd and 8.25 in both Mg-2Ag and Mg). After three days of cell culture, the pH of the three extracts decreased, more noticeably in Mg10Gd (7.16) than in Mg-2Ag and Mg (7.75 in Mg-2Ag; 7.64 in Mg).

Mg-2Ag and Mg conditions showed very similar pH values at every time point. Both conditions showed an increase after six days, getting close to the initial values, followed by a continuous and slow decrease until reaching similar values to the control.

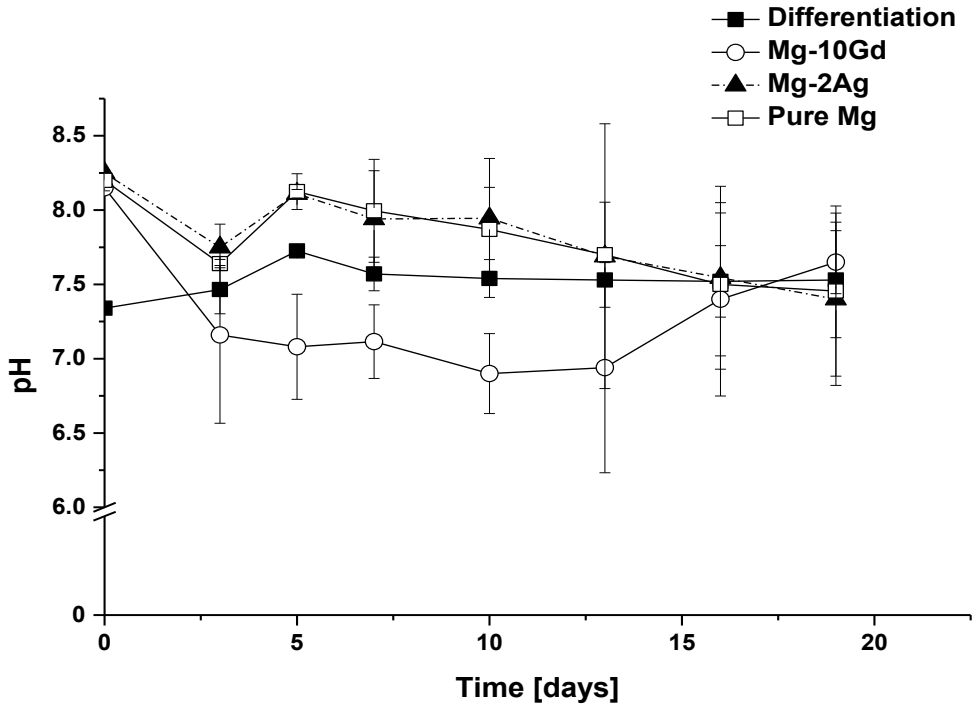

Figure 23. pH variations during ATDC5 cell culture. pH was measured prior to every change of medium (N=6). Stars indicate statistically significant differences regarding the control ($p < 0.05$ = *) calculated with Origin 9 software using one-way ANOVA and applying Bonferroni´s correction post t-test.

Unlike the tendency described with Mg-2Ag and Mg, the pH of Mg-10Gd extracts continued decreasing from day three till day 14, reaching acidic values (6.9), and afterwards an increase until values close to the ones in the other conditions (7.6).

8.2.3. Chondrogenic differentiation: gene expression

Evaluating the expression of chondrogenic and pre-hypertrophic gene markers, it is possible to determine in which stage of chondrogenic differentiation are the cells. The relative gene expression, normalized to the control in growth medium and to two reference genes (Actin, beta (B2m) and 40S ribosomal protein S18 (s18)), of ATDC5 cells was analyzed after seven, 14 and 21 days of culture with the extracts (Figure 24).

After seven days (Figure 24.A.), Col2a1 and Sox9 showed higher expression when stimulating the cells for chondrogenesis as well as with Mg-2Ag and Mg extracts, while Mg-10Gd showed no effects in the expression of any of the chondrogenic genes. Regarding the hypertrophic (Col10a1 and Runx2) and endochondral bone formation (Col1a1) gene markers, differentiation medium induced a slight increase in the expression of Runx2 and Col1a1. The most notable effects is detected with Mg-10Gd extract, inducing up-regulation of Col10a1 (1.95 times higher) and with Mg extract, which decreased the expression of Col10a1 to half (0.55) and even more of Runx2 (0.37) and Col1a1 (0.20). Mg-2Ag showed no effects over those three genes.

After 14 days (Figure 24.B.), the expression of the chondrogenic markers (Acan, Col2a1 and Sox9) was increased stimulating the cells with differentiation medium. Mg-10Gd and Mg-2Ag induced a much higher expression of Acan (2.35 and 2.93 times higher respectively), slight decrease in Col2a1 and no effects in Sox9 expression. Magnesium extracts increased expression of Sox9 (1.6 times). Differentiation medium decreased Col10a1 and Runx2 expression while Col1a1 was not altered. Up-regulation of hypertrophic (Col10a1, Runx2) and osteogenic (Col1a1) markers was detected with Mg-10Gd extract. Mg-2Ag and Mg extracts induced a higher expression of Col10a1 and a slight decrease in the expression of Runx2 regarding control in growth medium. Col1a1 expression was furthermore decreased with Mg-2Ag.

After 21 days of cell culture (Figure 24.C.), differentiation conditions showed an approximately double expression of Acan (2.2 times higher) and Sox9 (2.24 times higher) and a significant up-regulation of Col2a1 (5.2 times higher). Mg-10Gd induced significant up-regulation of Acan (4.57 times), a 2.3-fold increase in Col2a1 but did not affect Sox9 expressions. Mg-2Ag and Mg increased the expression of Col2a1 and showed the highest expression of Sox9. Expression of chondrogenic markers was increased under chondrogenic conditions. Mg-10Gd extracts induced a significant up-regulation of Col10a1 (5.9-fold increase) and Runx2 (4.02-fold increase).

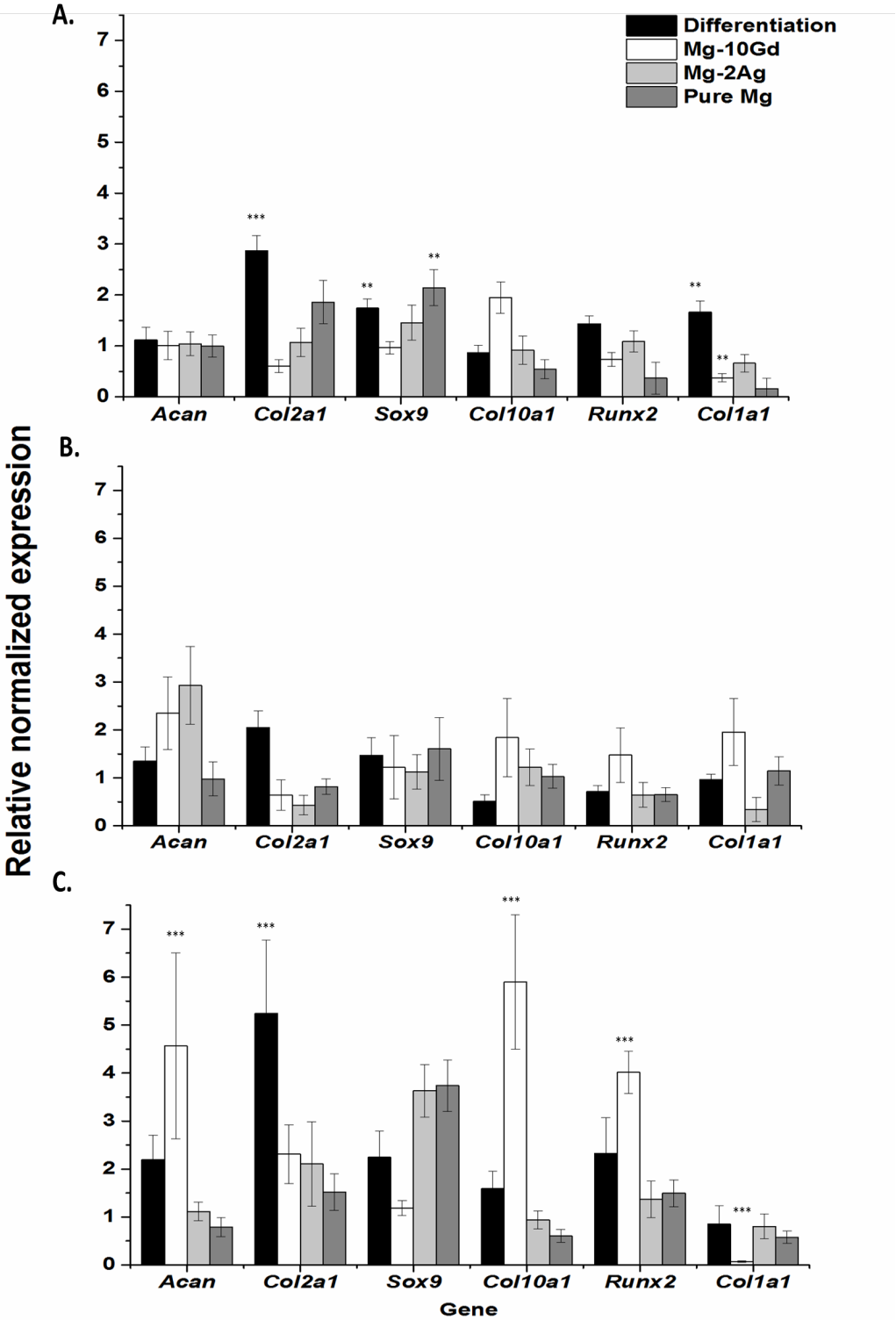

Figure 24. Relative normalized gene expression by ATDC5 chondrocytes after A) seven days, B) 14 days and C) 21 days of culture. The graph shows means ± standard deviation (N=12). Data normalized to control in growth medium (maintenance) and to two reference genes: Actin, beta (B2m) and 40S ribosomal protein S18 (s18). Stars indicate statistically significant differences regarding control in growth medium ($p < 0.01$ = **, $p < 0.001$ = ***) calculated with FCX manager software 3.1 using t-test method.

Mg showed a reduction in the expression of Col10a1 and an increase in the expression of Runx2 regarding the control. Mg-2Ag showed no effects in the expression of those genes. Col1a1 was slightly decreased to 0.85 with differentiation conditions and to 0.8 with Mg-2Ag extract. With Mg the expression of Col1a1 was reduced to almost half (0.58) and finally was significantly down-regulated with Mg-10Gd extract (0.074).

8.2.4. Cell reaction to direct contact with the material

- ***SEM images***

SEM images were obtained after seven days of cell culture, to evaluate cell morphology and distribution on the surface of the materials, which would indicate if the materials allow cell adhesion an homogenous distribution on the whole surface, being both properties desirable in an implant to obtain a good integration with the surrounding tissues. Additionally, information about cell health and phenotypic characteristics can be obtained from the morphology observed with SEM images.

Mg-2Ag and Mg-10Gd allowed cell attachment as indicated by the cellular extensions observed in contact with the surface of the materials (Figure 25). Both materials showed similar cell coverage, with a homogenous distribution through the whole surface. On the Mg-10Gd sample, some cells showed a spreaded and polygonal morphology, but most of the cells were forming part of aggregates and exhibiting a marked rounded shape, which is characteristic of chondrocytes. Layers of fibrils were surrounding the cell clusters.

On Mg-2Ag samples, most of the cells were spread on the surface. Some rounded cells are also noticed, but cell aggregation was lower than on Mg-10Gd samples.

Regarding Mg, the presence of cells was lower than in the other samples and its distribution was limited to some areas, where also high cell density and aggregation was detected, while other areas were unpopulated. Some cells showed a rounded morphology. Cells developed abundant surface extensions attaching to the material.

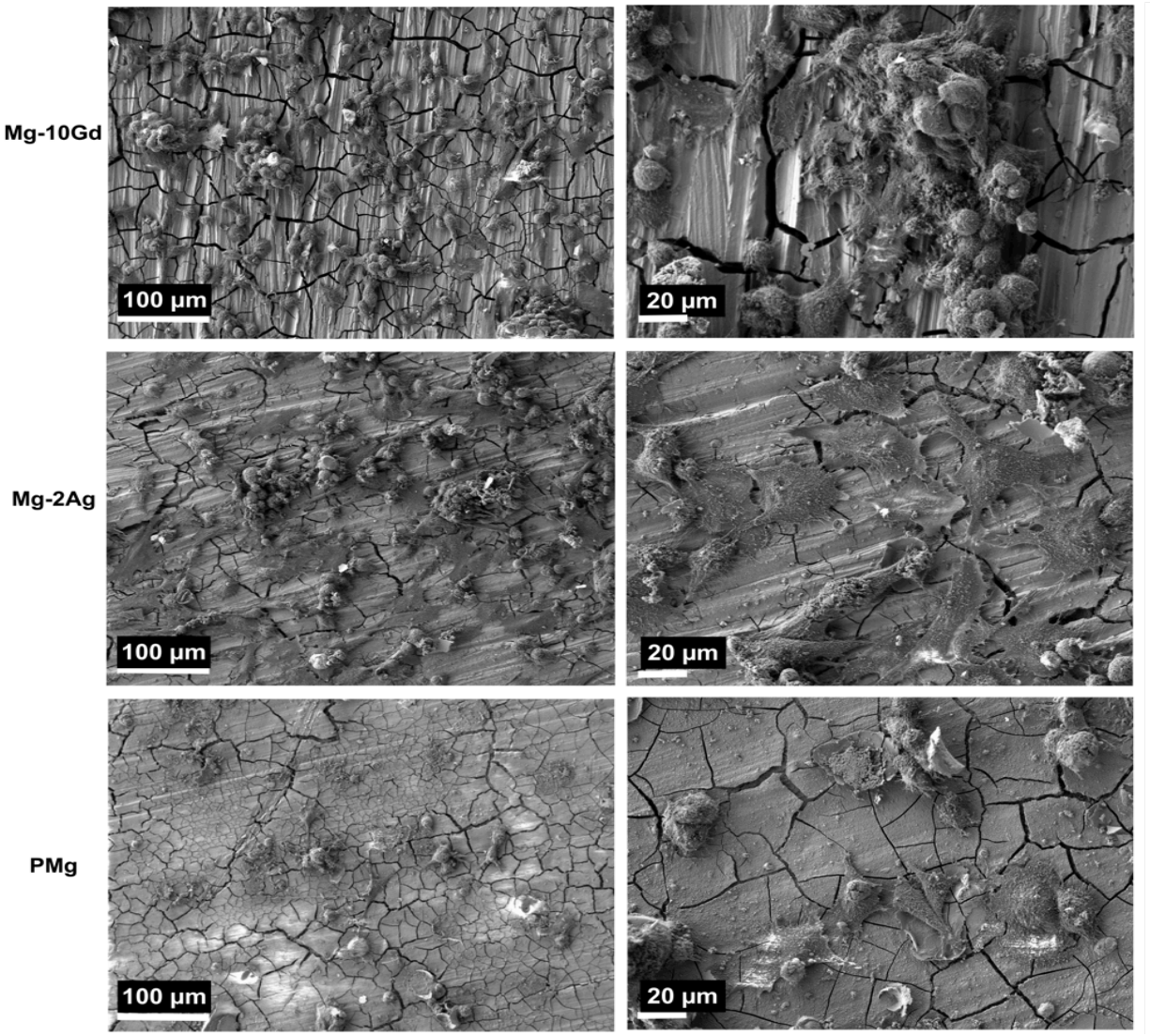

Figure 25. SEM images of ATDC5-chondrocytes on Mg-10Gd, Mg-2Ag and Mg samples after seven days of culture.

- ***Calcein staining***

Calcein staining was done to evaluate the distribution of viable cells on the materials, determining which one allows the highest cell viability and to confirm the results obtained with SEM.

Mg-10Gd surface was almost totally covered by cells after seven days (Figure 26). Cells showed a round-shaped morphology.

The distribution was very homogenous, and in areas with high cell density, ECM can be observed as homogenous layer embedding the cells.

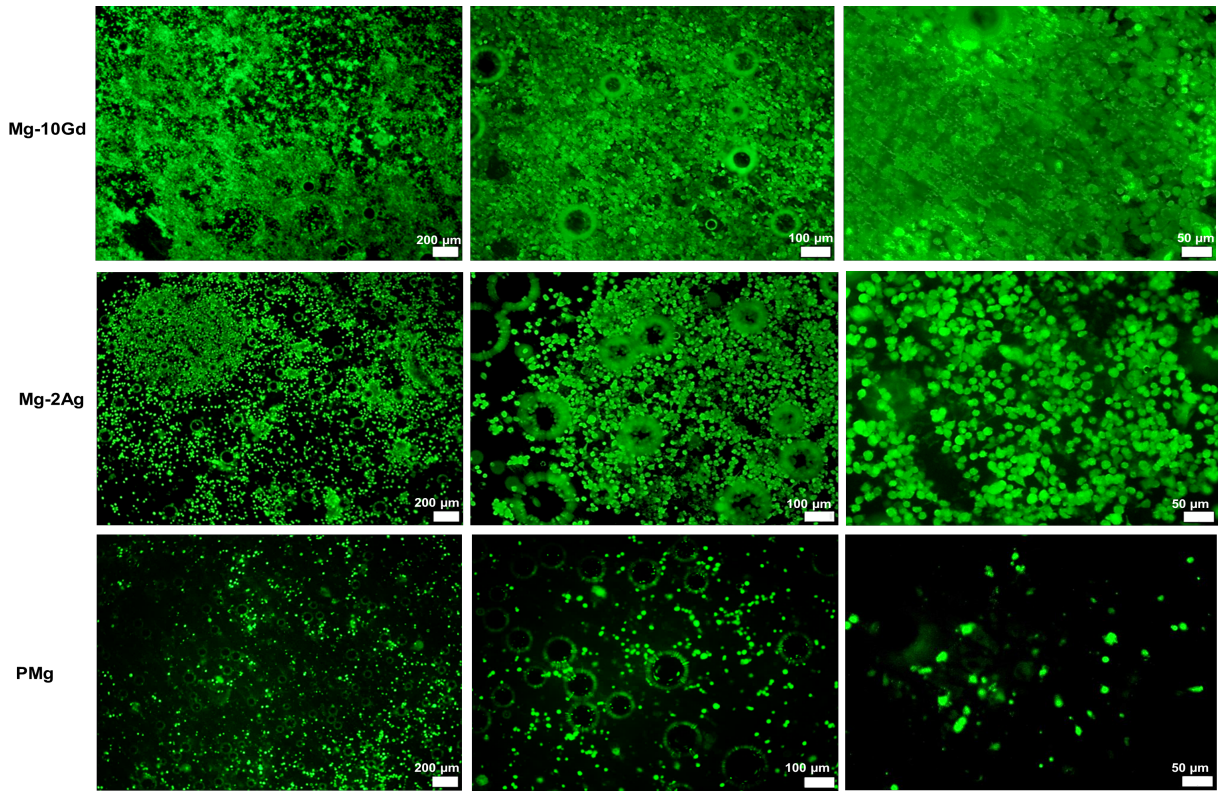

Figure 26. Calcein staining of living ATDC5 cells on the surface of Mg-10Gd, Mg-2Ag and Mg discs after seven days of culture.

Mg samples showed a lower and more localized cell presence than the alloys. ECM is negligible on those materials. Cells exhibited a similar size on all the materials.

On the Mg-2Ag samples also a homogenous distribution of the cells was observed, covering a lower area of the surface than in Mg-10Gd. ECM production is recognized locally (where cells form cartilage nodules). ATDC5 cells showed a tendency to follow an orientated distribution over both Mg-10Gd and Mg-2Ag alloys (can be appreciated as a diagonal linearity in Figure 27) that could be directed by the cutting lines of the samples.

- ***SEM and EDX of the degradation layer: element composition and thickness***

With the aim of better understanding the causes of the cell behavior observed on the different materials, the degradation layer formed during cell culture on the surface of the samples was also evaluated. The thickness and element composition may give information about the degradation behavior and why some samples are more populated by cells than others.

Figure 27 shows SEM pictures of the FIB processed transversal sections of the materials. The images contain the degradation layer below and without cells. It is possible to distinguish the degradation layer and cells on the materials surface.

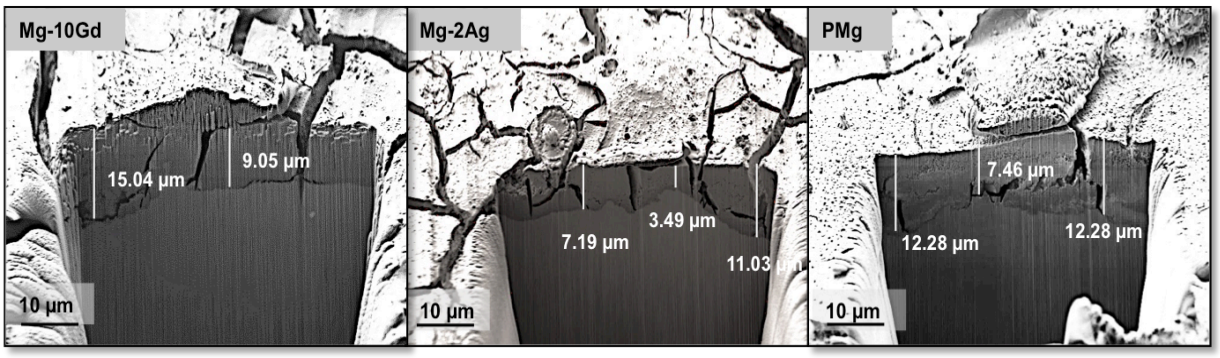

Figure 27. FIB-SEM image of Mg-10Gd, Mg-2Ag and Mg samples, showing variations in the thickness of the degradation layer, with and without cells on the surface.

Variations in the thickness along the degradation layer in the same sample are observed, regardless of the presence or lack of cells on the surface. Mg-2Ag has the thinnest degradation layer with a variable depth, corresponding with the lowest degradation rate (0.251 ± 0.022) showed in section 1.2.4.4. Mg-10Gd has the thickest layer (reaching 15.05 µm) and the most homogenous regarding size, which corresponds with the highest degradation rate (0.631 ± 0.21). Similarly, the degradation layer on Mg shows variations in the thickness.

Furthermore, qualitative (Figure 28) and quantitative (Table 12) element composition of the degradation layer was determined by EDX analysis. Apart from the alloying elements, the main differences are found in the content of Mg, Ca and P.

In the degradation layer on Mg-2Ag, Mg and O are homogenously distributed in the whole degradation layer. It shows a 1.5 times higher content of Mg than the other materials, and a low (0.30 wt%) Ag content that furthermore seems to be localized in some areas of the layer. In addition, Ca and P amounts are 1.4 times and 1.14 times higher (respectively) than in Mg-10Gd and 2.6 / 2.16 times higher (respectively) than in Mg. Magnesium content in the degradation layer of Mg-10Gd seems to be substituted by a high content of Gd (2.97 wt%) and in Mg samples by O.

Table 12. Element quantification in the degradation layer. Data obtained with EDAX ZAF Quantification (Standardless), element normalized. Wt%: weight percentage.

Element	wt %		
	Mg-10Gd	Mg-2Ag	Mg
C (K-line)	1.09	1.15	1.12
N (K-line)	0.03	0.06	0.07
O (K-line)	87.37	86.55	90.32
Na (K-line)	0.09	0.09	0.07
Ga (L-line)	0.81	0.50	0.81
Mg (K-line)	6.08	9.26	6.37
Si (K-line)	0.12	0.18	0.14
P (K-line)	0.70	0.80	0.37
Ag (L-line)	0.00	0.31	0.00
Ca (K-line)	0.46	0.65	0.25
Gd (L-line)	2.97	0.00	0.00
Total 100.00			

While in Mg-2Ag Ca is concentrated in the surface of the degradation layer, in Mg samples, Ca is distributed through the whole layer (even though the content is much lower). In Mg-10Gd samples, O and Mg are more concentrated in areas close to the surface. Gadolinium is distributed homogenously throughout the whole degradation layer.

Mg images showed a fragmented layer, with a very homogenous distribution of Ca. O and Mg followed the same distribution pattern in all the materials.

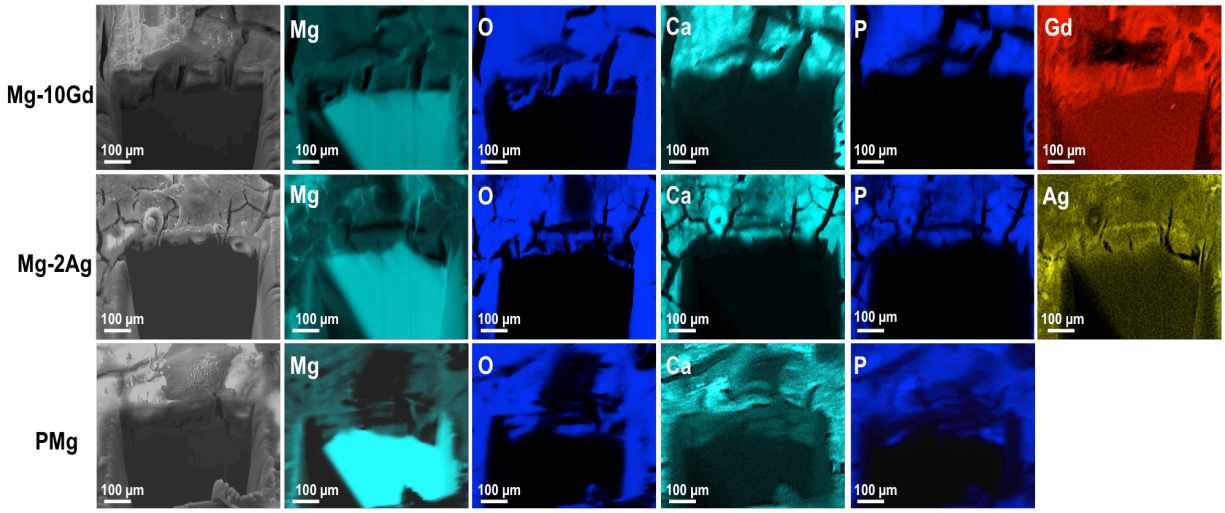

Figure 28. EDX mapping showing the distribution of magnesium (Mg), oxygen (O), calcium (Ca), phosphorous (P), silver (Ag) and gadolinium (Gd) in the transversal section of the materials. Images were taken at an accelerating voltage of 15 keV.

- ***Degradation rate of the samples***

The degradation rate of Mg-10Gd (0.631 ± 0.21) was significantly higher than in Mg-2Ag (0.251 ± 0.022) and Mg (0.293 ± 0.044), indicating a higher interaction of the surrounding environment with the material. The lower degradation rate detected in Mg-2Ag and Mg samples could be caused by the formation of a protective layer as a consequence of the precipitation of some components of the medium (as C, O, N and Mg, which amount was higher in the degradation layer of Mg-2Ag and Mg than in Mg-10Gd). Additionally, Mg-2Ag samples showed the highest content of P and Ca that may correspond to Ca-P phase precipitation, which tend to form a homogenous protecting layer.

8.1. HUCPV cell reaction to Mg, Mg-10Gd and Mg-2Ag

Due to the significant differences appreciated in cell behavior under the influence of Mg-10Gd regarding the other extracts (and mainly motivated by the notable changes in pH previously discussed in section 1.2.2.), influence of Mg-10Gd extract over cell metabolism was studied.

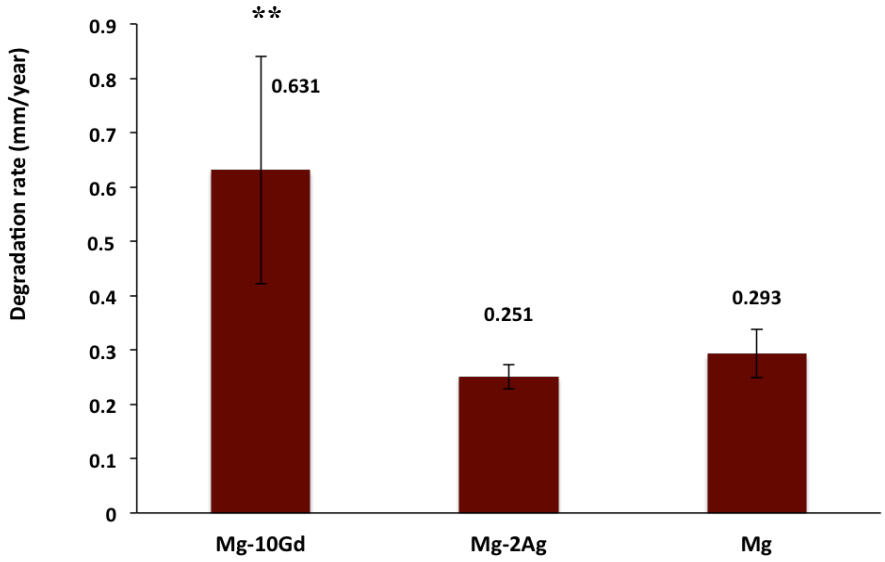

Figure 29. Degradation rate (mm/year) of Mg-10Gd, Mg-2Ag and Mg samples after 7 days of immersion under cell culture conditions. The solution is alpha-MEM with addition of 15% FBS and 1% antibiotics (penicilin and streptomycin) (N= 6 per sample). Stars indicate statistically significant differences regarding the control ($p < 0.01$ = **) calculated with Origin 9 software using one-way ANOVA and applying Bonferroni´s correction post t-test.

In addition, the cell viability was determined under the influence of the three extracts, as well as the chondrogenic differentiation of HUCPV based on the GAG production and gene expression. Regarding the cell reactions in direct contact with the samples, the evaluation was done focusing on the cell viability and distribution, as well as the expression of chondrogenic markers.

8.1.1. Cell metabolic activity under the influence of Mg-10Gd extracts.

Due to the different cell behavior observed in ATDC5 cells cultured in Mg-10Gd compared to the other conditions (as lower proliferation and higher expression of chondrogenic markers), and the controversy about the effects of Gd found in the literature, HUCPV cell viability was evaluated under the influence of Gd, after 24 and 72 hours. For this purpose, cells where culture in $GdCl_3$ with three different concentrations of Gd (0.5, 5, and 50 µM). Additinally, cells where cultured in Mg-10Gd extracts with the same Gd concentrations (obtained diluting the extract) in order to compare the results and to determine differences regarding $GdCl_3$.

Such differences would be due to the combination of Gd and/or Mg with another components of the culture medium. MTT ((3-(4, 5-dimethylthiazolyl-2)-2, 5-diphenyltetrazolium bromide) was used to meassure cell viability (% of viability regarding control cells in growth medium) and the results were normalized to the DNA content in order to obtain the metabolic activity of the cells (Figure 30).

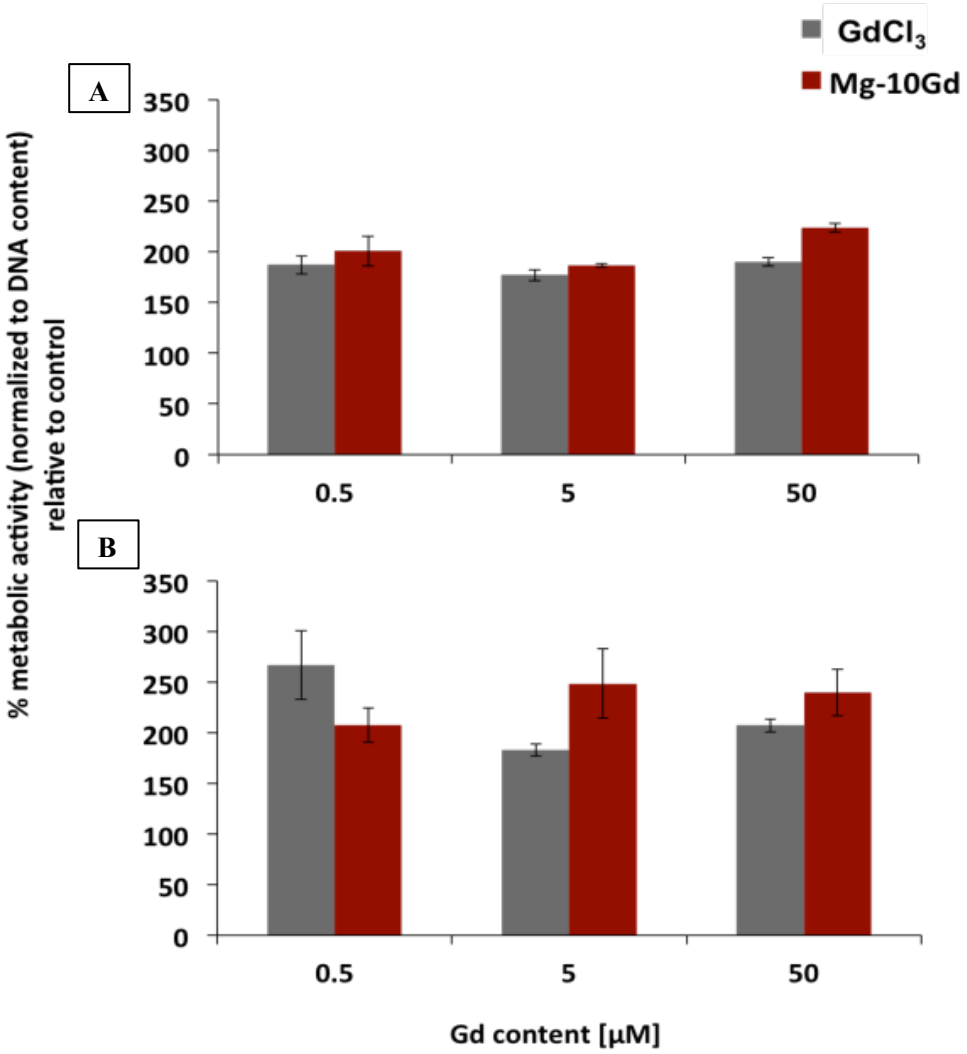

Figure 30. Metabolic activity of HUCPV cells after 24 (A) and 72 hours (B). The average metabolic rates obtained with MTT assay were normalized to the DNA content (N=12). Control condition corresponds to 100% of metabolic activity.

After both times, the metabolic activity was increased when cells where cultured with Gd in all evaluated concentrations (0.5, 5 and 50 µM). The increase was more notable after 72 hours than after 24 hours of culture. Mg-10Gd showed a stronger

effect on cell metabolism than $GdCl_3$ at same concentrations. Significant differences between $GdCl_3$ and Mg-10Gd were not observed.

8.1.2. Cell viability

HUCPV cells were cultured in 12 well-plates under the influence of the three extracts (Mg, Mg-10Gd and Mg-2Ag) for seven days.
Afterwards, cell viability was assessed by life/dead staining (Fisher Scientific GmbH). Cell pools and stringy cell connections between them are visualized in Figure 31. This is likely to be due to the high cell confluence and the washing step. It is possible to notice higher and more homogenous coverage in Mg-10Gd extracts (Figure 31.B and 31.F) than in Mg-2Ag (Figure 31.C and 31.G) and Mg (Figure 31.D and 31.H).

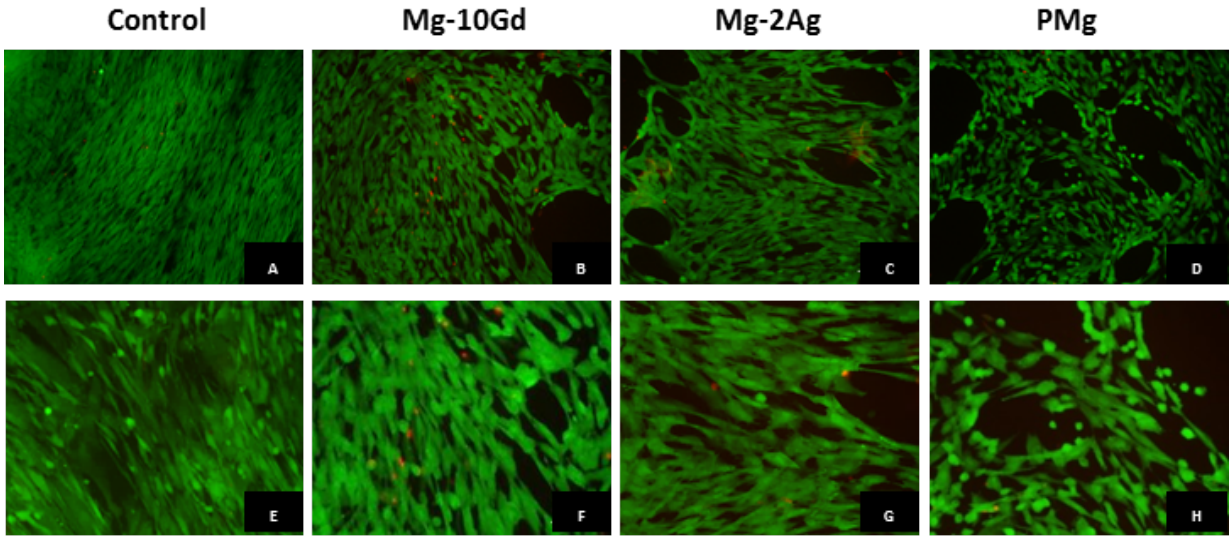

Figure 31. Life/dead staining images after seven days of cell culture in extracts, at 5% O_2. 10x magnification images (A-D); 20x magnification images (E-H).

Cells cultured in Mg-extracts show rounder morphology and larger size than the ones in control condition. Few dead cells are observed in the three extracts.

8.1.3. Chondrogenic differentiation

After 21 days of cell culture in chondrogenic medium (with and without the addition of Mg-extracts), the obtained micromasses were processed to evaluate the chondrogenic differentiation under the influence of the extracts (Mg, Mg-10Gd and Mg-2Ag) all with 6.08 mM of Mg.

- ***Cell growth and GAG production***

In section 1.1.3. we showed the GAG production of micromasses cultured with different concentrations of Mg extract. In this section we discuss the GAG production of micromasses cultured with Mg, Mg-10Gd and Mg-2Ag extracts, all with the same Mg concentration (6.08 mM).

Cell growth was determined quantifying the DNA content in the HUCPV micromasses after 21 days of culture (inducing chondrogenesis) under the effect of the extracts (Figure 32). On the one side, higher DNA content was observed in those micromasses cultured with Mg (320.74 ± 53.85 ng/mL) and Mg-2Ag (356.96 ± 32.22 ng/mL) extracts than in the control (284.19 ± 14.99 ng/mL), indicating an induction of proliferation. The increase in DNA amount is stronger with Mg-2Ag extracts than with Mg.

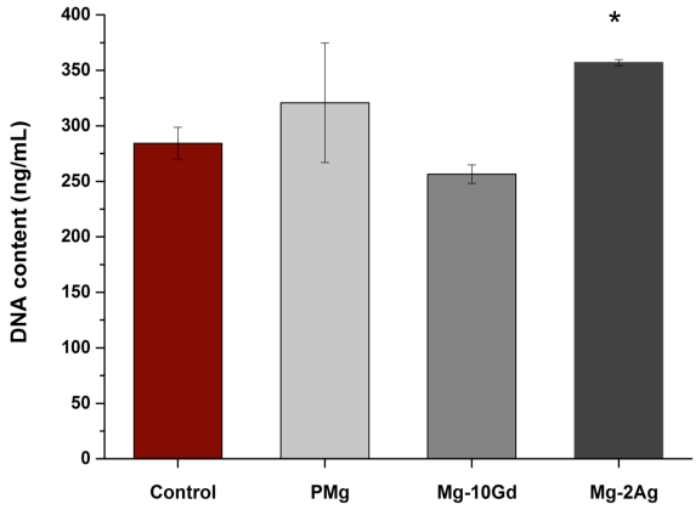

Figure 32. DNA content of the micromasses after 21 days of chondrogenic differentiation. Control was performed in differentiation medium. N=9. Stars indicate statistically significant differences regarding the control ($p < 0.05$ = *) calculated with Origin 9 software using one-way ANOVA and applying Bonferroni´s correction post t-test.

The total GAG content in the ECM of each micromass was normalized to the DNA content in order to calculate the GAG production per micromass (Figure 33). The highest value was detected in micromasses cultured in Mg-2Ag extracts (29.82 ± 2.69 ng/mL), being significantly higher than in control conditions. Mg-10Gd

samples showed higher production (23.9 ± 0.76 ng/mL) than the control in differentiation medium (20.01 ng/mL) and Mg (16.59 ± 2.78 ng/mL). GAG production was lower in samples cultured in Mg than in control.

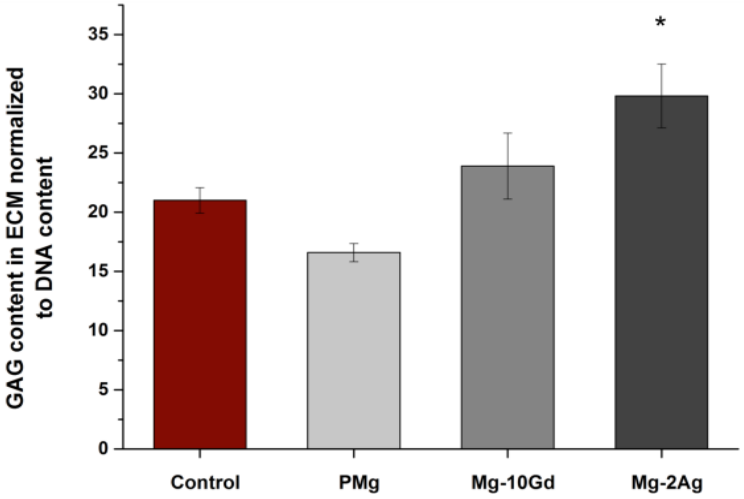

Figure 33. GAG content in the ECM of the micromasses (ng/mL) normalized to DNA content (ng/mL) after 21 days of chondrogenic differentiation. Control was performed in differentiation medium. N=9. Stars indicate statistically significant differences regarding the control ($p < 0.05$ = *) calculated with Origin 9 software using one-way ANOVA and applying Bonferroni´s correction post t-test.

- ***Gene expression***

Relative gene expression of HUCPV cells micromasses was evaluated after 21 days of culture under the influence of the extracts, and compared to the gene expression of HUCPV cells at day 0. The results were normalized to the control (differentiation medium) and to two reference genes (ribosomal protein L10 (RLP10) and valosin containing protein (VCP)). HUCPV cells analyzed before inducing differentiation showed only low amounts of ACAN, COL2A1, SOX9 and COL1A1 gene expression (figure 34). Pellets cultured with Mg-10Gd extracts showed an increased expression of ACAN (1.19-folds) and SOX9 (1.13-folds), as well as no difference of COL2A1 expression compared to differentiation medium. Mg-2Ag induced a decrease of ACAN (0.88-fold) and SOX9 (0.72-fold) expression and a 1.12-fold increase of the expression of COL2A1. Magnesium increased the expression of chondrogenic markers COL2 and SOX9, and did not influence expression of ACAN.

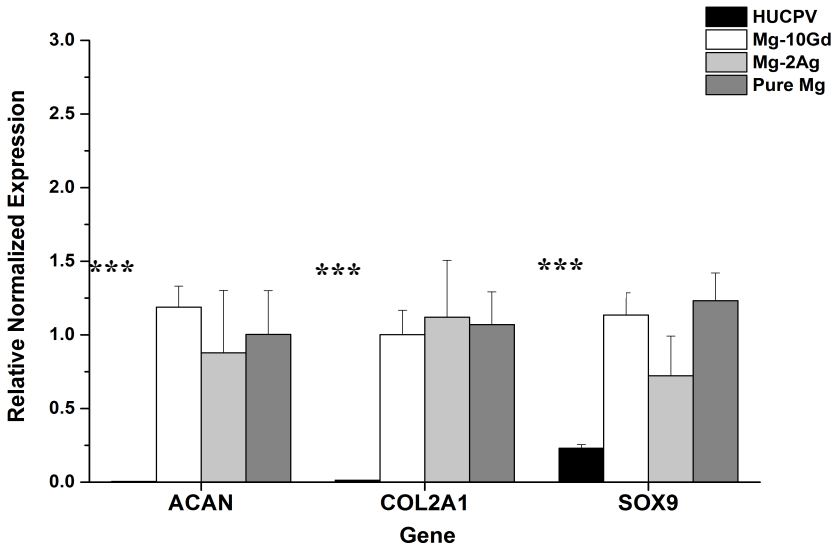

Figure 34. Relative normalized gene expression of chondrogenic markers. The graph shows means ± standard deviation (N=9). Data normalized to two reference genes (ribosomal protein L10 (RLP10) and valosin containing protein (VCP)) and to control in differentiation medium. Stars indicate statistically significant differences regarding control in growth medium ($p < 0.05$ = *, $p < 0.01$ = **, $p < 0.001$ = ***) calculated with FCX manager software 3.1 using t-test method.

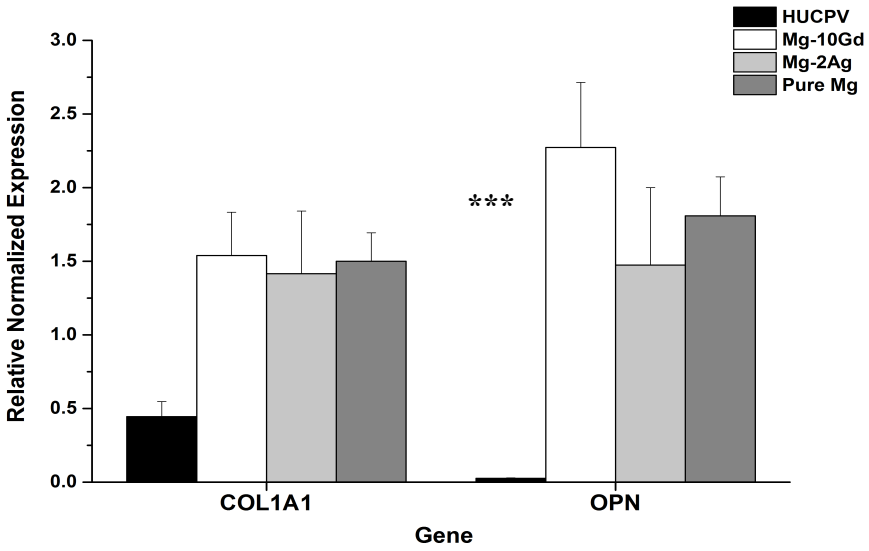

Figure 35. Relative normalized gene expression of pre-osteogenic markers. The graph shows means ± standard deviation (N=9). Data normalized to two reference genes (ribosomal protein L10 (RLP10) and valosin containing protein (VCP)) and to control in differentiation medium. Stars indicate statistically significant differences regarding control in growth medium ($p < 0.05$ = *, $p < 0.01$ = **, $p < 0.001$ = ***) calculated with FCX manager software 3.1 using t-test method.

Figure 35 shows the expression of pre-osteogenic markers. With Mg-10Gd both COL1A1 (1.54-folds) and OPN (2.27-folds) showed the highest expression values. Mg-2Ag induced a 1.42-fold increase of COL1A1 and 1.47 of OPN expression. The expression of the pre-osteogenic markers OPN and COL1 was increased 1.8 and 1.5 fold respectively under the influence of Mg.

8.1.4. Cell reactions to direct contact with the materials

40 000 HUCPV cells were seeded on the surface of the materials. Those cells were cultured for seven days with 5% oxygen in order to avoid intrinsic tendency of HUCPV to differentiate into osteoblasts, and approach the hypoxic conditions of the cartilage tissue (1% of oxygen or lower).

- ***Life/dead staining***

After seven days of culture, life/dead staining was performed to evaluate the viability and cell distribution of the cells after culture on the materials (Figure 36).
Cells cultured on Mg-10Gd disks tended to form aggregates homogenously distributed on the surface. In some areas, large aggregates of cells were also found, where it was possible to observe a group of dead cells (red) in the central part.

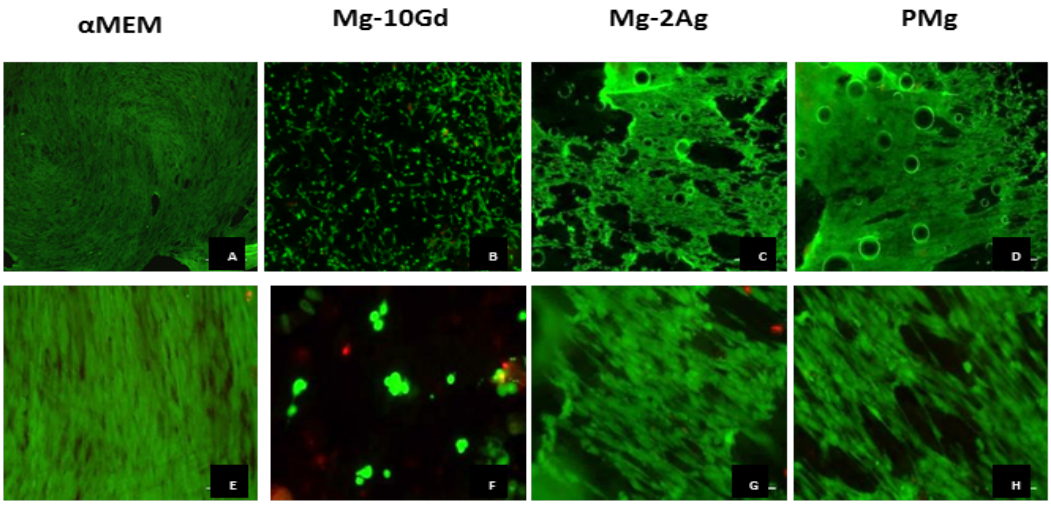

Figure 36. Images showing life/dead staining after seven days of culture in direct contact with the materials, under 5% O_2. Cells cultured in tissue culture plates were used as controls. Live cells are stained with Calcein (green). Dead cells are stained with Ethidium Bromide (red). 4x images (A-D); 20x images (E-H).

Mg-2Ag and Mg showed similar cell coverage of the surface of the materials. HUCPV cells on those samples showed a tendency to arrange linearly. Regarding the dead cells (red), only a low amount was detected.

- ***Expression of chondrogenic markers***

To evaluate the chondrogenic potential of the materials, 40 000 HUCPV cells were cultured during seven days in direct contact with the surface, in a 5% O_2 atmosphere and in growth culture medium. Additionally, cells were cultured in wells from 12 well-plates with growth medium as control condition. The expression of ECM-markers (Acan, Col-II and Col-X), as well as cartilage specific transcription factors (Nfat5 and SOX9) was analyzed. Nfat5 is a transcription factor activated as response to osmotic stress. Due to the increased in osmosis produced as a result of the degradation of the samples, this marker was also evaluated in the direct contact test. The expression of Acan, Col-II and Sox9 was increased when cells were in contact with the three materials (Mg, Mg-10Gd and Mg-2Ag) as occurred with the genes expressed under the influence of the extracts.

Cells covered the whole surface of the three materials. It was possible to perceive cell aggregation on Mg-10Gd samples and in some areas also on Mg-2Ag samples (Figure 37). Mg-10Gd exhibited the highest expression and most homogenous distribution of Acan and Col-II, closely followed by Mg-2Ag. In Mg samples, the expression of Acan and Col-II was lower than in the other conditions and more localized. Regarding the expression of Col-X, Mg-10Gd showed a high presence of this marker, while in control conditions, Mg-2Ag and Mg samples, Col-X expression was barely detected (Figure 37).

Nfat5 was observed in cells over the three materials. In Mg samples, Naft5 was distributed throughout the cytoplasm, while in Mg-10Gd and Mg-2Ag was more concentrated around the nuclear region (Figure 38).

Expression of the transcription factor Sox9 was observed in cells cultured under control conditions, and it was much higher in cells culture on Mg-10Gd and Mg-2Ag. In Mg samples, Sox9 expression was limited to areas with high cell density (Figure 38).

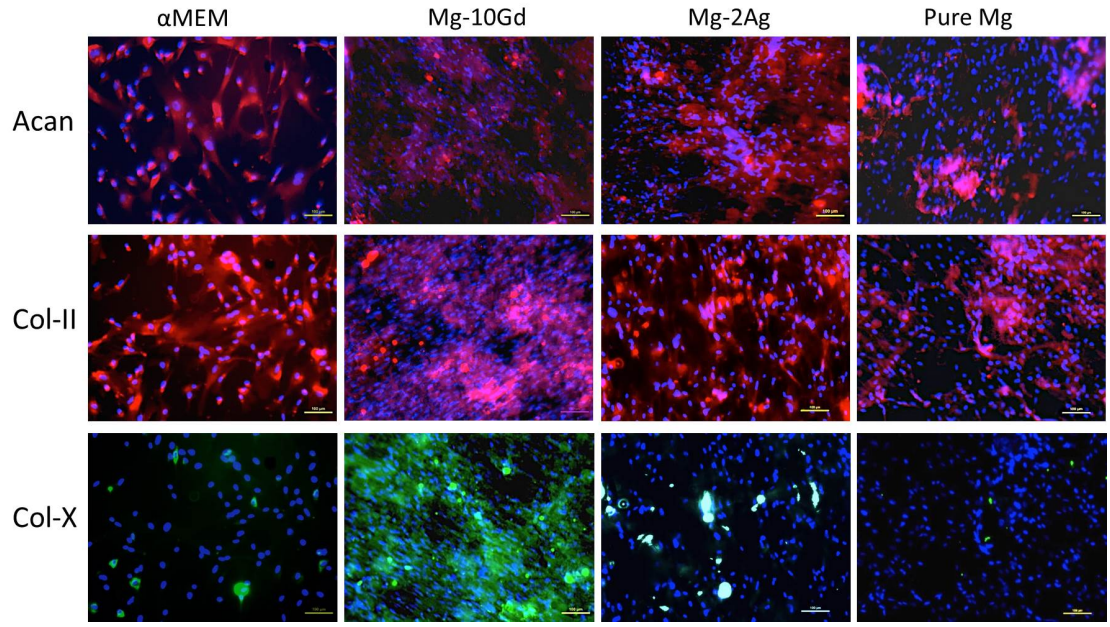

Figure 37. Effects of Mg-materials on cartilage-specific ECM markers detected by immunofluorescence in cultured HUCPV cells at day seven. Cells were stained for Acan (red), Col- II (red), Col-X (green) and nuclei were stained with DAPI (blue). Bar= 100 µm.

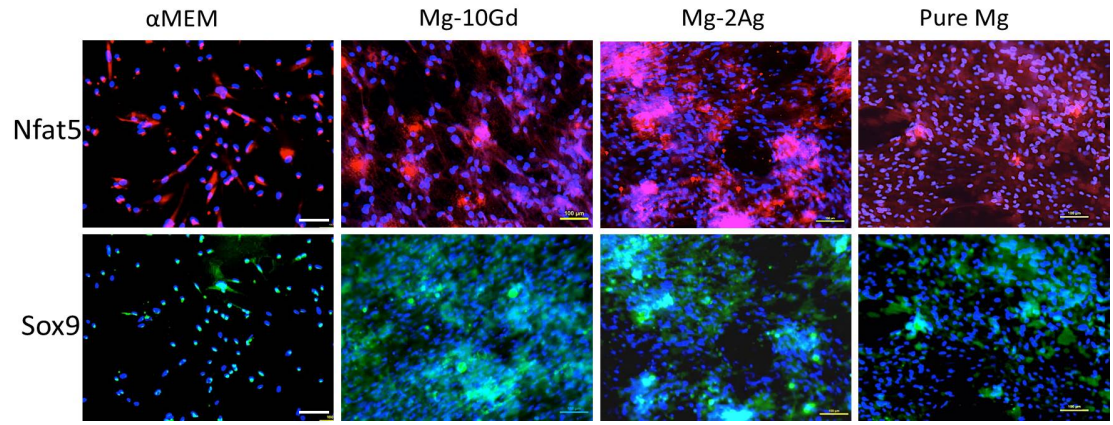

Figure 38. Effects of Mg-materials on cartilage-specific transcription factor markers detected by immunofluorescence in cultured HUCPV cells at day seven. Cells were stained for Nfat5 (red), Sox9 (green) and nuclei were stained with DAPI (blue). Bar= 100 µm.

8.2. Proteomic evaluation of HUCPV cells micromasses under the influence of Mg-10Gd, Mg-2Ag and Mg extracts

In order to determine the influence of pure Mg and two Mg alloys (Mg-10Gd and Mg-2Ag) on HUCPV cells, proteins were extracted, tryptic digested, and analyzed by LC-MS/MS for label-free quantification (LFQ) analysis.

Significantly regulated proteins (246 proteins) under the influence of the extracts were found (from the mean value of the regulated proteins normalized to control) and are listed in Supplementary Table 1.

136 proteins were up-regulated by Mg-10Gd, Mg-2Ag and Pure-Mg, from which 134 were common for the three extracts. Regarding the proteins down-regulated, 110 were down-regulated by the three extracts respectively, being 109 common.

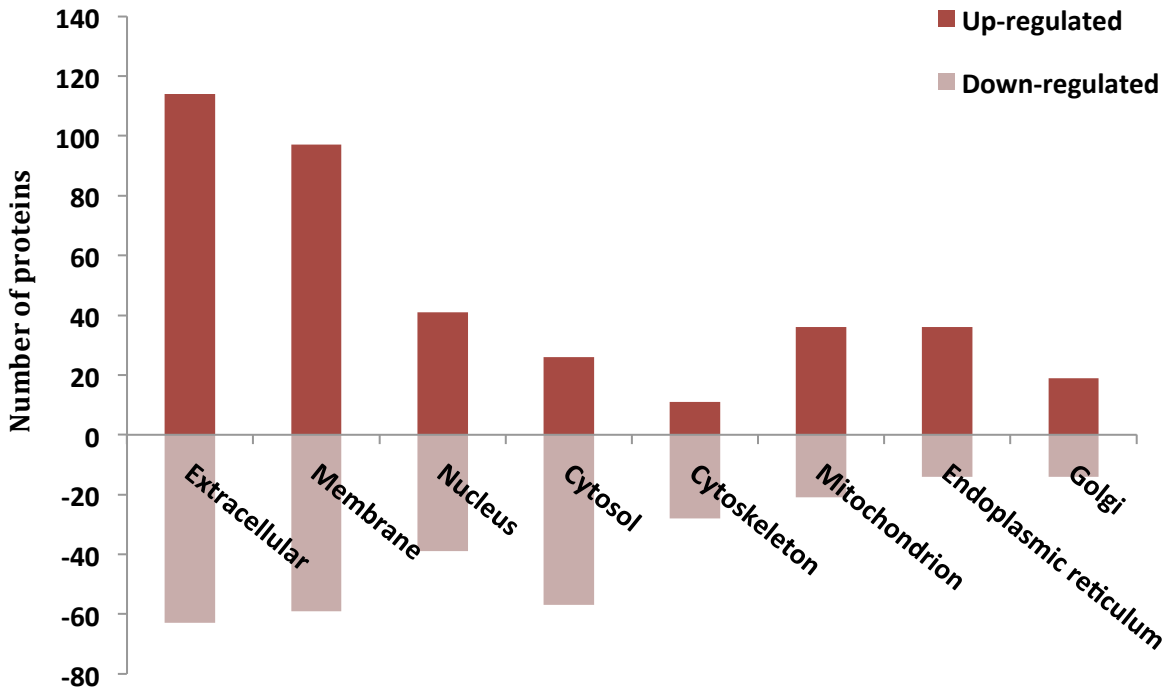

Figure 39. The number of regulated proteins with more than two-fold change in at least one of the Mg-alloys sorted regarding their location in the cells. Some proteins are attributed to more than one cell location, therefore the number of proteins shown in the graph is higher than the total amount of protein regulated with the extracts (246 proteins).

Further investigation of the processed data was performed based on Gene Ontology (GO) annotation downloaded from UniProt. Clustering the regulated proteins regarding their location in the cells (cellular component) (Figure 39) indicated the number of up-regulated extracellular proteins and membrane proteins (either involved in ECM composition or not) is considerably higher than down-regulated ones. Additionally, the number of regulated cytosolic proteins is high. Cytosolic and cytoskeletal proteins are mostly down-regulated.

Figure 40 shows the most affected biological processes. The highest number of regulated proteins were involved in cell binding, differentiation and apoptosis, followed by cell proliferation and miscellaneous function. To a lesser extent, proteins involved in angiogenesis, energy metabolism, bone development and chondrogenesis were influenced by the extracts.

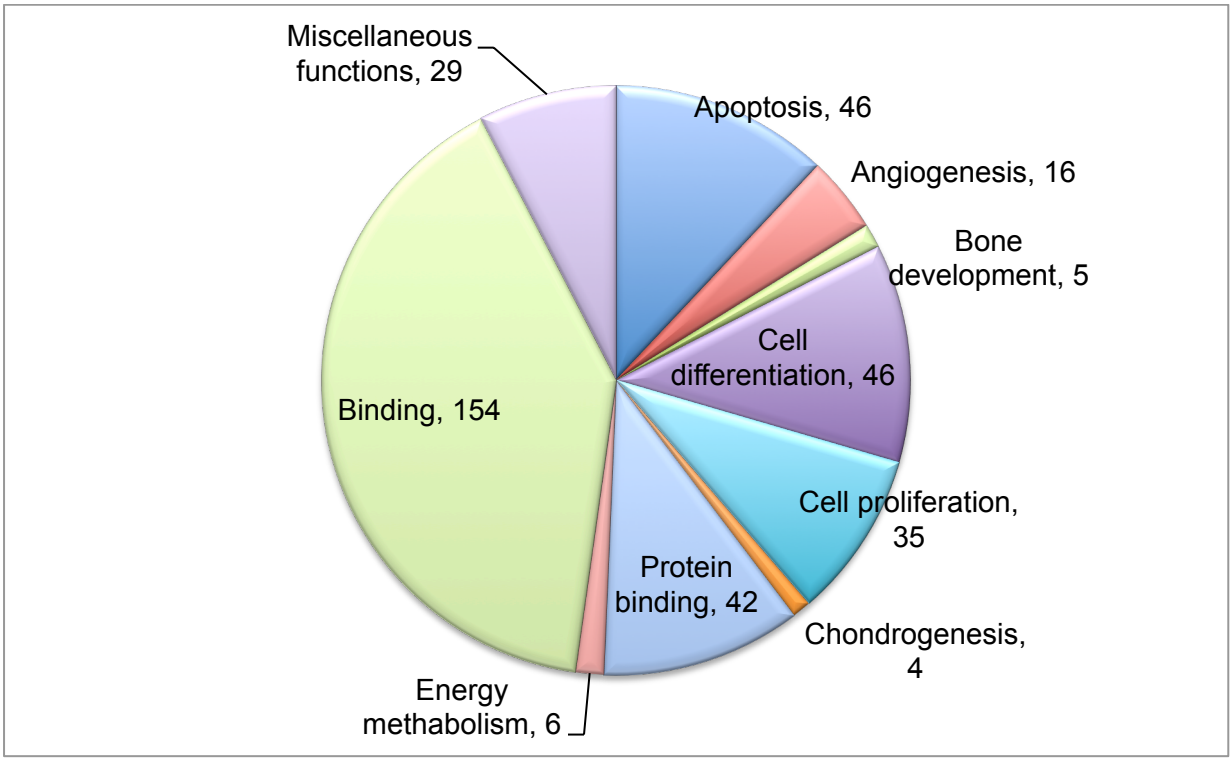

Figure 40. The number of regulated proteins with more than two-fold change in at least one of the extracts sorted regarding their involvement in the biological process. The total amount of proteins in this scheme is 383 (while the total number of regulated proteins is 246), because some proteins are attributed to more than one biological process.

Tables 13-17 contain the list of proteins, regulated by the three extracts, clustered respectively according to their involvement in angiogenesis, apoptosis, response to cell toxicity, bone development and chondrogenesis or cartilage formation.

8.2.1. Regulated proteins involved in chondrogenesis and cartilage formation

Table 16 lists regulated proteins related to chondrogenesis with reproducibility in at least two of three biological replicates.

Four chondrogenesis-related proteins were up-regulated by the extracts: phosphatidylinositol-glycan-specific phospholipase D (GPLD1) was present only in the presence of Mg-alloys, while beta-hexosaminidase subunit beta (HEXB) and transforming growth factor-beta-induced protein ig-h3 (TGFBI) were up-regulated compared to the control.

Table 16. List of significantly up- and down-regulated proteins with all the extracts, involved in chondrogenesis and cartilage formation (P-value< 0.05; min. fold-change of two). Comparison of the mean values of the biological replicates (normalized to Control).

Protein name	Gene name	Regulation	Fold change		
			Mg-10Gd	Mg-2Ag	Mg
Phosphatidylinositol glycan specific phospholipase D	PIGPLD1	Up-regulated	Not detected in the control	Not detected in the control	Not detected in the control
Beta hexosaminidase subunit beta	HEXB		2.23	3.18	3.19
Intercellular adhesion molecule 1	ICAM1		Not detected in control	Not detected in control	Not detected in control
Tenascin	TNC		Not detected in control	Not detected in control	Not detected in control
Vitronectin	VTN		Not detected in control	Not detected in control	Not detected in control
Transforming growth factor beta induced protein igh3	TGFBI		11.22	12.02	11.90
Collagen alpha 3(VI) chain	COL6A3		5.51	3.49	3.92
Basement membrane-specific heparan sulfate proteoglycan core protein	HSPG2		4.10	60	3.18
Fibronectin	FN1		3.78	4.13	3.18
Integrin alpha V	ITGAV		3.65	3.25	3.74
Integrin alpha 2	ITGA2		3.31	2.54	3.24
Beta hexosaminidase subunit beta	HEXB		2.23	3.18	3.19
oxoglutarate 5-dioxygenase 2	PLOD2		2.36	2.09	2.37
oxoglutarate 5-dioxygenase 1	PLOD1		2.01	1.82	2.11
Integrin alpha 5	ITGA5		2.07	1.52	1.86
Collagen alpha 1(I) chain	COL1A1	Down-regulated	2.94	2.44	2.76

In addition, proteins involved in cartilage ECM formation and organization were

up-regulated in presence of Mg: fibronectin (FN1), collagen type VI (COL6), tenascin (TNC), ICAM1, vitronectin (VTN), basement membrane-specific heparan sulfate proteoglycan core protein (HSPG2), procollagen-lysine 2-oxoglutarate 5 dioxygenase 1 and 2 (PLOD1 and PLOD2) and integrins alpha-2 (ITGA2), alpha-V (ITGAV). Collagen type I was down-regulated by all the extracts. Integrin alpha-5 was up-regulated in the presence of Mg-10Gd but not with the other extracts.

With regards to the proteins transcripted from the chondrogenic gene markers previously evaluated (ACAN, COL2A1 and SOX9), its expression was not significantly influenced by the extracts, which correlates with the gene expression observed with HUCPV cells and with ATDC5 after seven days.

8.2.2. Regulated proteins involved in bone development

Two proteins involved in bone development were only expressed in the presence of Mg-alloys (Table 17): prostaglandin G/H synthase 2 (PTGS2) and phosphatidylinositol-glycan-specific phospholipase D (GPLD1). Plastin-3 and collagen alpha-1(I) chain (COL1A1) were down-regulated in HUCPV cells in the presence of Mg-alloys compared to control cells.

The angiogenesis is the process that directs the vascularization of tissues. In the growth plate, angiogenesis plays a key role in coupling chondrogenesis and bone formation.

Table 17. List of significantly up- and down-regulated proteins with all the extracts, involved in bone development (P-value< 0.05; min. fold-change of 2). Comparison of the mean values of the biological replicates (normalized to Control).

Protein name	Gene name	Regulation	Fold change		
			Mg-10Gd	Mg-2Ag	Mg
Prostaglandin G/H synthase 2	PTGS2	Up-regulated	Not detected in the control	Not detected in the control	Not detected in the control
Phosphatidylinositol glycan specific phospholipase D	PIGPLD1		Not detected in the control	Not detected in the control	Not detected in the control
Collagen alpha 1(I) chain	COL1A1	Down-regulated	2.945	2.44	2.76
Plastin 3	PLS3		2.088	1.99	2.06

8.2.3. Regulated proteins involved in angiogenesis

Among the angiogenesis-related proteins, 16 were regulated in the presence of Mg-alloys, and the amount of 15 of these proteins was significantly raised in the presence of at least one of the Mg-alloys. Vascular invasion of cartilage leads to chondrocytes apoptosis, and some of the proteins regulated by the extracts are involved in both processes (angiogenesis and apoptosis).

Apolipoprotein D (APOD), complement C3 (C3), prostaglandin G/H synthase 2 (PTGS2), phosphatidylinositol-glycan-specific phospholipase D (GPLD1), and angiopoietin-related protein 4 (ANGPTL4) were present in at least two biological replicates of the HUCPV cells incubated with Mg-alloys, and not present in the absence of Mg-alloys in control (Table 13).

Table 13. List of significantly up- and down-regulated proteins with all the extracts, involved in angiogenesis (P-value< 0.05; min. fold-change of 2). Comparison of the mean values of the biological replicates (normalized to control).

Protein name	Gene name	Regulation	Fold change		
			Mg-10Gd	Mg-2Ag	Mg
Aminopeptidase N	ANPEP	Up-regulated	6.84	8.34	6.78
Collagen alpha 2(IV) chain	COL4A2		5.80	5.89	4.91
Transforming growth factor beta induced protein igh3	TGFBI		11.22	12.02	11.90
Integrin alpha 5	ITGA5		2.07	1.52	1.86
Prolyl endopeptidase FAP	FAP		2.42	2.17	2.03
Thrombospondin 1	TSP1		2.20	2.02	2.00
ATP synthase subunit beta	ATP5B		2.29	2.66	2.86
Integrin alpha V	ITGAV		3.65	3.25	3.74
Basement membrane specific heparan sulfate proteoglycan core protein	HSPG2		3.18	4.10	2.60
Fibronectin	FN1FN		3.78	4.13	3.18
Prostaglandin G/H synthase 2	PTGS2		Not detected in control	Not detected in control	Not detected in control
Angiopoietin related protein 4	ANGPTL4		Not detected in control	Not detected in control	Not detected in control
Phosphatidylinotsitol glycan specific phospholipase D	PIGPLD1		Not detected in control	Not detected in control	Not detected in control
Apolipoprotein D	APOD		Not detected in control	Not detected in control	Not detected in control
Complement C3	CPAMD1		Not detected in control	Not detected in control	Not detected in control
Ribonuclease inhibitor	RNH1	Down-regulated	1.39	2.011	1.60

Ribonuclease inhibitor (RNH1) was down-regulated in the presence of all Mg-alloys. However, down-regulation of this protein is significant in the presence of Mg-2Ag compared to the other Mg-alloys.

Moreover, Integrin alpha-5 (ITGA5) was significantly up-regulated in the presence of Mg-10Gd, while there was no significant change in the presence of the other Mg-alloys. Thrombospondin-1 (THBS1) was up-regulated with all the extracts.
The up-regulation of the other angiogenesis-related proteins was significant in all Mg-alloys.

8.2.4. Regulated proteins involved in apoptosis

Regulated proteins involved in apoptosis are listed in Table 14. From the total 44 proteins identified, 27 were up-regulated, while 17 were down-regulated in the presence of Mg-alloys. Some of those proteins are also involved in another biological processes, mainly in response to toxicity and angiogenesis. Thus, PAIRBP1 is furthermore involved in angiogenesis, bone development and chondrogenesis, ICAM1 in response to toxicity and chondrogenesis, CPAMD1 in response to toxicity and angiogenesis, PTGS2 in angiogenesis and bone development, ANGPTL4, FNI1FN and TSP1 are furthermore involved in angiogenesis, ITGAV in angiogenesis and chondrogenesis, LAMP1, ASNS and PARK7 in response to toxicity.

Protein S100A-9 (S100A9) was completely absent in the presence of Mg-alloys. Galectin-3 (LGALS3) was down-regulated in the presence of Mg-2Ag, and absent in any biological replicates in the presence of the other Mg-alloys.

Regarding the down-regulated proteins in the presence of the extracts, programmed cell death protein 5 (PDCD5) and PRKC apoptosis WT1 regulator protein (PAWR) are positive regulators of apoptosis.

The regulation of the other apoptotic-related proteins is significant in all Mg-alloys.

Table 14. List of significantly up- and down-regulated proteins with all the extract, involved in apoptosis (P-value< 0.05; min. fold-change of two in all Mg-alloys). Comparison of the mean values of the biological replicates (normalized to Control).

Protein name	Gene name	Regulation	Fold change		
			Mg-10Gd	Mg-2Ag	Mg
Phosphatidylinositol glycan specific phospholipase D	PIGPLD1	Up-regulated	Not detected in control	Not detected in control	Not detected in control
Intercellular adhesion molecule 1	ICAM1		Not detected in control	Not detected in control	Not detected in control
Kininogen 1	KNG1		Not detected in control	Not detected in control	Not detected in control
Complement C3	CPAMD1		Not detected in control	Not detected in control	Not detected in control
TAR DNA binding protein 43	TARDBP		Not detected in control	Not detected in control	Not detected in control
Prostaglandin G/H synthase 2	PTGS2		Not detected in control	Not detected in control	Not detected in control
Niban like protein 1	FAM129B		Not detected in control	Not detected in control	Not detected in control
Angiopoietin related protein 4	ANGPTL4		Not detected in control	Not detected in control	Not detected in control
Serum albumin	ALB		44.83	65.22	61.32
Superoxide dismutase	SOD2		7.42	10.73	10.28
Gelsolin	GSN		2.37	3.53	3.26
Prohibitin	PHB		3.15	3.35	3.88
Prohibitin 2	PHB2		3.08	3.19	3.49
Voltage dependent anion selective channel protein1	VDAC1		2.85	3.38	3.39
ERO1 like protein alpha	ERO1A		3.72	3.46	3.86
Integrin alpha V	ITGAV		3.65	3.25	3.74
Fibronectin	FN1FN		3.78	4.13	3.18
3 ketoacyl CoA thiolase	ACAA2		1.75	2.68	1.97
Complement component 1 Q subcomponent binding protein	C1QBP		1.59	2.14	2.17
Non POU domain containing octamer binding protein	NONO		1.94	2.22	2.43
10 kDa heat shock protein	HSPE1		1.91	2.25	2.22
60 kDa heat shock protein	HSP60		1.91	1.20	2.16
Lysosome associated membrane glycoprotein 1	LAMP1		2.25	2.31	2.51

Prolyl endopeptidase FAP	FAP		2.42	2.17	2.03
Thrombospondin 1	TSP1		2.20	2.02	2.00
Alpha crystallin B chain	CRYAB		1.86	2.43	2.00
Galectin 3	LGALS3	Down- regulated	---	1.65	----
Protein S100 A9	S100A9		---	---	---
Asparagine synthetase	ASNS		4.19	5.09	1077.38
14+3+3 protein beta/alpha	YWHAB		2.76	815.75	2.22
Protein deglycase DJ1	PARK7		617.94	1.82	2.18
Plasminogen activator inhibitor 1 RNA binding protein	PAIRBP1		1.84	1.47	2.11
Y box binding protein 3	YBX3		1.84	1.49	2.43
14 3 3 protein zeta/delta	YWHAZ		2.12	1.72	1.93
14 3 3 protein epsilon	YWHAE		2.22	1.55	2.09
Filamin A	FLNA		1.99	2.08	2.15
Alpha actinin 4	ACTN4		2.21	1.91	2.10
Alanine tRNA ligase	AARS		1.49	2.12	1.80
Reticulon 4	RTN4		1.32	2.16	2.16
Catenin alpha 1	CTNNA1		2.11	2.95	2.40
Programmed cell death protein 5	PDCD5		3.01	2.60	3.67
Keratin. type I cytoskeletal 18	KRT18		2.74	2.33	2.51
Keratin. type II cytoskeletal 8	KRT8		2.71	2.32	2.78

8.2.5. Regulated proteins involved in the cellular response to toxicity

Table 15 contains the nine regulated proteins involved in cellular response to a toxic substrate (present in at least two biological replicates) in the presence of Mg-alloys. Six of the ten proteins were up-regulated while four of them were down-regulated.

ICAM1, Complement C3 (C3), and serum paraoxonase/arylesterase 1 were only present in the HUCPV cells incubated with Mg-alloys.

Table 15. List of significantly up- and down-regulated proteins with all the extracts, involved in the cellular response to toxicity (P-value< 0.05; min. fold-change of two). Comparison of the mean values of the biological replicates (normalized to Control).

Protein name	Gene name	Regulation	Fold change		
			Mg-10Gd	Mg-2Ag	Mg
Intercellular adhesion molecule 1	ICAM1	Up-regulated	Not detected in the control	Not detected in the control	Not detected in the control
Serum paraoxonase/arylesterase 1	PON1		Not detected in the control	Not detected in the control	Not detected in the control
Complement C3	CPAMD1		Not detected in the control	Not detected in the control	Not detected in the control
Lysosome associated membrane glycoprotein 1	LAMP1		5	2.31	2.51
HLA class I histocompatibility antigen	HLAA		2.02	2.26	2.02
Serum albumin	ALB		44.83	65.22	61.33
Bleomycin hydrolase	BLMH	Down-regulated	2.18	1.43	Not detected in control
Asparagine synthetase	ASNS		4.19	5.09	1077.38
Protein deglycase DJ1	PARK7		617.947	1.82	2.18

9. DISCUSSION

Magnesium-based materials are potential candidates as temporary implants in children. The growth plates (hyaline cartilage discs) in growing bones require specific analysis of the possible effects of the Mg implants. Therefore in this study, *in vitro* evaluation of variations in normal chondrogenesis due to the degradation of Mg and two binary alloys (Mg-10Gd and Mg-2Ag) was performed.

9.1. Cell reactions under the influence of Mg-10Gd, Mg-2Ag and Mg extracts

A complete evaluation requires the study of the cell reactions in direct contact with the materials and reactions to the degradation products released into the degradation solution. The last one is relevant due to the diffusion that would take place *in vivo* through the body fluids. Evaluation of Mg, Gd and Ag in the literature is mainly based on the use of salts (*e.g.* $MgCl_2$, $GdCl_3$). Nevertheless, the degradation products can react with the compounds of the degradation solution, altering its composition. As an example, Ca-containing compounds were formed and precipitated in the extracts used in this study, as indicated by the strong decrease observed with the element composition of the media after pre-incubation with the materials (Table 2) and the high presence of Ca observed in the degradation layer (Figure 28). Therefore, previously to the analysis of cell reactions to the three extracts, the effects of $MgCl_2$ and Mg-extract (with the same concentration of Mg) on cell proliferation were compared (Figures 17 and 18). The results indicated a stronger effect of Mg-extract with respect to $MgCl_2$, therefore further evaluation was done exclusively with extracts. The concentration of Mg in the three extracts (Mg, Mg-10Gd and Mg-2Ag) was kept at a concentration of 6.08 mM, since it enhanced cell proliferation and chondrogenic differentiation of the HUCPV cells, as indicated by the higher expression of chondrogenic genes and GAG production (Figures 19 and 20). Thus, with an equal Mg content in the extracts, cell reactions to the alloying elements can be detected.

9.1.1. Cell viability

In order to use the materials as implants, one of the most important requirements is the lack of toxic effects on cells. Viability of both, HUCPV primary cells and ATDC5 cell line was determined after seven days under the influence of Mg, Mg-10Gd and Mg-2Ag extracts. On the one hand, the quantification of living ATDC5 cells showed no significant differences in the viability (an increase of 1.7% when cultured in Mg-10Gd and a decrease of 3.2% when cultured in Mg) (Figure 21). On the other hand, life/dead staining of HUCPV cells showed few dead cells with the three extracts, indicating the lack of cytotoxic effects. Furthermore, less cell density was observed when cultured in the extracts, but this was due to the larger size and round-shaped morphology of the cells compared to cells in control conditions (Figure 31).

9.1.2. Chondrogenic differentiation

After proving the lack of toxic effect on cells, variations in the chondrogenic differentiation were determined with both HUCPV and ATDC5 cells.

In growing bones, bone formation and development starts with the condensation of stem cells [101]. In those condensation areas, a small percentage of cells can undergo osteogenesis (mainly in flat bones of the skull) and become osteoblasts. Those cells are producing an ECM rich in type I collagen. But in growth plates, stem cells undergo chondrogenesis giving rise to the primary cells of the cartilage, the chondrocytes. Chondrocyte differentiation is a process constituted by different stages, each one characterized by variations in cell proliferation, morphology and expression of some transcription factors (as Sox9 and Runx2) and ECM molecules (as Col1, Col2, Col10 and Acan). Therefore HUCPV cells allow the evaluation of the whole process of chondrogenesis and bone formation. HUCPV cells can differentiate in different mesenchyme lineages, including osteoblasts and chondrocytes. Its proliferative and differentiation potential is furthermore higher than in other MSCs, as *e.g.* bone marrow stem cells. Additionally, self-renewal capability is maintained *in vitro* regardless passaging [102]. The ATDC5 cell line is derived from mouse teratocarcinoma cells and characterized as a chondrogenic cell line, which goes through a sequential process analogy to chondrocyte differentiation during endochondral bone formation [103]. ATDC5 cells are a well established *in*

vitro model of endochondral ossification; however, current methods are limited for mineralization studies [84] and transformed cells do not reflect the way cells function *in vivo* as closely as primary cells. The use of both cell types allows a deeper and easier analysis of the effects of Mg-materials on chondrogenic differentiation and guaranties the reliability of the results obtained.

Cartilage tissue enlarges during chondrocyte proliferation and ECM production. In the central areas of the growth plate, chondrocytes undergo hypertrophy, which implicates cease of proliferation, an increase in cell size and changes in the composition of the ECM. Col10 becomes then one of the main components of ECM [64]. In articular cartilage, chondrocyte proliferation is strongly limited, and cell hypertrophy can give rise to cartilage degeneration. Nevertheless, in growth plate cartilage, hypertrophy is required for endochondral ossification that consists of mineralization of the matrix and blood vessel formation within hypertrophic cartilage (during fracture healing or bone elongation). Therefore, terminal maturation or hypertrophy of HUCPV and ATDC5 cells would resemble the normal process of endochondral ossification in the growth plate.

Sox9 expression is essential for chondrocyte proliferation, differentiation and maturation [104, 105], and it also avoids chondrocytes to become hypertrophic [106, 107]. Sox9 has also been suggested to direct cell condensation and cell survival in the condensation stage [108]. This gene furthermore stimulates the expression of other cartilage matrix genes as Col2 and Acan [109]. Col2 and Acan are the main components of chondrocyte ECM, being the most recognized markers for cartilage tissue. The results obtained with ATDC5 cells showed a clear correlation between Sox9 and Col2 expression after seven and 14 days. Runx2 is a transcription factor involved in different cell pathways. While it has been shown to be a pre-osteogenic marker, indicating that certain degree of ossification is starting to take place, it is more recognized as a marker of chondrocyte hypertrophy [110-112]. During chondrocyte maturation, the increase in ColX and Runx2 has been reported to be a marker of advanced chondrocyte hypertrophy [113, 114], which takes place prior to endochondral ossification *in vivo*. ATDC5 chondrocytes showed a very similar pattern of expression of ColX and Runx2 at all the analysed time points. As a marker of bone cells and mineralization of ECM, Col1 gene expression was also

evaluated [115] which showed a down-regulation of this gene under the influence of the extracts. Additionally, an increased Col2/Col1 ratio when cells were cultured in the extracts indicate that chondrogenesis and not osteogenesis is taking place [116,117]. All the extracts increased the expression of chondrogenic markers compared to the control in growth medium, although in Mg-10Gd the effect was delayed until the last time point. After 21 days of culture, Mg-10Gd induced the highest expression of Acan. Nevertheless, the influence of Mg and Mg-2Ag became less notable with time, while Mg-10Gd showed significant induction of cell maturation and hypertrophy, which increased as time went by.

Based on the high expression of hypertrophic markers observed with Mg-10Gd extract, increased expression of Col1 would also be expected, as marker of mineralization. However, Col1 was inhibited by the three extracts, and contrary to the hypertrophic markers, Mg-10Gd extract induced down-regulation of this gene.

Gene expression of chondrogenic markers by HUCPV cells showed no significant differences compared to the control, apart from an increased expression of COL2 and SOX9 by Mg. As occurred with ATDC5 cells after 21 days, an increased expression of ACAN was observed in cells under the effects of Mg-10Gd (being the highest gene expression among all the conditions). An up-regulation of pre-osteogenic genes was induced by the three extracts, being more notable with Mg-10Gd than with the other two extracts, which suggests an induction of chondrocyte maturation and beginning of osteogenesis. Differently to what was observed in ATDC5 cells, expression of COL1 was up-regulated by the three extracts. In agreement with the high expression of ACAN found in both cell types cultured in Mg-10Gd extract, GAG production was increased in HUCPV micromasses cultured with Mg-10Gd compared to the control condition. Mg-2Ag also induced synthesis of GAG, while Mg showed a reduction of its content.

The examination of pH fluctuations during 21 days of ATDC5 cells culture under the influence of extracts was carried out due to strong variations seen in the color of the culture media already after three days. The pH values indicated that the strongest fluctuation occurred with Mg-10Gd extracts (Figure 23). Optimal pH for most of the cell types to grow in cell culture is about 7.4. A decrease of pH could reflect an increase in cell metabolism. Therefore right after cell seeding, a decrease is

expected due to the high initial cell proliferation. Even though the pH in the extracts was initially higher than in control medium, the fast reduction during the first three days indicated a high cell metabolism and proliferation, confirming the lack of toxicity of the extracts. Extracellular pH of chondrocytes *in vivo* is more acidic than in the rest of the tissues; a pH of 6.9 has been registered in the ECM of articular cartilage. Among others, a reason for the low pH in cartilage is the positive charge of proteoglycans, that attract and bind high number of negative charges modifying the extracellular ionic composition [118]. Hence, the gradual decrease of pH showed in Mg-2Ag and Mg extracts after 6 days could indicate an increase in ECM synthesis. Nevertheless, Mg-10Gd exhibited a significantly stronger drop of pH than in the other conditions after three days, reaching acidic values, and remained acidic until 13th day of culture. In contradiction, the optical microscopy images of ATDC5 cells cultured in Mg-10Gd extracts showed similar confluence as in the other conditions after six days. After 12 days an increase in cell size is appreciated while cell confluence remained constant, so that cell proliferation does not explain the decrease of pH in that extract. A higher production of ECM synthesis would not completely explain the drop in pH, because the same reaction would be expected under differentiation conditions. For this reason, the effects of Gd on cell metabolism (both as $GdCl_3$ and as Mg-10Gd extracts), with a concentration of 0.5, 5 and 50 µM were evaluated to prove if the effects were due to alterations in the metabolism or not. Results showed an induction of the metabolic activity of HUCPV cells by Gd, after 24 and 72 hours (Figure 30), suggesting that the reason for the acidic pH in Mg-10Gd relies in the hypertrophic stage of the cells: while in articular cartilage hypertrophic chondrocytes reduce their metabolic activity, during development, growth or bone repair, mature hypertrophic chondrocytes exhibit a high metabolic activity that is also related with an increase in ECM production [119]. After 21 days, the pH was restored in all the extracts until almost the same values as those in control condition. This pH regulation could be due to the action of the buffering system of the medium and to the cells activity, showing the capability of the chondrocytes to osmoregulate the extracellular pH (in the extracts). Those results indicate that Mg extract increases cell proliferation but decreases chondrogenic potential of HUCPV and ATDC5 cells. On the other side, Mg-10Gd and Mg-2Ag induce chondrogenic differentiation of both cell types. Mg-2Ag also enhances cell proliferation, while Mg-10Gd decreases it.

In the diluted extracts used in this experiments, the only relevant difference of the composition is the presence of Gd or Ag in Mg-10Gd and Mg-2Ag respectively (table 2). Therefore, common effects from the three extracts regarding control in growth medium are attributed to Mg itself, while differences on ATDC5 with Mg-10Gd and Mg-2Ag regarding Mg can be attributed to the alloying elements.

Accordingly to the presented results, previous studies with ATDC5 cells have shown that a concentration of 4.2 mM of Mg^{2+} ion reduces the effects of Ca ion excess and inhibitis mineralization of ATDC5, by reducing the effects of Ca ion excess [120]. The explanation is that as an antagonist for Ca^{2+}, high concentration of Mg^{2+} could lead to changes in the intracellular Ca^{2+}/Mg^{2+} balance, interfering in Ca^{2+}-dependent cellular processes, such as extracellular matrix mineralization. High Mg^{2+} (>1.3 mM), was proven to negatively influence osteogenesis and mineralization of stem cells in a dose dependent manner [121], and chondrogenic induction of stem cells [122]. Furthermore, a reduction of osteoblasts intracellular Ca^{2+} is produced due to the competition for the same transporters, which inhibits osteoblast mineralizing activity *in vitro* [123, 124]. Inversely, when using Mg-based materials both *in vitro* (instead of extracts) and *in vivo* (bone implants) mineralization and bone apposition is observed. The cause for such difference between the effect of Mg-based materials and Mg^{2+} ions could be the precipitation of calcium phosphate promoted by the materials over its surface [4, 125-127].

The precipitation of Ca on the samples during immersion in culture medium is indicated by the reduction in Ca content in the extract regarding the control without materials. Nevertheless, the reduction of Ca in the extract was restored by diluting in culture medium, so that no additional effects due to the variation on this ion should be considered. Regardless of the hypertrophic phenotype appreciated in HUCPV cells, the low expression of Col1 in ATDC5 cells confirms the inhibitory effect of Mg on the mineralization of chondrocytes. The differences observed between the results obtained with ATDC5 and HUCPV are due to the cell nature (mouse vs human and cell line vs primary cell). As previously mentioned in the introduction section, human primary cells better resemble the physiological conditions and therefore the results are more reliable than the ones obtained with the murine cell line.

Accordingly to this study, Mg (in form of extract) shows no toxic effects at doses used in this work, increased cell proliferation and a reduction of terminal differentiation and mineralization of stem cells and chondrocytes.

Toxic effects of Ag on articular chondrocytes are detected at doses approximately five times higher than the one present in the extract (5 mg/L) [128]. Interestingly, when cells were in a 3D model (as with HUCPV micromasses) the toxic limit increased to almost double concentrations (9 mg/L) [128]. The optical images taken during the whole culture period of ATDC5 chondrocytes showed no toxic effects. The initial drop on the pH of Mg-2Ag and further gradual decrease until reaching levels similar to the ones in maintenance conditions, is also indicating high cell proliferation. The cell growth of HUCPV micromasses is increased regarding control conditions and the other extracts. Gene expression under the influence of Mg-2Ag and Mg showed no significant differences in both cell types. Nevertheless, the GAG production on HUCPV micromasses was significantly higher than with the other conditions.

Studies specifically investigating the effect of silver on stem cell differentiation are rare [129-131] and controversial. On the one side, some have shown no effects on stem cell differentiation even at toxic concentrations. [132]. Thus, Ag concentrations close to the ones which were used in this study showed no effects on morphology and Acan production during chondrogenesis of stem cells [49, 131]. On the other side, increased expression of Acan, Col2 and Sox9 during stem cell differentiation has been reported [133], which agrees with the increased expression of Col2 in ATDC5 cells and the highest GAG production in HUCPV cells after 21 days of culture in Mg-2Ag extracts. In summary, the only significant difference found between Mg-2Ag and Mg is the higher cell proliferation and GAG production in HUCPV micromasses. Further studies are necessary in order to clarify those findings.

The strongest effects on cell behavior regarding any other condition were found with Mg-10Gd extract. As previously discussed, the decrease in the pH of Mg-10Gd extracts by ATDC5 is due to an increased metabolic activity. In accordance with the hypertrophic effect we observed, a low pH has been associated with a faster chondrogenic differentiation of MSC [134]. *In vivo*, the pH also exhibits focal

variations in the growth plate, being higher in central regions of maturing and early hypertrophic chondrocytes (>8) and lower close to the late hypertrophic and calcifying cells (6.5-7.2) [135]. Gadolinium has been associated with an enhanced cell cycle progression, by the up-regulation of proteins involved in the G1/S transition [44, 45]. Additionally, the decrease in cell proliferation and increased synthesis of ECM observed with HUCPV micromasses is characteristic of stem cells chondrogenesis, which suggests that Mg-10Gd extracts induce chondrogenic differentiation.

Gd action starts extracellularly, activating an extracellular signal-regulated kinase (ERK) member of mitogen-activated protein kinas (MAPK) and phosphoinositide 3-kinase (PI3K) signaling cascade. The increase of cellular activity is caused by the ion species and not by the nanoparticles [46]. But as ion, Gd^{3+} in the blood stream binds phosphates, citrates, hydroxides or carbonates and form precipitates [47]. As in the blood, under physiological conditions *in vitro* Gd was proved to form those precipitates that will locate in contact with the cell surface. The possible reason is that such precipitates containing Gd would release ions depending on thermodynamic conditions, and due to the proximity with cell surfaces, would enhance the effect of the extracellular Gd^{3+} ions [44]. This hypothesis explains the strong effect obtained with the extract even though Gd content is really low (1.27×10^{-3} mg/mL).

Mg-10Gd induced an increase in the production of GAG and ACAN expression. Similarly, Gd (as Gadiodiamide) has been proven to enhance proteoglycan production until concentrations of 20 mM [136]. Articular chondrocytes detect and react to mechanical, ionic or osmotic signals by modifying their metabolic activity. This is important *in vivo* because it allows the regulation of the synthesis and degradation rates as well as varying the composition of the ECM [137] but, how is it related to the results showed in this work?. The answer could be the increased osmolarity produced as a result of the degradation of the materials, and the osmotic stress this could cause to the cells. *In vivo,* mechanical compression on the cartilage will increase interstitial osmotic pressure and this will give rise to the activation of osmotic recovery pathways that require ion transport. As an example, the response to the hyper-osmotic stress and for regulating cell volume, Ca influx occurs from the

extracellular space in order to recover cell morphology. The transduction of mechanical or osmotic stress is carried out by mechanosensitive channels (MC) [138]. Those MC are also present in growth plate chondrocytes reacting to mechanical strains [139, 140]. Apart from interfering with other channels, Gd^{3+} has the capability of inhibiting mechanical responses blocking most of MCs already at low concentrations (lower than 0.1 mM) [41, 42]. It is possible that the action of Gd^{3+} is not on the channel protein at all, but on the surrounding lipids, pulling them tightly together so the membrane surrounding the channel is rigid or somehow unable to support a change in channel dimensions [141, 142]. Gadolinium ions can furthermore block L-type Ca^{+2} voltage channels present in chondrocytes, when undergoing mechanical pressure, but not under resting conditions. This results in the decrease of Ca influx also under osmotic stress, but not under normal conditions [43]. Even though Ca is indispensable for chondrocyte maturation, the intracellular concentrations of this ion should be kept much lower than outside so that mineralization is avoided [143]. These channels should be taken into account since during material degradation the osmolality is increased, and in chondrocytes hyperosmotic stress cause the same effects as mechanical load. Both mineralization of adjacent areas and increase of osmotic stress have been furthermore related to an increase in ROS species and enhancement of cell apoptosis in chondrocytes [144, 145]. ROS species are known to regulate inhibition of cell proliferation and to induce hypertrophy of chondrocytes. Reactive oxygen species induce chondrocyte hypertrophy in endochondral ossification [144]. Taking together, this information would explain not only the hypertrophic effect of Mg-10Gd extracts on ATDC5 chondrocytes and the stronger effect inhibiting mineralization than in Mg extracts, but also an inhibition of apoptosis: in Mg-10Gd, Mg reduces Ca influx and therefore mineralization, but Gd is also playing an important role in this regard. Even though ROS species production due to osmotic stress is enough to induce hypertrophy of ATDC5 chondrocytes, Gd seems to inhibit the apoptotic effect expected from those species. Gadolinium effects can therefore be especially relevant in cartilage application during first periods of direct contact test with materials (*in vitro*) or after implantation (*in vivo*), when osmolality is increased due to material degradation, so that osmotic stress will take place.

9.1.3. Proteomic evaluation

A detailed evaluation of the proteins regulated in presence of Mg-extracts allowed the confirmation of the results previously described, and provided additional information about the mechanisms underlying its chondrogenic potential.

246 proteins were regulated under the influence of Mg extracts. Most of those proteins were extracellular, membrane, cytosolic and cytoskeletal (Figure 39). Extracellular proteins were mostly up-regulated, probably due to the synthesis of ECM and reorganization needed during chondrogenesis and cartilage formation. Membrane proteins were also mostly up-regulated, which is explained by the need of transporters for Mg and Mg-alloys degradation products uptake. (Figure 40) shows the most affected biological processes. The highest number of regulated proteins were involved in cell binding, differentiation and apoptosis, followed by cell proliferation and miscellaneous function (proteins with diverse functions). To a lesser extent, proteins involved in angiogenesis, energy metabolism, bone development and chondrogenesis were influenced by the extracts. Some of the proteins have been related with all the functions here described (as phosphatidylinositol-glycan-specific phospholipase D). Therefore conclusions regarding their role cannot be taken without further investigations.

Proteins involved in apoptosis and cell response to toxicity:

In agreement with the effects of the extracts on cell viability previously discussed, the regulation of proteins involved in apoptosis and cell response to toxicity also revealed the lack of toxic effects. Apoptosis is a tightly regulated process, inevitable and essential during development, particularly during formation of articular cartilage and endochondral ossification of growth plate [146]. Apoptosis also happens in osteoblasts via fracture healing process [147-151]. Nevertheless, increased apoptosis in native cartilage is associated with matrix degradation. Induction of MSC chondrogenesis *in vitro* using micromass formation models increases the possibility of apoptosis due to the severe hypoxic conditions that cells suffer in the center of the spheres. Nevertheless, some differences in protein expression (involved in both positive and negative regulation of apoptosis) were found due to the action of the extracts (Table 14). On the one hand, nine apoptosis-related proteins were found only in presence of extracts: five were stimulators of apoptosis (complement C3

(C3), bradykinin, prostaglandin G/H synthase 2, TAR DNA-binding protein 43 (TARDBP), and phosphatidylinositol-glycan-specific phospholipase D (GPLD1)) and four inhibitors (APOE, ICAM1, niban-like protein 1 (FAM129B), and angiopoietin-related protein 4 (ANGPTL4). On the other hand, two proteins that stimulate apoptosis were down-regulated, protein S100A-9 (S100A9) and galectin-3 (LGALS3). Protein S100A-9 was completely absent in the presence of Mg-alloys. This protein also has a role in actin cytoskeleton reorganization, proinflammatory response and oxidant-scavenging (uniprot). Galectin-3 (LGALS3) was down-regulated in the presence of Mg-2Ag, and absent in the presence of Pure-Mg and Mg-10Gd. Galectin-3 (LGALS3) is also found to be a potent inhibitor for osteoclastogenesis *in vitro* [152]. Those results show a clear influence on apoptosis and suggest a reduction of cell death by the extracts.

As indicated in Table 15, six from the nine regulated proteins showed increased expression in the presence of extracts. From those six, four proteins were not found in the absence of the extracts, which might suggest a response of the cells toward toxicity; however, these proteins have other roles in the cells. For instance, complement C3 (C3) is one of the stimulators for angiogenesis and ICAM1 is involved in cell migration and adhesion, therefore reinforcing cartilage and bone repair.

Proteins involved in cell metabolism:

Regarding the proteins involved in cell metabolism, an up-regulation of ATP synthase mitochondrial, subunits alpha (ATP5A1), gamma (ATP5C1), beta (ATP5B), O (ATP5O), and ATP synthase F(0) complex subunit B1 (ATP5F1), mitochondria was observed under the influence of the extracts, which is associated with increased cell metabolism. Those results show that not only Mg-10Gd, but also Mg-2Ag and Mg are increasing cell metabolism (the two last ones to a lesser extent). Those results correlate with the increased metabolic activity observed with ATDC5, detected by the strong decrease in pH during culture with Mg-10Gd, and with HUCPV cells by MTT assay. Magnesium ion enhances the activity of ATP synthase [153], the enzyme responsible for ATP generation. Therefore, higher metabolic activity is expected for cells influenced by Mg. Similarly, up-regulation of voltage-dependent anion-selective channel protein 1 (VDAC1) was induced by the extracts.

This protein interacts with hexokinase and creatine kinase to convert newly generated ATP into high-energy storage molecules. Therefore the overexpression of VDAC1 is also associated with high metabolically active and energy-demanding cells [154].

Proteins involved in cholesterol metabolism were strongly up-regulated by the extracts (see supplementary Table 1). Phosphatidylcholine-sterol acyltransferase (LCAT) showed two-fold higher expression with Mg-10Gd and Pure-Mg compared to Mg-2Ag. This protein is the central enzyme involved in the extracellular metabolism of lipoproteins. Apolipoprotein A-I (APOA1) is the most potent phosphatidylcholine-sterol acyltransferase activator in plasma (although it can be also activated by APOE, APOCI and APOAIV). All those apolipoproteins involved in cholesterol efflux (as well as additional ones as APOD) were strongly up-regulated with the three extracts. Lack or deficiency of phosphatidylcholine-sterol acyltransferase (LCAT) and APOI gives rise to cartilage degeneration and the development of osteoarthritis (OA) [155, 156] making interesting future investigations about the possible effects of the materials on cartilage regeneration.

Some of the proteins were up- or down-regulated exclusively by an extract or showed significant differences in one extract (see supplementary tables 2, 3 and 4). Among those proteins, glutaminyl-tRNA synthetase showed a three times higher up-regulation with Mg-10Gd than with Mg-2Ag and Mg extracts. Interestingly, this enzyme is required for protein synthesis (UniProt) and its up-regulation is again confirming a higher metabolic activity in cells influenced by Mg-10Gd extracts.

Proteins involved in chondrogenesis and cartilage formation:

Although the proteomic analysis did not show significant regulation of the proteins encoded by the chondrogenic gene markers here evaluated (probably because of the two-folds filter used), variations in the expression of other proteins involved in chondrogenesis and cartilage formation were detected. The results confirmed an inductive effect on the up-regulation of proteins involved in cartilage development (both ECM integrity and ECM-cell adhesion). Among the proteins detected, tenascin (TNC) is notably up-regulated during cartilage development, and it is involved in ECM remodeling and cell differentiation [157], therefore its up-regulation is desirable in growing bones, and probably it would not influence the normal growth if the

implant induces its up-regulation. Basement membrane-specific heparan sulfate proteoglycan core protein (HSPG2) is involved in the metabolism (synthesis and catabolism) of GAG, one of the main components of cartilage ECM. It is required for cartilage development, where it plays a role in ECM organization. ICAM1 has multiple functions, being relevant in cell adhesion (specifically integrin-mediated adhesion). Its expression in human chondrocytes can be induced by exogenous Interleukin 1 alpha (IL1- alpha), which was added to the culture medium in order to induce chondrogenesis [158]. Those results suggest an increased effect of IL1-alpha in the presence of Mg-extracts or a direct effect of the Mg^{2+} ions on ICAM1 expression. In one way or another, the enhancement of cell adhesion would be relevant in the cells surrounding the tissue, therefore, evaluation of the expression of ICAM in bone would be interesting in order to predict the cell-material interaction after implantation. Similarly, another up-regulated group of proteins, the integrins, are involved in several roles, like cell adhesion and differentiation. They are responsible for primary adhesion of cells to orthopedic or dental implants, therefore addition of Mg^{2+} ions to the surface of biomaterials enhance cell-material interaction, reducing the possibilities of implant rejection by the body [159]. Hence, it seems that Mg-based implants would favor the integration of the implant on the surrounding tissues, as the cortical bone in contact with the extremes of the intramedullary nails. Furthermore, the integrin family of cell surface receptors appears to play a major role in mediating cell-matrix interactions that are important in regulating cartilage development and repair. Integrins and cell-matrix interactions have been shown to be involved in chondrogenesis of MSC [157] and enhance MSC attachment to endochondral defects (enhancing its repair). Additionally, integrins avoid apoptosis. Up-regulation of integrins by Mg extracts seems therefore to be beneficial, not only for enhancing chondrogenesis of HUCPV cells, but also for generating a good quality cartilaginous matrix. In native cartilage, chondrocytes express several members of the integrin family which can serve as receptors for relevant proteins in the structure of the ECM: Integrin alpha-5 is a receptor for fibronectin; integrin alpha-1, alpha-2 and alpha-10 are receptors for types II and VI collagen; integrin alpha-6 is a receptor for laminin and integrin alpha-V is a receptor for vitronectin (VTN) and osteopontin. Among all those proteins, Mg-extracts induced the up-regulation of integrin alpha-2 (ITGA2), integrin alpha-5 (ITGA5) (only significant up-regulation with Mg-10Gd) and

integrin alpha-V (ITGAV), as well as its corresponding signaling proteins, type VI collagen (COL6), fibronectin (FN1) and vitronectin (VTN), respectively. Since divalent cations, including Mg^{2+}, are ligands for integrins and activate them, an increased cell adhesion of HUCPV cells is expected under the influence of the three extracts.

The previously mentioned integrin-signaling proteins are important components of the cartilage ECM. Vitronectin interacts with GAG and proteoglycans and serves as a cell-to-substrate adhesion molecule. Furthermore, it inhibits the membrane-damaging effect of the terminal cytolytic complement pathway (UniProt). Fibronectin is involved in early chondrocyte differentiation events after birth being up-regulated since the condensation of stem cells to form the growth plate [160]. Type VI collagen is found in connective tissues. A notable up-regulation of this protein has been reported during early stages of human MSC (after 10 days), possibly due to the influence of this protein on Sox9 [161]. A schematic representation of how the extracts are inducing chondrogenic differentiation is illustrated in Figure 41. Two additional chondrogenesis-related proteins were up-regulated by the three extracts: phosphatidylinositol-glycan-specific phospholipase D (GPLD1) (not detected in control samples), which stimulates chondrocyte differentiation, and beta-hexosaminidase subunit beta (HEXB), which has a role in the catabolic process of chondroitin sulfate.

The use of Mg-extracts on HUCPV cells during chondrogenesis also induced the up-regulation of transforming growth factor-beta-induced protein ig-h3 (TGFBI), a protein involved in the cell-collagen interaction and important for ECM remodeling during chondrocyte differentiation. Furthermore, the overexpression of Beta ig-h3 positively enhances the proliferation and chondrogenic potential of hSD-MSCs [162]. It has been shown that beta ig-h3 induces up-regulation of integrins [163]. Therefore it is feasible to assume that Mg extracts induce an enhancement of beta ig-h3 protein, that would up-regulate integrin production, and subsequently, integrin-mediated cell adhesion and chondrogenesis. In addition, TGF-beta induces expression of procollagen-lysine 2-oxoglutarate 5-dioxygenase 1 and 2 (PLOD1 and PLOD2) protein up-regulated in regenerated cartilage *in vivo* (regarding the natural cartilage).

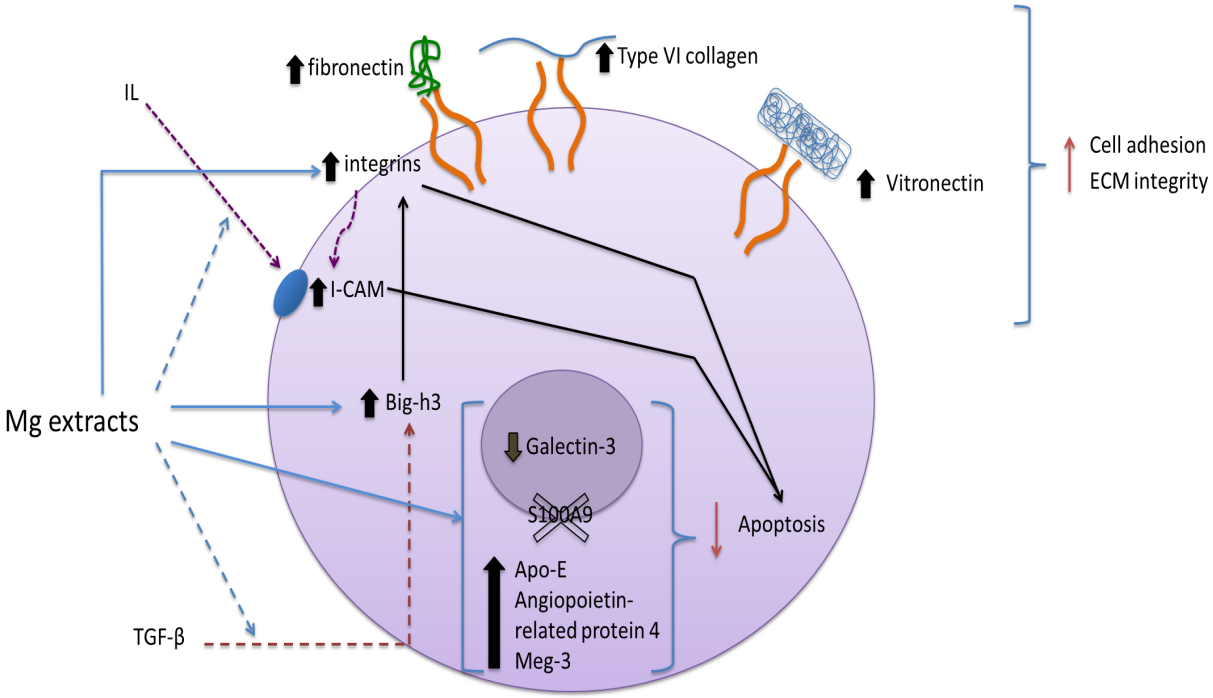

Figure 41. Schematic representation of the influence of Mg extracts on the proteins involved in chondrogenesis and cartilage formation. TGF-β: transforming growth factor beta; IL: interleukin; I-CAM: intercellular adhesion molecule; Big-h3: transforming growth factor-beta-induced protein ig-h3; Apo-E: apolipoprotein E; Meg-3: Very putative protein from MEG3 locus.

All those up-regulated proteins indicate that Mg-based materials have a strong potential to be use in cartilage regeneration or repair. The effect of the up-regulation of those specific proteins on growth plate (and bone growth) should be evaluated *in vivo*, in order to determine if an increased chondrogenesis is also taking place and if it has any undesirable consequence on bone elongation.

Angiogenesis and bone development:

Angiogenesis is a fundamental component of bone repair due to the development of blood vessels in the fracture callus [164] and a vital part of bone formation [164, 165]. Hypertrophic cartilage produces angiogenic stimulators [166-168], unlike angiogenesis inhibitors, which are secreted by immature chondrocytes [169, 170]. The three processes, chondrogenesis, angiogenesis and bone formation are closely related. Hence, some of the regulated proteins are involved in all of them (*e.g.* Integrin alpha-5 and Collagen alpha-1(I) chain).

Up-regulation of 15 of the 16 regulated proteins involved in angiogenesis shows a predictable progression of chondrogenesis followed by bone formation in the

presence of Mg-alloys *in vivo*. Nevertheless, thrombospondin-1 (THBS1) up-regulation could be of interest for further investigations since it has been shown that this protein inhibits vascular endothelial growth factor (VEGF)-induced migration in human microvascular cells [171].

Apart from its role in cartilage development, collagen alpha-1(I) chain is involved in bone trabecula formation. The down-regulation of this protein together with the lack of effect on Col II production in presence of Mg-extracts is indicating an increase in the ratio of Col II/Col I, which is characteristic in cartilage tissue. Plastin-3 (PLS3) is involved in bone development, and its down-regulation in the presence of Mg-alloys might avoid cartilage mineralization. Consequently, the down-regulation of those two proteins is beneficial in order to keep the chondrogenic phenotype of the differentiated HUCPV cells. Differently, two proteins that enhance bone mineralization, prostaglandin G/H synthase 2 (PTGS2) and phosphatidylinositol-glycan-specific phospholipase D (GPLD1), were only detected in the presence of extracts. Those results suggest a stimulation of bone formation by the extracts, but prostaglandin G/H synthase 2 (PTGS2) is also associated with increased cell adhesion, phenotypic changes and resistance to apoptosis.

9.2. Cell reactions in direct contact with Mg-10Gd, Mg-2Ag and Mg materials

The previous section addressed the effects of the degradation products contained in the extracts. In this section, the cell reactions in direct contact with the materials will be discussed. In the direct contact test, the degradation rate and homogeneity, as well as the composition of the degradation layer will be the main factors determining cell adhesion, distribution and changes in chondrocytes phenotypes. This method resembles better *in vivo* conditions, even though *in vivo* higher cell resistance and lower degradation rate is expected [172].

Although the degradation rate seems to be the most determining factor for cell reactions, the best cell coverage and matrix production was obtained with Mg-10Gd, the materials that exhibited the highest degradation rate, followed by Mg-2Ag, with the lowest degradation rate. Magnesium showed the lowest cell presence and exhibited a less homogenous distribution on the surface.

The degradation layer of Mg-10Gd and Mg-2Ag exhibited a higher tendency to precipitate Ca and P (probably as hydroxyapatite) than Mg, which also correlates with the high levels of Ca found in Mg extracts (non-diluted) regarding the other extracts. Magnesium samples showed higher content of O compared to the other materials, which suggests the main components of the corrosion layer are $Mg(OH)_2$ and MgO.

Even though the content of Ca and P is higher in Mg-2Ag than in Mg-10Gd, a thicker and more intense layer of Ca below the cells in Mg-10Gd samples was found. Furthermore, in Mg-10Gd extracts a strong drop of Ca and P is observed after 72 hours, also indicating a higher precipitation. Differently, Mg samples induce a low precipitation of Ca and phosphorous. Cells on Mg samples exhibited the lowest cell density although the degradation rate was lower than in Mg-10Gd and similar to Mg-2Ag, and in the case of ATDC5 furthermore the cell presence was limited to some areas. Therefore, Ca deposition on the surface may also be contributing to form a degradation layer that leads to a more homogenous degradation.

The composition of the degradation layer gives also relevant information about the degradation behavior. Gadolinium and Ag^+ cations incorporated in the degradation layer would help to have a more homogenous degradation (independently from the rate), and therefore a better distribution of cells in Mg-10Gd and Mg-2Ag samples. Those cations can interact with Cl^- anions (forming $GdCl_3$ and $AgCl_3$), slowing down the harmful effect of Cl^- on the hydroxide layer formed during Mg-materials degradation [19]. This would explain why the highest degradation rate corresponds with the highest and most homogenous cell coverage of the samples in the Mg-10Gd samples.

Although Mg-10Gd samples contain 10% of Gd, and Mg-2Ag 2% of Ag, the content of Gd detected in the extracts was lower than the content of Ag (1.27×10^{-3} and 11×10^{-3} mg/mL respectively). Furthermore, the degradation layer of Mg-10Gd samples shows a high content of Gd while in Mg-2Ag degradation layer a low content of Ag is observed. Both findings indicate that most of the Gd is being retained in the degradation layer while the Ag is being released. This could be due to the fact that Gd^{3+} ions can substitute Mg^{2+} cations in the brucite lattice [173]. The high content of Gd in the layer has also effects on cell behavior: higher cell and ECM

density on Mg-10Gd may also be enhanced by the higher amount of Mg^{2+} ions released into the medium, and to the high availability of Gd^{3+} ions present in the degradation layer. Such Gd^{3+} ions are in direct contact with the cell surface, increasing the effects of Gd on the membrane (channels) or the ion transfer of the ion (as previously explained with nanoparticles). As a result micro-cell aggregates of chondrocytes as the ones found on Mg-10Gd with both cell types can form, enhancing the synthesis of cartilaginous ECM and neo-cartilage formation (both *in vitro* and *in vivo*) [174]. Additionally, an increase in the expression of chondrogenic markers (Acan, Col2, Sox9) was observed when HUCPV cells were cultured on those samples. Therefore, Mg-10Gd samples seem to induce spontaneous chondrogenic differentiation of ATDC5 chondrocytes seeded on their surface.

Finally, the content of Ag is localized in some areas of the degradation layer of Mg-2Ag samples while in Mg-10Gd, the Gd is homogenously distributed throughout the whole layer. This fact could be contributing to the lower coverage (even if not too relevant) on Mg-2Ag than in Mg-10Gd.

10. SUMMARY AND FUTURE WORK

The three materials are well tolerated by both, HUCPV and ATDC5 cells. Magnesium and Mg-2Ag extracts showed no significant effects apart from a slight increase in chondrogenic differentiation. Mg-10Gd extracts induced chondrocyte maturation or hypertrophy. Magnesium samples exhibited the lowest cell coverage among the three materials, probably due to a non-homogenous degradation behavior. Mg-10Gd materials showed good cell attachment, high proliferation and wide coverage of the materials surface, followed closely by Mg-2Ag. The tree materials exhibited a chondrogenic effect on the cells in direct contact. Furthermore, Mg-10Gd samples induced cell aggregates formation and stimulated matrix production. Accordingly, many proteins were regulated in response to Mg-alloys. Regulation of specific proteins confirmed a positive effect on chondrogenesis (i.e. integrins, Beta Ig-h3, fibronectin, vitronectin, calmodulin, nonO protein) and cell viability (apoptotic-related proteins), as well as possible influence on reducing or inhibiting OA (cholesterol metabolism-related proteins and SERPINE2) and acute-phase response (APOA2, ATIII and Alpha-1-antitrypsin).

Cell maturation and hypertrophy is a normal and necessary process in growth plate. Nevertheless, an accelerated growing or maturation in the growing skeleton could result in adverse effects i.e. legs length discrepancy or premature closure of the physis. Thus, these results need to be proved in animal models and in long lasting experiments, evaluating possible disturbances on the *in vivo* growth process as well as the long-term effects of the alloying systems.

Furthermore, the chondrogenic effect exhibited by the three materials, which was not significant evaluating only the gene expression, but was detected from the proteomic study, indicates possible potential for an additional application: treatment of cartilage damage due to trauma or degeneration and application as implants for growth plate fractures. Therefore, *in vitro* investigations of the role in diverse pathways of those and other cartilage or chondrogenic-related proteins are highly recommended, in order to get in-depth insight into the effect of Mg-alloys on stimulating/inhibiting various processes involved in cartilage and bone formation *in vivo.*

11. BIBLIOGRAPHY

[1] Kraus T, Fischerauer SF, Hanzi AC, Uggowitzer PJ, Loffler JF, Weinberg AM. Magnesium alloys for temporary implants in osteosynthesis: in vivo studies of their degradation and interaction with bone. Acta Biomater 2012;8:1230-8.
[2] Lindtner RA, Castellani C, Tangl S, Zanoni G, Hausbrandt P, Tschegg EK, et al. Comparative biomechanical and radiological characterization of osseointegration of a biodegradable magnesium alloy pin and a copolymeric control for osteosynthesis. J Mech Behav Biomed Mater 2013;28:232-43.
[3] Ragamouni S, Kumar JM, Mushahary D, Nemani H, Pande G. Histological analysis of cells and matrix mineralization of new bone tissue induced in rabbit femur bones by Mg-Zr based biodegradable implants. Acta histochemica 2013;115:748-56.
[4] Witte F, Kaese V, Haferkamp H, Switzer E, Meyer-Lindenberg A, Wirth CJ, et al. In vivo corrosion of four magnesium alloys and the associated bone response. Biomaterials 2005;26:3557-63.
[5] Lhotka C, Szekeres T, Steffan I, Zhuber K, Zweymuller K. Four-year study of cobalt and chromium blood levels in patients managed with two different metal-on-metal total hip replacements. Journal of orthopaedic research : official publication of the Orthopaedic Research Society 2003;21:189-95.
[6] Persaud-Sharma D, McGoron A. Biodegradable Magnesium Alloys: A Review of Material Development and Applications. Journal of biomimetics, biomaterials, and tissue engineering 2012;12:25-39.
[7] Staiger MP, Pietak AM, Huadmai J, Dias G. Magnesium and its alloys as orthopedic biomaterials: a review. Biomaterials 2006;27:1728-34.
[8] Lambotte A. L'utilisation du magnesium comme materiel perdu dans l'osteosynthèse. Bull Mém Soc Nat Chir
1932;28:1325–34.
[9] Castellani C, Lindtner RA, Hausbrandt P, Tschegg E, Stanzl-Tschegg SE, Zanoni G, et al. Bone-implant interface strength and osseointegration: Biodegradable magnesium alloy versus standard titanium control. Acta biomaterialia 2011;7:432-40.
[10] Saris NE, Mervaala E, Karppanen H, Khawaja JA, Lewenstam A. Magnesium. An update on physiological, clinical and analytical aspects. Clinica chimica acta; international journal of clinical chemistry 2000;294:1-26.
[11] Zhang E, Xu L, Yu G, Pan F, Yang K. In vivo evaluation of biodegradable magnesium alloy bone implant in the first 6 months implantation. Journal of biomedical materials research Part A 2009;90:882-93.
[12] Song G. Control of biodegradation of biocompatable magnesium alloys. Corrosion Science 2007;49:1696-701.
[13] Brar HS, Platt MO, Sarntinoranont M, Martin PI, Manuel MV. Magnesium as a biodegradable and bioabsorbable material for medical implants. JOM 2009;61:31-4.
[14] Agarwal S, Curtin J, Duffy B, Jaiswal S. Biodegradable magnesium alloys for orthopaedic applications: A review on corrosion, biocompatibility and surface modifications. Materials Science and Engineering: C 2016;68:948-63.
[15] Martinez Sanchez AH, Luthringer BJ, Feyerabend F, Willumeit R. Mg and Mg alloys: how comparable are in vitro and in vivo corrosion rates? A review. Acta biomaterialia 2015;13:16-31.
[16] Witte F, Hort N, Vogt C, Cohen S, Kainer KU, Willumeit R, et al. Degradable biomaterials based on magnesium corrosion. Curr Opin Solid State Mater Sci 2008;12:63-72.

[17] Angrisani N, Reifenrath J, Seitz J-M, Meyer-Lindenberg A. Rare earth metals as alloying components in magnesium implants for orthopaedic applications. DNA 2012;35:36.
[18] Hort N, Huang Y, Fechner D, Störmer M, Blawert C, Witte F, et al. Magnesium alloys as implant materials – Principles of property design for Mg–RE alloys. Acta Biomaterialia 2010;6:1714-25.
[19] Tie D, Feyerabend F, Muller WD, Schade R, Liefeith K, Kainer KU, et al. Antibacterial biodegradable Mg-Ag alloys. European cells & materials 2013;25:284-98; discussion 98.
[20] Fujimori E, Tomosue Y, Haraguchi H. Determination of rare earth elements in blood serum reference sample by chelating resin preconcentration and inductively coupled plasma mass spectrometry. The Tohoku journal of experimental medicine 1996;178:63-74.
[21] Zaichick S, Zaichick V, Karandashev V, Nosenko S. Accumulation of rare earth elements in human bone within the lifespan. Metallomics : integrated biometal science 2011;3:186-94.
[22] Mi P, Dewi N, Yanagie H, Kokuryo D, Suzuki M, Sakurai Y, et al. Hybrid Calcium Phosphate-Polymeric Micelles Incorporating Gadolinium Chelates for Imaging-Guided Gadolinium Neutron Capture Tumor Therapy. ACS Nano 2015;9:5913-21.
[23] Feyerabend F, Fischer J, Holtz J, Witte F, Willumeit R, Drucker H, et al. Evaluation of short-term effects of rare earth and other elements used in magnesium alloys on primary cells and cell lines. Acta biomaterialia 2010;6:1834-42.
[24] Bidlack WR. The Biological Chemistry of Magnesium Edited by J. A. Cowan (The Ohio State University). VCH Publishers, Inc.: New York. 1995. xvi + 254 pp. $59.95. ISBN 1-56081-627-9. J Am Chem Soc 1996;118:6-7.
[25] Swaminathan R. Magnesium metabolism and its disorders. The Clinical biochemist Reviews 2003;24:47-66.
[26] de Baaij JHF, Hoenderop JGJ, Bindels RJM. Magnesium in Man: Implications for Health and Disease. Physiol Rev 2015;95:1-46.
[27] de Baaij JHF, Hoenderop JGJ, Bindels RJM. Regulation of magnesium balance: lessons learned from human genetic disease. Clinical Kidney Journal 2012;5:i15-i24.
[28] Alfrey AC, Miller NL, Trow R. Effect of Age and Magnesium Depletion on Bone Magnesium Pools in Rats. J Clin Invest 1974;54:1074-81.
[29] Ebel H, Gunther T. Magnesium metabolism: a review. J Clin Chem Clin Biochem 1980;18:257-70.
[30] Laires MJ, Monteiro CP, Bicho M. Role of cellular magnesium in health and human disease. Frontiers in bioscience : a journal and virtual library 2004;9:262-76.
[31] Rubin AH, Terasaki M, Sanui H. Magnesium reverses inhibitory effects of calcium deprivation on coordinate response of 3T3 cells to serum. Proc Natl Acad Sci U S A 1978;75:4379-83.
[32] Rubin AH, Terasaki M, Sanui H. Major intracellular cations and growth control: correspondence among magnesium content, protein synthesis, and the onset of DNA synthesis in BALB/c3T3 cells. Proc Natl Acad Sci U S A 1979;76:3917-21.
[33] Banai S, Haggroth L, Epstein SE, Casscells W. Influence of extracellular magnesium on capillary endothelial cell proliferation and migration. Circulation research 1990;67:645-50.
[34] Rude RK, Gruber HE, Norton HJ, Wei LY, Frausto A, Mills BG. Bone loss induced by dietary magnesium reduction to 10% of the nutrient requirement in rats is associated with increased release of substance P and tumor necrosis factor-α. The Journal of nutrition 2004;134:79-85.

[35] Shimaya M, Muneta T, Ichinose S, Tsuji K, Sekiya I. Magnesium enhances adherence and cartilage formation of synovial mesenchymal stem cells through integrins. Osteoarthritis and cartilage / OARS, Osteoarthritis Research Society 2010;18:1300-9.
[36] Rubin H, Vidair C, Sanui H. Restoration of normal appearance, growth behavior, and calcium content to transformed 3T3 cells by magnesium deprivation. Proceedings of the National Academy of Sciences of the United States of America 1981;78:2350-4.
[37] Heinrich MC, Kuhlmann MK, Kohlbacher S, Scheer M, Grgic A, Heckmann MB, et al. Cytotoxicity of iodinated and gadolinium-based contrast agents in renal tubular cells at angiographic concentrations: in vitro study. Radiology 2007;242:425-34.
[38] Drynda A, Deinet N, Braun N, Peuster M. Rare earth metals used in biodegradable magnesium-based stents do not interfere with proliferation of smooth muscle cells but do induce the up-regulation of inflammatory genes. Journal of biomedical materials research Part A 2009;91:360-9.
[39] Maiseyeu A, Mihai G, Kampfrath T, Simonetti OP, Sen CK, Roy S, et al. Gadolinium-containing phosphatidylserine liposomes for molecular imaging of atherosclerosis. Journal of lipid research 2009;50:2157-63.
[40] Haley TJ, Raymond K, Komesu N, Upham HC. Toxicological and pharmacological effects of gadolinium and samarium chlorides. British Journal of Pharmacology and Chemotherapy 1961;17:526-32.
[41] Hansen DE, Borganelli M, Stacy GP, Jr., Taylor LK. Dose-dependent inhibition of stretch-induced arrhythmias by gadolinium in isolated canine ventricles. Evidence for a unique mode of antiarrhythmic action. Circulation research 1991;69:820-31.
[42] Lebert M, Hader DP. How Euglena tells up from down [letter]. Nature 1996;379:590.
[43] Mancilla EE, Galindo M, Fertilio B, Herrera M, Salas K, Gatica H, et al. L-type calcium channels in growth plate chondrocytes participate in endochondral ossification. Journal of cellular biochemistry 2007;101:389-98.
[44] Fu LJ, Li JX, Yang XG, Wang K. Gadolinium-promoted cell cycle progression with enhanced S-phase entry via activation of both ERK and PI3K signaling pathways in NIH 3T3 cells. Journal of biological inorganic chemistry : JBIC : a publication of the Society of Biological Inorganic Chemistry 2009;14:219-27.
[45] Li JX, Fu LJ, Yang XG, Wang K. Integrin-mediated signaling contributes to gadolinium-containing-particle-promoted cell survival and G(1) to S phase cell cycle transition by enhancing focal adhesion formation. Journal of biological inorganic chemistry : JBIC : a publication of the Society of Biological Inorganic Chemistry 2012;17:375-85.
[46] Li JX, Liu JC, Wang K, Yang XG. Gadolinium-containing bioparticles as an active entity to promote cell cycle progression in mouse embryo fibroblast NIH3T3 cells. Journal of biological inorganic chemistry : JBIC : a publication of the Society of Biological Inorganic Chemistry 2010;15:547-57.
[47] Carrasco Muñoz S, Calles Blanco C, Marcin J, Fernández Álvarez C, Lafuente Martínez J. Contrastes basados en gadolinio utilizados en resonancia magnética. Radiología 2014;56, Supplement 1:21-8.
[48] Lubick N. Nanosilver toxicity: ions, nanoparticles--or both? Environmental science & technology 2008;42:8617.
[49] Greulich C, Kittler S, Epple M, Muhr G, Koller M. Studies on the biocompatibility and the interaction of silver nanoparticles with human mesenchymal stem cells

(hMSCs). Langenbeck's archives of surgery / Deutsche Gesellschaft fur Chirurgie 2009;394:495-502.
[50] Pascarelli NA, Moretti E, Terzuoli G, Lamboglia A, Renieri T, Fioravanti A, et al. Effects of gold and silver nanoparticles in cultured human osteoarthritic chondrocytes. Journal of applied toxicology : JAT 2013;33:1506-13.
[51] Greulich C, Braun D, Peetsch A, Diendorf J, Siebers B, Epple M, et al. The toxic effect of silver ions and silver nanoparticles towards bacteria and human cells occurs in the same concentration range. RSC Advances 2012;2:6981-7.
[52] Pichler K, Kraus T, Martinelli E, Sadoghi P, Musumeci G, Uggowitzer PJ, et al. Cellular reactions to biodegradable magnesium alloys on human growth plate chondrocytes and osteoblasts. International orthopaedics 2014;38:881-9.
[53] Ligier JN, Metaizeau JP, Prevot J. [Closed flexible medullary nailing in pediatric traumatology]. Chirurgie pediatrique 1983;24:383-5.
[54] Hosalkar HS, Pandya NK, Cho RH, Glaser DA, Moor MA, Herman MJ. Intramedullary nailing of pediatric femoral shaft fracture. The Journal of the American Academy of Orthopaedic Surgeons 2011;19:472-81.
[55] Simanovsky N, Tair MA, Simanovsky N, Porat S. Removal of flexible titanium nails in children. Journal of pediatric orthopedics 2006;26:188-92.
[56] Flynn JM, Skaggs DL, Sponseller PD, Ganley TJ, Kay RM, Leitch KK. The surgical management of pediatric fractures of the lower extremity. Instructional course lectures 2003;52:647-59.
[57] Lindaman LM. Bone healing in children. Clinics in podiatric medicine and surgery 2001;18:97-108.
[58] Chung R, Foster BK, Xian CJ. Injury responses and repair mechanisms of the injured growth plate. Frontiers in bioscience (Scholar edition) 2011;3:117-25.
[59] Pichler K, Schmidt B, Fischerauer EE, Rinner B, Dohr G, Leithner A, et al. Behaviour of human physeal chondro-progenitorcells in early growth plate injury response in vitro. International orthopaedics 2012;36:1961-6.
[60] Heinegard D, Saxne T. The role of the cartilage matrix in osteoarthritis. Nature reviews Rheumatology 2011;7:50-6.
[61] Gentili C, Cancedda R. Cartilage and bone extracellular matrix. Current pharmaceutical design 2009;15:1334-48.
[62] Omelyanenko NP, Slutsky LI, Mironov SP. Connective Tissue: Histophysiology, Biochemistry, Molecular Biology: CRC Press; 2016.
[63] Bhosale AM, Richardson JB. Articular cartilage: structure, injuries and review of management. British medical bulletin 2008;87:77-95.
[64] Kronenberg HM. Developmental regulation of the growth plate. Nature 2003;423:332-6.
[65] Cooper KL, Oh S, Sung Y, Dasari RR, Kirschner MW, Tabin CJ. Multiple phases of chondrocyte enlargement underlie differences in skeletal proportions. Nature 2013;495:375-8.
[66] Hunziker EB. Mechanism of longitudinal bone growth and its regulation by growth plate chondrocytes. Microscopy research and technique 1994;28:505-19.
[67] Nilsson O, Parker EA, Hegde A, Chau M, Barnes KM, Baron J. Gradients in bone morphogenetic protein-related gene expression across the growth plate. The Journal of endocrinology 2007;193:75-84.
[68] Bannister AJ, Oehler T, Wilhelm D, Angel P, Kouzarides T. Stimulation of c-Jun activity by CBP: c-Jun residues Ser63/73 are required for CBP induced stimulation in vivo and CBP binding in vitro. Oncogene 1995;11:2509-14.

[69] Nasu M, Takayama S, Umezawa A. Endochondral Ossification Model System: Designed Cell Fate of Human Epiphyseal Chondrocytes During Long-Term Implantation. Journal of Cellular Physiology 2015;230:1376-88.
[70] Zhong L, Huang X, Karperien M, Post JN. The Regulatory Role of Signaling Crosstalk in Hypertrophy of MSCs and Human Articular Chondrocytes. International Journal of Molecular Sciences 2015;16:19225-47.
[71] Matsiko A, Levingstone T, #039, Brien F. Advanced Strategies for Articular Cartilage Defect Repair. Materials 2013;6:637.
[72] Alini M, Matsui Y, Dodge GR, Poole AR. The extracellular matrix of cartilage in the growth plate before and during calcification: changes in composition and degradation of type II collagen. Calcified tissue international 1992;50:327-35.
[73] De la Fuente A, Mateos J, Lesende-Rodriguez I, Calamia V, Fuentes-Boquete I, de Toro FJ, et al. Proteome analysis during chondrocyte differentiation in a new chondrogenesis model using human umbilical cord stroma mesenchymal stem cells. Molecular & cellular proteomics : MCP 2012;11:M111.010496.
[74] Ji YH, Ji JL, Sun FY, Zeng YY, He XH, Zhao JX, et al. Quantitative proteomics analysis of chondrogenic differentiation of C3H10T1/2 mesenchymal stem cells by iTRAQ labeling coupled with on-line two-dimensional LC/MS/MS. Molecular & cellular proteomics : MCP 2010;9:550-64.
[75] Wang D, Park JS, Chu JS, Krakowski A, Luo K, Chen DJ, et al. Proteomic profiling of bone marrow mesenchymal stem cells upon transforming growth factor beta1 stimulation. The Journal of biological chemistry 2004;279:43725-34.
[76] Ishihara T, Kakiya K, Takahashi K, Miwa H, Rokushima M, Yoshinaga T, et al. Discovery of novel differentiation markers in the early stage of chondrogenesis by glycoform-focused reverse proteomics and genomics. Biochimica et biophysica acta 2014;1840:645-55.
[77] Pan C, Kumar C, Bohl S, Klingmueller U, Mann M. Comparative Proteomic Phenotyping of Cell Lines and Primary Cells to Assess Preservation of Cell Type-specific Functions. Molecular & cellular proteomics : MCP 2009;8:443-50.
[78] Burdall SE, Hanby AM, Lansdown MR, Speirs V. Breast cancer cell lines: friend or foe? Breast cancer research : BCR 2003;5:89-95.
[79] Masters JR. Human cancer cell lines: fact and fantasy. Nature reviews Molecular cell biology 2000;1:233-6.
[80] Sarugaser R, Lickorish D, Baksh D, Hosseini MM, Davies JE. Human umbilical cord perivascular (HUCPV) cells: a source of mesenchymal progenitors. Stem cells (Dayton, Ohio) 2005;23:220-9.
[81] Baksh D, Yao R, Tuan RS. Comparison of proliferative and multilineage differentiation potential of human mesenchymal stem cells derived from umbilical cord and bone marrow. Stem cells (Dayton, Ohio) 2007;25:1384-92.
[82] Zhang L, Su P, Xu C, Yang J, Yu W, Huang D. Chondrogenic differentiation of human mesenchymal stem cells: a comparison between micromass and pellet culture systems. Biotechnology Letters 2010;32:1339-46.
[83] Tsang WP, Shu Y, Kwok PL, Zhang F, Lee KK, Tang MK, et al. CD146+ human umbilical cord perivascular cells maintain stemness under hypoxia and as a cell source for skeletal regeneration. PLoS One 2013;8:e76153.
[84] Newton PT, Staines KA, Spevak L, Boskey AL, Teixeira CC, Macrae VE, et al. Chondrogenic ATDC5 cells: an optimised model for rapid and physiological matrix mineralisation. International journal of molecular medicine 2012;30:1187-93.
[85] Shukunami C, Shigeno C, Atsumi T, Ishizeki K, Suzuki F, Hiraki Y. Chondrogenic differentiation of clonal mouse embryonic cell line ATDC5 in vitro:

differentiation-dependent gene expression of parathyroid hormone (PTH)/PTH-related peptide receptor. The Journal of cell biology 1996;133:457-68.
[86] Myrissa A, Agha NA, Lu Y, Martinelli E, Eichler J, Szakács G, et al. In vitro and in vivo comparison of binary Mg alloys and pure Mg. Materials Science and Engineering: C 2016;61:865-74.
[87] ISO 10993-5. Biological evaluation of medical devices -- Part 5: Tests for in vitro cytotoxicity: International Organization for standardization; 2009.
[88] ISO 10993-12. Biological evaluation of medical devices -- Part 12: Sample preparation and reference materials: International Organization for standardization; 20012.
[89] Willumeit R, Mohring A, Feyerabend F. Optimization of cell adhesion on mg based implant materials by pre-incubation under cell culture conditions. Int J Mol Sci 2014;15:7639-50.
[90] Cecchinato F, Agha NA, Martinez-Sanchez AH, Luthringer BJC, Feyerabend F, Jimbo R, et al. Influence of Magnesium Alloy Degradation on Undifferentiated Human Cells. PLoS ONE 2015;10:e0142117.
[91] Johnson CW, Timmons DL, Hall PE. Essential laboratory mathematics : concepts and applications for the chemical and clinical laboratory technician. Clifton Park, N.Y.: Delmar Learning; 2003.
[92] Seelenfreund E, Robinson WA, Amato CM, Tan AC, Kim J, Robinson SE. Long term storage of dry versus frozen RNA for next generation molecular studies. PLoS One 2014;9:e111827.
[93] Macherauch E, Zoch H-W. Rasterelektronenmikroskopie. Praktikum in Werkstoffkunde: 91 ausführliche Versuche aus wichtigen Gebieten der Werkstofftechnik. Wiesbaden: Vieweg+Teubner; 2011. p. 289-96.
[94] Taylor G. Disintegration of Water Drops in an Electric Field. Proceedings of the Royal Society of London Series A Mathematical and Physical Sciences 1964;280:383-97.
[95] Giannuzzi LA, Stevie FA. Introduction to focused ion beams : instrumentation, theory, techniques, and practice. New York: Kluwer Academic Publishers; 2005.
[96] Grandfield K, Engqvist H. Focused Ion Beam in the Study of Biomaterials and Biological Matter. Advances in Materials Science and Engineering 2012;2012:6.
[97] Graves PR, Haystead TA. Molecular biologist's guide to proteomics. Microbiology and molecular biology reviews : MMBR 2002;66:39-63; table of contents.
[98] Ho CS, Lam CW, Chan MH, Cheung RC, Law LK, Lit LC, et al. Electrospray ionisation mass spectrometry: principles and clinical applications. The Clinical biochemist Reviews 2003;24:3-12.
[99] Faia-Torres AB, Guimond-Lischer S, Rottmar M, Charnley M, Goren T, Maniura-Weber K, et al. Differential regulation of osteogenic differentiation of stem cells on surface roughness gradients. Biomaterials 2014;35:9023-32.
[100] Sanchez AHM, Luthringer BJC, Feyerabend F, Willumeit R. Mg and Mg alloys: How comparable are in vitro and in vivo corrosion rates? A review. Acta Biomaterialia 2015;13:16-31.
[101] Hall BK, Miyake T. All for one and one for all: condensations and the initiation of skeletal development. BioEssays : news and reviews in molecular, cellular and developmental biology 2000;22:138-47.
[102] Sarugaser R, Hanoun L, Keating A, Stanford WL, Davies JE. Human mesenchymal stem cells self-renew and differentiate according to a deterministic hierarchy. PloS one 2009;4:e6498.

[103] Yao Y, Wang Y. ATDC5: an excellent in vitro model cell line for skeletal development. Journal of cellular biochemistry 2013;114:1223-9.
[104] Chung UI. Essential role of hypertrophic chondrocytes in endochondral bone development. Endocrine journal 2004;51:19-24.
[105] Shum L, Nuckolls G. The life cycle of chondrocytes in the developing skeleton. Arthritis Research 2002;4:94-106.
[106] Ikeda T, Kawaguchi H, Kamekura S, Ogata N, Mori Y, Nakamura K, et al. Distinct roles of Sox5, Sox6, and Sox9 in different stages of chondrogenic differentiation. Journal of bone and mineral metabolism 2005;23:337-40.
[107] Huang W, Chung U-i, Kronenberg HM, de Crombrugghe B. The chondrogenic transcription factor Sox9 is a target of signaling by the parathyroid hormone-related peptide in the growth plate of endochondral bones. Proceedings of the National Academy of Sciences 2001;98:160-5.
[108] Akiyama H, Chaboissier MC, Martin JF, Schedl A, de Crombrugghe B. The transcription factor Sox9 has essential roles in successive steps of the chondrocyte differentiation pathway and is required for expression of Sox5 and Sox6. Genes & development 2002;16:2813-28.
[109] Hino K, Saito A, Kido M, Kanemoto S, Asada R, Takai T, et al. Master Regulator for Chondrogenesis, Sox9, Regulates Transcriptional Activation of the Endoplasmic Reticulum Stress Transducer BBF2H7/CREB3L2 in Chondrocytes. The Journal of Biological Chemistry 2014;289:13810-20.
[110] Bond SR, Lau A, Penuela S, Sampaio AV, Underhill TM, Laird DW, et al. Pannexin 3 is a novel target for Runx2, expressed by osteoblasts and mature growth plate chondrocytes. Journal of bone and mineral research : the official journal of the American Society for Bone and Mineral Research 2011;26:2911-22.
[111] Enomoto H, Furuichi T, Zanma A, Yamana K, Yoshida C, Sumitani S, et al. Runx2 deficiency in chondrocytes causes adipogenic changes in vitro. Journal of Cell Science 2004;117:417-25.
[112] Zhang Y, Yang TL, Li X, Guo Y. Functional analyses reveal the essential role of SOX6 and RUNX2 in the communication of chondrocyte and osteoblast. Osteoporosis international : a journal established as result of cooperation between the European Foundation for Osteoporosis and the National Osteoporosis Foundation of the USA 2015;26:553-61.
[113] Schmid TM, Linsenmayer TF. Type X Collagen A2 - BURGESON, RICHARD MAYNEROBERT E. Structure and Function of Collagen Types: Academic Press; 1987. p. 223-59.
[114] Marriott A, Ayad S, Grant ME. The synthesis of type X collagen by bovine and human growth-plate chondrocytes. Journal of cell science 1991;99 (Pt 3):641-9.
[115] Meury T, Akhouayri O, Jafarov T, Mandic V, St-Arnaud R. Nuclear alpha NAC influences bone matrix mineralization and osteoblast maturation in vivo. Molecular and cellular biology 2010;30:43-53.
[116] Chen CW, Tsai YH, Deng WP, Shih SN, Fang CL, Burch JG, et al. Type I and II collagen regulation of chondrogenic differentiation by mesenchymal progenitor cells. J Orthop Res 2005;23:446-53.
[117] Marlovits S, Hombauer M, Truppe M, Vecsei V, Schlegel W. Changes in the ratio of type-I and type-II collagen expression during monolayer culture of human chondrocytes. The Journal of bone and joint surgery British volume 2004;86:286-95.
[118] Wilkins RJ, Hall AC. Control of matrix synthesis in isolated bovine chondrocytes by extracellular and intracellular pH. Journal of cellular physiology 1995;164:474-81.

[119] Bruckner P, Hörler I, Mendler M, Houze Y, Winterhalter KH, Eich-Bender SG, et al. Induction and prevention of chondrocyte hypertrophy in culture. The Journal of Cell Biology 1989;109:2537-45.
[120] Nakatani S, Mano H, Ryanghyok IM, Shimizu J, Wada M. Excess magnesium inhibits excess calcium-induced matrix-mineralization and production of matrix gla protein (MGP) by ATDC5 cells. Biochemical and biophysical research communications 2006;348:1157-62.
[121] Zhang L, Yang C, Li J, Zhu Y, Zhang X. High extracellular magnesium inhibits mineralized matrix deposition and modulates intracellular calcium signaling in human bone marrow-derived mesenchymal stem cells. Biochemical and biophysical research communications 2014;450:1390-5.
[122] Yoshizawa S, Brown A, Barchowsky A, Sfeir C. Magnesium ion stimulation of bone marrow stromal cells enhances osteogenic activity, simulating the effect of magnesium alloy degradation. Acta biomaterialia 2014;10:2834-42.
[123] Abed E, Moreau R. Importance of melastatin-like transient receptor potential 7 and cations (magnesium, calcium) in human osteoblast-like cell proliferation. Cell proliferation 2007;40:849-65.
[124] Leidi M, Dellera F, Mariotti M, Maier JA. High magnesium inhibits human osteoblast differentiation in vitro. Magnesium research : official organ of the International Society for the Development of Research on Magnesium 2011;24:1-6.
[125] Li L, Gao J, Wang Y. Evaluation of cyto-toxicity and corrosion behavior of alkali-heat-treated magnesium in simulated body fluid. Surface and Coatings Technology 2004;185:92-8.
[126] Kuwahara H, Al-Abdullat Y, Mazaki N, Tsutsumi S, Aizawa T. Precipitation of magnesium apatite on pure magnesium surface during immersing in Hank's solution. Materials Transactions 2001;42:1317-21.
[127] Yang JX, Cui FZ, Lee IS, Zhang Y, Yin QS, Xia H, et al. In vivo biocompatibility and degradation behavior of Mg alloy coated by calcium phosphate in a rabbit model. Journal of biomaterials applications 2012;27:153-64.
[128] Stojkovska J, Kostić D, Jovanović Ž, Vukašinović-Sekulić M, Mišković-Stanković V, Obradović B. A comprehensive approach to in vitro functional evaluation of Ag/alginate nanocomposite hydrogels. Carbohydrate Polymers 2014;111:305-14.
[129] Liu X, He W, Fang Z, Kienzle A, Feng Q. Influence of silver nanoparticles on osteogenic differentiation of human mesenchymal stem cells. Journal of biomedical nanotechnology 2014;10:1277-85.
[130] Pauksch L, Hartmann S, Rohnke M, Szalay G, Alt V, Schnettler R, et al. Biocompatibility of silver nanoparticles and silver ions in primary human mesenchymal stem cells and osteoblasts. Acta biomaterialia 2014;10:439-49.
[131] Sengstock C, Diendorf J, Epple M, Schildhauer TA, Koller M. Effect of silver nanoparticles on human mesenchymal stem cell differentiation. Beilstein journal of nanotechnology 2014;5:2058-69.
[132] Samberg ME, Loboa EG, Oldenburg SJ, Monteiro-Riviere NA. Silver nanoparticles do not influence stem cell differentiation but cause minimal toxicity. Nanomedicine (London, England) 2012;7:1197-209.
[133] He W, Kienzle A, Liu X, Muller WEG, Feng Q. In vitro 30 nm silver nanoparticles promote chondrogenesis of human mesenchymal stem cells. RSC Advances 2015;5:49809-18.
[134] Moghadam FH, Tayebi T, Dehghan M, Eslami G, Nadri H, Moradi A, et al. Differentiation of Bone Marrow Mesenchymal Stem Cells into Chondrocytes after

Short Term Culture in Alkaline Medium. International Journal of Hematology-Oncology and Stem Cell Research 2014;8:12-9.
[135] Simão AMS, Bolean M, Hoylaerts MF, Millán JL, Ciancaglini P. Effects of pH on the Production of Phosphate and Pyrophosphate by Matrix Vesicles' Biomimetics. Calcified tissue international 2013;93:222-32.
[136] Greisberg JK, Wolf JM, Wyman J, Zou L, Terek RM. Gadolinium inhibits thymidine incorporation and induces apoptosis in chondrocytes. Journal of orthopaedic research : official publication of the Orthopaedic Research Society 2001;19:797-801.
[137] Mobasheri A, Barrett-Jolley R, Carter SD, Martin-Vasallo P, Schulze-Tanzil G, Shakibaei M. Functional Roles of Mechanosensitive Ion Channels, ss1 Integrins and Kinase Cascades in Chondrocyte Mechanotransduction. In: Kamkin A, Kiseleva I, editors. Mechanosensitivity in Cells and Tissues. Moscow: Academia
Academia Publishing House Ltd.; 2005.
[138] Erickson GR, Alexopoulos LG, Guilak F. Hyper-osmotic stress induces volume change and calcium transients in chondrocytes by transmembrane, phospholipid, and G-protein pathways. Journal of biomechanics 2001;34:1527-35.
[139] Amini S, Veilleux D, Villemure I. Tissue and cellular morphological changes in growth plate explants under compression. Journal of biomechanics 2010;43:2582-8.
[140] Mobasheri A, Carter SD, Martin-Vasallo P, Shakibaei M. Integrins and stretch activated ion channels; putative components of functional cell surface mechanoreceptors in articular chondrocytes. Cell biology international 2002;26:1-18.
[141] Sukharev SI, Martinac B, Arshavsky VY, Kung C. Two types of mechanosensitive channels in the Escherichia coli cell envelope: solubilization and functional reconstitution. Biophysical journal 1993;65:177-83.
[142] Sachs F, Morris CE. Mechanosensitive ion channels in nonspecialized cells. Reviews of physiology, biochemistry and pharmacology 1998;132:1-77.
[143] Mobasheri A, Mobasheri R, Francis MJ, Trujillo E, Alvarez de la Rosa D, Martin-Vasallo P. Ion transport in chondrocytes: membrane transporters involved in intracellular ion homeostasis and the regulation of cell volume, free [Ca2+] and pH. Histology and histopathology 1998;13:893-910.
[144] Morita K, Miyamoto T, Fujita N, Kubota Y, Ito K, Takubo K, et al. Reactive oxygen species induce chondrocyte hypertrophy in endochondral ossification. The Journal of experimental medicine 2007;204:1613-23.
[145] Mansfield K, Pucci B, Adams CS, Shapiro IM. Induction of apoptosis in skeletal tissues: phosphate-mediated chick chondrocyte apoptosis is calcium dependent. Calcified tissue international 2003;73:161-72.
[146] Pirog KA, Irman A, Young S, Halai P, Bell PA, Boot-Handford RP, et al. Abnormal chondrocyte apoptosis in the cartilage growth plate is influenced by genetic background and deletion of CHOP in a targeted mouse model of pseudoachondroplasia. PLoS One 2014;9:e85145.
[147] Chao DT, Korsmeyer SJ. BCL-2 family: regulators of cell death. Annual review of immunology 1998;16:395-419.
[148] Earnshaw WC, Martins LM, Kaufmann SH. Mammalian caspases: structure, activation, substrates, and functions during apoptosis. Annual review of biochemistry 1999;68:383-424.
[149] Hengartner MO. The biochemistry of apoptosis. Nature 2000;407:770-6.
[150] Olmedo ML, Landry PS, Sadasivan KK, Albright JA, Marino AA. Programmed cell death in post-traumatic bone callus. Cellular and molecular biology (Noisy-le-Grand, France) 2000;46:89-97.

[151] Olmedo ML, Landry PS, Sadasivan KK, Albright JA, Meek WD, Routh R, et al. Regulation of osteoblast levels during bone healing. Journal of orthopaedic trauma 1999;13:356-62.
[152] Yun Y, Dong Z, Yang D, Schulz MJ, Shanov VN, Yarmolenko S, et al. Biodegradable Mg corrosion and osteoblast cell culture studies. Materials Science and Engineering: C 2009;29:1814-21.
[153] Ko YH, Hong S, Pedersen PL. Chemical mechanism of ATP synthase. Magnesium plays a pivotal role in formation of the transition state where ATP is synthesized from ADP and inorganic phosphate. The Journal of biological chemistry 1999;274:28853-6.
[154] Shoshan-Barmatz V, Golan M. Mitochondrial VDAC1: function in cell life and death and a target for cancer therapy. Current medicinal chemistry 2012;19:714-35.
[155] Triantaphyllidou IE, Kalyvioti E, Karavia E, Lilis I, Kypreos KE, Papachristou DJ. Perturbations in the HDL metabolic pathway predispose to the development of osteoarthritis in mice following long-term exposure to western-type diet. Osteoarthritis and cartilage 2013;21:322-30.
[156] Papachristou DJ, Blair HC. Bone and high-density lipoprotein: The beginning of a beautiful friendship. World journal of orthopedics 2016;7:74-7.
[157] Kozhemyakina E, Lassar AB, Zelzer E. A pathway to bone: signaling molecules and transcription factors involved in chondrocyte development and maturation. Development (Cambridge, England) 2015;142:817-31.
[158] Davies ME, Dingle JT, Pigott R, Power C, Sharma H. Expression of intercellular adhesion molecule 1 (ICAM-1) on human articular cartilage chondrocytes. Connective tissue research 1991;26:207-16.
[159] Zreiqat H, Howlett CR, Zannettino A, Evans P, Schulze-Tanzil G, Knabe C, et al. Mechanisms of magnesium-stimulated adhesion of osteoblastic cells to commonly used orthopaedic implants. Journal of biomedical materials research 2002;62:175-84.
[160] Kulyk WM, Upholt WB, Kosher RA. Fibronectin gene expression during limb cartilage differentiation. Development (Cambridge, England) 1989;106:449-55.
[161] Cui J, Liu Y, Matumoto R, Uemura T. Highly Expression and Biological Function of Type VI Collagen on the Early Events of Chondrogenesis in Human Mesenchymal Stem Cells. Journal of Oral Tissue Engineering 2013;11:29-41.
[162] Kim YI, Ryu J-S, Yeo JE, Choi YJ, Kim YS, Ko K, et al. Overexpression of TGF-β1 enhances chondrogenic differentiation and proliferation of human synovium-derived stem cells. Biochemical and Biophysical Research Communications 2014;450:1593-9.
[163] Imabuchi R, Ohmiya Y, Kwon HJ, Onodera S, Kitamura N, Kurokawa T, et al. Gene expression profile of the cartilage tissue spontaneously regenerated in vivo by using a novel double-network gel: comparisons with the normal articular cartilage. BMC musculoskeletal disorders 2011;12:213.
[164] Hankenson KD, Dishowitz M, Gray C, Schenker M. Angiogenesis in bone regeneration. Injury 2011;42:556-61.
[165] Maes C, Carmeliet P, Moermans K, Stockmans I, Smets N, Collen D, et al. Impaired angiogenesis and endochondral bone formation in mice lacking the vascular endothelial growth factor isoforms VEGF164 and VEGF188. Mechanisms of development 2002;111:61-73.
[166] Alini M, Marriott A, Chen T, Abe S, Poole AR. A novel angiogenic molecule produced at the time of chondrocyte hypertrophy during endochondral bone formation. Developmental biology 1996;176:124-32.

[167] Carlevaro MF, Albini A, Ribatti D, Gentili C, Benelli R, Cermelli S, et al. Transferrin promotes endothelial cell migration and invasion: implication in cartilage neovascularization. The Journal of cell biology 1997;136:1375-84.
[168] Vu TH, Shipley JM, Bergers G, Berger JE, Helms JA, Hanahan D, et al. MMP-9/gelatinase B is a key regulator of growth plate angiogenesis and apoptosis of hypertrophic chondrocytes. Cell 1998;93:411-22.
[169] Moses MA, Wiederschain D, Wu I, Fernandez CA, Ghazizadeh V, Lane WS, et al. Troponin I is present in human cartilage and inhibits angiogenesis. Proceedings of the National Academy of Sciences of the United States of America 1999;96:2645-50.
[170] Shukunami C, Iyama K, Inoue H, Hiraki Y. Spatiotemporal pattern of the mouse chondromodulin-I gene expression and its regulatory role in vascular invasion into cartilage during endochondral bone formation. The International journal of developmental biology 1999;43:39-49.
[171] Norbert S. Angiogenesis in Osteoarthritis. Current Rheumatology Reviews 2008;4:206-9.
[172] Sanchez AHM, Luthringer BJC, Feyerabend F, Willumeit R. Mg and Mg alloys: How comparable are in vitro and in vivo corrosion rates? A review. Acta biomaterialia 2015;13:16-31.
[173] KubÁSek J, VojtĚCh D. Structural and corrosion characterization of biodegradable Mg–RE (RE=Gd, Y, Nd) alloys. Transactions of Nonferrous Metals Society of China 2013;23:1215-25.
[174] Moreira Teixeira LS, Leijten JC, Sobral J, Jin R, van Apeldoorn AA, Feijen J, et al. High throughput generated micro-aggregates of chondrocytes stimulate cartilage formation in vitro and in vivo. European cells & materials 2012;23:387-99.

12. SUPPLEMENTARY MATERIAL

Supplementary Table 1. Proteins up- and down-regulated with Mg, Mg-10Gd and Mg-2Ag extracts.

Protein ID	Protein names	Gene names	Difference regarding Control (log10)		
			Mg-10Gd	*Mg-2Ag*	*Mg*
P05090	Apolipoprotein D (Apo-D) (ApoD)	APOD	8.628	8.611	8.627
P00747	Plasminogen (EC 3.4.21.7)	PLG	8.617	8.602	8.626
P04003	C4b-binding protein alpha chain (C4bp) (Proline-rich protein) (PRP)	C4BPA C4BP	8.505	8.566	8.657
P01857	Ig gamma-1 chain C region	IGHG1	8.482	8.544	8.554
P01876	Ig alpha-1 chain C region	IGHA1	8.426	8.503	8.497
P00450	Ceruloplasmin (EC 1.16.3.1) (Ferroxidase)	CP	8.507	8.500	8.607
P01834	Ig kappa chain C region	IGKC	8.425	8.476	8.482
P02774	Vitamin D-binding protein (DBP) (VDB) (Gc protein-derived macrophage activating factor) (Gc-MAF) (GcMAF) (Gc-globulin) (Group-specific component) (Gc) (Vitamin D-binding protein-macrophage activating factor) (DBP-maf)	GC	8.289	8.371	8.406
P01024	Complement C3 (C3 and PZP-like alpha-2-macroglobulin domain-containing protein 1)	C3 CPAMD1	8.326	8.345	8.381
P01871	Ig mu chain C region	IGHM	8.312	8.305	8.357
P27169	Serum paraoxonase/arylesterase 1 (PON 1) (EC 3.1.1.2) (EC 3.1.1.81) (EC 3.1.8.1) (Aromatic esterase 1) (A-esterase 1) (K-45) (Serum aryldialkylphosphatase 1)	PON1 PON	8.351	8.273	8.330
P06727	Apolipoprotein A-IV (Apo-AIV) (ApoA-IV) (Apolipoprotein A4)	APOA4	8.200	8.242	8.244
P24821	Tenascin (TN) (Cytotactin) (GMEM) (GP 150-225) (Glioma-associated-extracellular matrix antigen) (Hexabrachion) (JI) (Myotendinous antigen) (Neuronectin) (Tenascin-C) (TN-C)	TNC HXB	8.138	8.182	8.181
P02649	Apolipoprotein E (Apo-E)	APOE	8.047	8.139	8.112
P35542	Serum amyloid A-4 protein (Constitutively expressed serum amyloid A protein) (C-SAA)	SAA4 CSAA	5.285	8.112	8.000
O95445	Apolipoprotein M (Apo-M) (ApoM) (Protein G3a)	APOM G3A NG20 HSPC33 6	8.126	8.068	8.085
P02766	Transthyretin (ATTR) (Prealbumin) (TBPA)	TTR PALB	7.946	7.996	7.983
P02652	Apolipoprotein A-II (Apo-AII) (ApoA-II) (Apolipoprotein A2) [Cleaved into: Proapolipoprotein A-II (ProapoA-II);Truncated apolipoprotein A-II (Apolipoprotein A-II(1-76))]	APOA2	5.320	7.961	7.880

P02790	Hemopexin (Beta-1B-glycoprotein)	HPX	7.649	7.954	7.864
P01859	Ig gamma-2 chain C region	IGHG2	7.764	7.885	7.839
P00739	Haptoglobin-related protein	HPR	5.267	7.884	7.869
P02656	Apolipoprotein C-III (Apo-CIII) (ApoC-III) (Apolipoprotein C3)	APOC3	7.968	7.873	7.924
Q14112	Nidogen-2 (NID-2) (Osteonidogen)	NID2	7.599	7.818	7.766
P04217	Alpha-1B-glycoprotein (Alpha-1-B glycoprotein)	A1BG	7.708	7.801	7.806
P19827	Inter-alpha-trypsin inhibitor heavy chain H1 (ITI heavy chain H1) (ITI-HC1) (Inter-alpha-inhibitor heavy chain 1) (Inter-alpha-trypsin inhibitor complex component III) (Serum-derived hyaluronan-associated protein) (SHAP)	ITIH1 IGHEP1	7.563	7.756	7.759
P01042	Kininogen-1 (Alpha-2-thiol proteinase inhibitor) (Fitzgerald factor) (High molecular weight kininogen) (HMWK) (Williams-Fitzgerald-Flaujeac factor) [Cleaved into: Kininogen-1 heavy chain;T-kinin (Ile-Ser-Bradykinin);Bradykinin (Kallidin I);Lysyl-bradykinin (Kallidin II);Kininogen-1 light chain;Low molecular weight growth-promoting factor]	KNG1 BDK KNG	7.580	7.737	7.691
Q8IUX7	Adipocyte enhancer-binding protein 1 (AE-binding protein 1) (Aortic carboxypeptidase-like protein)	AEBP1 ACLP	7.616	7.722	7.623
Q99541	Perilipin-2 (Adipophilin) (Adipose differentiation-related protein) (ADRP)	PLIN2 ADFP	7.593	7.678	7.597
O14791	Apolipoprotein L1 (Apolipoprotein L) (Apo-L) (ApoL) (Apolipoprotein L-I) (ApoL-I)	APOL1 APOL	7.610	7.670	7.609
P04206	Ig kappa chain V-III region GOL (Rheumatoid factor)		7.679	7.664	7.747
Q9GZM7	Tubulointerstitial nephritis antigen-like (Glucocorticoid-inducible protein 5) (Oxidized LDL-responsive gene 2 protein) (OLRG-2) (Tubulointerstitial nephritis antigen-related protein) (TIN Ag-related protein) (TIN-Ag-RP)	TINAGL1 GIS5 LCN7 OLRG2 TINAGL PP6614 PSEC0088 UNQ204/PRO230	7.540	7.660	7.655
P22352	Glutathione peroxidase 3 (GPx-3) (GSHPx-3) (EC 1.11.1.9) (Extracellular glutathione peroxidase) (Plasma glutathione peroxidase) (GPx-P) (GSHPx-P)	GPX3 GPXP	7.585	7.594	7.622
P02747	Complement C1q subcomponent subunit C	C1QC C1QG	7.319	7.578	7.372
P19652	Alpha-1-acid glycoprotein 2 (AGP 2) (Orosomucoid-2) (OMD 2)	ORM2 AGP2	7.308	7.542	7.510
P02654	Apolipoprotein C-I (Apo-CI) (ApoC-I) (Apolipoprotein C1) [Cleaved into: Truncated apolipoprotein C-I]	APOC1	7.334	7.509	7.399

P00748	Coagulation factor XII (EC 3.4.21.38) (Hageman factor) (HAF) [Cleaved into: Coagulation factor XIIa heavy chain;Beta-factor XIIa part 1;Coagulation factor XIIa light chain (Beta-factor XIIa part 2)]	F12	5.040	7.486	5.000
P01008	Antithrombin-III (ATIII) (Serpin C1)	SERPINC1 AT3 PRO0309	4.873	7.467	7.445
Q92743	Serine protease HTRA1 (EC 3.4.21.-) (High-temperature requirement A serine peptidase 1) (L56) (Serine protease 11)	HTRA1 HTRA PRSS11	7.272	7.441	7.411
P02743	Serum amyloid P-component (SAP) (9.5S alpha-1-glycoprotein) [Cleaved into: Serum amyloid P-component(1-203)]	APCS PTX2	7.295	7.391	7.541
P05362	Intercellular adhesion molecule 1 (ICAM-1) (Major group rhinovirus receptor) (CD antigen CD54)	ICAM1	7.277	7.358	7.336
P01011	Alpha-1-antichymotrypsin (ACT) (Cell growth-inhibiting gene 24/25 protein) (Serpin A3) [Cleaved into: Alpha-1-antichymotrypsin His-Pro-less]	SERPINA3 AACT GIG24 GIG25	4.889	7.307	4.976
P07093	Glia-derived nexin (GDN) (Peptidase inhibitor 7) (PI-7) (Protease nexin 1) (PN-1) (Protease nexin I) (Serpin E2)	SERPINE2 PI7 PN1	7.337	7.296	4.825
Q9Y3B8	Oligoribonuclease, mitochondrial (EC 3.1.-.-) (RNA exonuclease 2 homolog) (Small fragment nuclease)	REXO2 SFN SMFN CGI-114	4.804	7.255	7.265
Q14165	Malectin	MLEC KIAA0152	7.352	7.208	7.254
P80108	Phosphatidylinositol-glycan-specific phospholipase D (PI-G PLD) (EC 3.1.4.50) (Glycoprotein phospholipase D) (Glycosyl-phosphatidylinositol-specific phospholipase D) (GPI-PLD) (GPI-specific phospholipase D)	GPLD1 PIGPLD1	7.220	7.160	7.263
O00264	Membrane-associated progesterone receptor component 1 (mPR)	PGRMC1 HPR6.6 PGRMC	2.392	7.156	4.829
P04004	Vitronectin (VN) (S-protein) (Serum-spreading factor) (V75) [Cleaved into: Vitronectin V65 subunit;Vitronectin V10 subunit;Somatomedin-B]	VTN	6.918	6.937	6.978
P01009	Alpha-1-antitrypsin (Alpha-1 protease inhibitor) (Alpha-1-antiproteinase) (Serpin A1) [Cleaved into: Short peptide from AAT (SPAAT)]	SERPINA1 AAT PI PRO0684 PRO2209	6.514	6.624	6.682
Q96TA1	Niban-like protein 1 (Meg-3) (Melanoma invasion by ERK) (MINERVA) (Protein FAM129B)	FAM129B C9orf88	5.100	5.034	7.590
Q9BY76	Angiopoietin-related protein 4 (Angiopoietin-like protein 4) (Hepatic	ANGPTL4 ARP4	4.863	4.869	7.374

	fibrinogen/angiopoietin-related protein) (HFARP)	HFARP PGAR PP1158 PSEC0166 UNQ171/PRO197			
Q13148	TAR DNA-binding protein 43 (TDP-43)	TARDBP TDP43	7.255	4.866	4.854
P35555	Fibrillin-1 [Cleaved into: Asprosin]	FBN1 FBN	7.276	4.838	4.802
P35354	Prostaglandin G/H synthase 2 (EC 1.14.99.1) (Cyclooxygenase-2) (COX-2) (PHS II) (Prostaglandin H2 synthase 2) (PGH synthase 2) (PGHS-2) (Prostaglandin-endoperoxide synthase 2)	PTGS2 COX2	7.328	4.822	7.276
P04180	Phosphatidylcholine-sterol acyltransferase (EC 2.3.1.43) (Lecithin-cholesterol acyltransferase) (Phospholipid-cholesterol acyltransferase)	LCAT	7.012	4.670	7.048
P04114	Apolipoprotein B-100 (Apo B-100) [Cleaved into: Apolipoprotein B-48 (Apo B-48)]	APOB	3.060	2.945	2.969
P47897	Glutamine--tRNA ligase (EC 6.1.1.18) (Glutaminyl-tRNA synthetase) (GlnRS)	QARS	7.420	2.469	2.501
Q9BWM7	Sideroflexin-3	SFXN3	7.292	2.425	7.292
P02647	Apolipoprotein A-I (Apo-AI) (ApoA-I) (Apolipoprotein A1) [Cleaved into: Proapolipoprotein A-I (ProapoA-I);Truncated apolipoprotein A-I (Apolipoprotein A-I(1-242))]	APOA1	1.872	1.892	1.839
P02768	Serum albumin	ALB GIG20 GIG42 PRO0903 PRO1708	1.652	1.814	1.788
P00738	Haptoglobin (Zonulin) [Cleaved into: Haptoglobin alpha chain;Haptoglobin beta chain]	HP	1.578	1.698	1.693
P02787	Serotransferrin (Transferrin) (Beta-1 metal-binding globulin) (Siderophilin)	TF PRO1400	1.208	1.482	1.372
Q15582	Transforming growth factor-beta-induced protein ig-h3 (Beta ig-h3) (Kerato-epithelin) (RGD-containing collagen-associated protein) (RGD-CAP)	TGFBI BIGH3	1.050	1.080	1.076
P04179	Superoxide dismutase [Mn], mitochondrial (EC 1.15.1.1)	SOD2	0.870	1.031	1.012
P15144	Aminopeptidase N (AP-N) (hAPN) (EC 3.4.11.2) (Alanyl aminopeptidase) (Aminopeptidase M) (AP-M) (Microsomal aminopeptidase) (Myeloid plasma membrane glycoprotein CD13) (gp150) (CD antigen CD13)	ANPEP APN CD13 PEPN	0.835	0.921	0.831
P08572	Collagen alpha-2(IV) chain [Cleaved into: Canstatin]	COL4A2	0.764	0.770	0.691

P02751	Fibronectin (FN) (Cold-insoluble globulin) (CIG) [Cleaved into: Anastellin;Ugl-Y1;Ugl-Y2;Ugl-Y3]	FN1 FN	0.577	0.616	0.503
P98160	Basement membrane-specific heparan sulfate proteoglycan core protein (HSPG) (Perlecan) (PLC) [Cleaved into: Endorepellin;LG3 peptide]	HSPG2	0.503	0.613	0.415
P31930	Cytochrome b-c1 complex subunit 1, mitochondrial (Complex III subunit 1) (Core protein I) (Ubiquinol-cytochrome-c reductase complex core protein 1)	UQCRC1	0.523	0.594	0.656
P22695	Cytochrome b-c1 complex subunit 2, mitochondrial (Complex III subunit 2) (Core protein II) (Ubiquinol-cytochrome-c reductase complex core protein 2)	UQCRC2	0.540	0.581	0.584
P01023	Alpha-2-macroglobulin (Alpha-2-M) (C3 and PZP-like alpha-2-macroglobulin domain-containing protein 5)	A2M CPAMD5 FWP007	0.673	0.572	0.506
Q9UJZ1	Stomatin-like protein 2, mitochondrial (SLP-2) (EPB72-like protein 2) (Paraprotein target 7) (Paratarg-7)	STOML2 SLP2 HSPC108	0.512	0.560	0.613
P06396	Gelsolin (AGEL) (Actin-depolymerizing factor) (ADF) (Brevin)	GSN	0.375	0.548	0.514
P12111	Collagen alpha-3(VI) chain	COL6A3	0.741	0.543	0.594
Q96HE7	ERO1-like protein alpha (ERO1-L) (ERO1-L-alpha) (EC 1.8.4.-) (Endoplasmic oxidoreductin-1-like protein) (Endoplasmic reticulum oxidoreductase alpha) (Oxidoreductin-1-L-alpha)	ERO1A ERO1L UNQ434/PRO865	0.571	0.539	0.587
P12110	Collagen alpha-2(VI) chain	COL6A2	0.778	0.530	0.590
P21796	Voltage-dependent anion-selective channel protein 1 (VDAC-1) (hVDAC1) (Outer mitochondrial membrane protein porin 1) (Plasmalemmal porin) (Porin 31HL) (Porin 31HM)	VDAC1 VDAC	0.454	0.529	0.530
P35232	Prohibitin	PHB	0.498	0.525	0.588
P06756	Integrin alpha-V (Vitronectin receptor subunit alpha) (CD antigen CD51) [Cleaved into: Integrin alpha-V heavy chain;Integrin alpha-V light chain]	ITGAV MSK8 VNRA	0.562	0.512	0.573
Q99623	Prohibitin-2 (B-cell receptor-associated protein BAP37) (D-prohibitin) (Repressor of estrogen receptor activity)	PHB2 BAP REA	0.489	0.504	0.542
P07686	Beta-hexosaminidase subunit beta (EC 3.2.1.52) (Beta-N-acetylhexosaminidase subunit beta) (Hexosaminidase subunit B) (Cervical cancer proto-oncogene 7 protein) (HCC-7) (N-acetyl-beta-glucosaminidase subunit beta) [Cleaved into: Beta-hexosaminidase subunit beta chain B;Beta-hexosaminidase subunit beta chain A]	HEXB HCC7	0.348	0.503	0.504
P07954	Fumarate hydratase, mitochondrial (Fumarase) (EC 4.2.1.2)	FH	0.390	0.475	0.460

Q9UBS4	DnaJ homolog subfamily B member 11 (APOBEC1-binding protein 2) (ABBP-2) (DnaJ protein homolog 9) (ER-associated DNAJ) (ER-associated Hsp40 co-chaperone) (Endoplasmic reticulum DNA J domain-containing protein 3) (ER-resident protein ERdj3) (ERdj3) (ERj3p) (HEDJ) (Human DnaJ protein 9) (hDj-9) (PWP1-interacting protein 4)	DNAJB11 EDJ ERJ3 HDJ9 PSEC0121 UNQ537/PRO1080	0.406	0.482	0.478
P36542	ATP synthase subunit gamma, mitochondrial (F-ATPase gamma subunit)	ATP5C1 ATP5C ATP5CL1	0.405	0.468	0.485
Q13011	Delta(3,5)-Delta(2,4)-dienoyl-CoA isomerase, mitochondrial (EC 5.3.3.-)	ECH1	0.397	0.456	0.468
P36957	Dihydrolipoyllysine-residue succinyltransferase component of 2-oxoglutarate dehydrogenase complex, mitochondrial (EC 2.3.1.61) (2-oxoglutarate dehydrogenase complex component E2) (OGDC-E2) (Dihydrolipoamide succinyltransferase component of 2-oxoglutarate dehydrogenase complex) (E2K)	DLST DLTS	0.403	0.455	0.488
P48047	ATP synthase subunit O, mitochondrial (Oligomycin sensitivity conferral protein) (OSCP)	ATP5O ATPO	0.418	0.453	0.435
Q99880	Histone H2B type 1-L (Histone H2B.c) (H2B/c)	HIST1H2BL H2BFC	0.337	0.436	0.354
P12109	Collagen alpha-1(VI) chain	COL6A1	0.676	0.433	0.510
P42765	3-ketoacyl-CoA thiolase, mitochondrial (EC 2.3.1.16) (Acetyl-CoA acyltransferase) (Beta-ketothiolase) (Mitochondrial 3-oxoacyl-CoA thiolase) (T1)	ACAA2	0.243	0.428	0.295
P40926	Malate dehydrogenase, mitochondrial (EC 1.1.1.37)	MDH2	0.332	0.426	0.422
P06576	ATP synthase subunit beta, mitochondrial (EC 3.6.3.14)	ATP5B ATPMB ATPSB	0.360	0.425	0.456
P62805	Histone H4	HIST1H4A H4/A H4FA;HIST1H4B H4/I H4FI;	0.413	0.419	0.345
Q9H444	Charged multivesicular body protein 4b (Chromatin-modifying protein 4b) (CHMP4b) (SNF7 homolog associated with Alix 1) (SNF7-2) (hSnf7-2) (Vacuolar protein sorting-associated protein 32-2) (Vps32-2) (hVps32-2)	CHMP4B C20orf178 SHAX1	0.359	0.414	-2.164
Q16778	Histone H2B type 2-E (Histone H2B-GL105) (Histone H2B.q) (H2B/q)	HIST2H2BE H2BFQ	0.366	0.407	0.315
P17301	Integrin alpha-2 (CD49 antigen-like family member B) (Collagen receptor) (Platelet membrane glycoprotein Ia) (GPIa) (VLA-2	ITGA2 CD49B	0.520	0.404	0.511

	subunit alpha) (CD antigen CD49b)				
P21589	5'-nucleotidase (5'-NT) (EC 3.1.3.5) (Ecto-5'-nucleotidase) (CD antigen CD73)	NT5E NT5 NTE	0.407	0.400	0.431
P80723	Brain acid soluble protein 1 (22 kDa neuronal tissue-enriched acidic protein) (Neuronal axonal membrane protein NAP-22)	BASP1 NAP22	0.305	0.399	0.358
P00505	Aspartate aminotransferase, mitochondrial (mAspAT) (EC 2.6.1.1) (EC 2.6.1.7) (Fatty acid-binding protein) (FABP-1) (Glutamate oxaloacetate transaminase 2) (Kynurenine aminotransferase 4) (Kynurenine aminotransferase IV) (Kynurenine--oxoglutarate transaminase 4) (Kynurenine--oxoglutarate transaminase IV) (Plasma membrane-associated fatty acid-binding protein) (FABPpm) (Transaminase A)	GOT2	0.267	0.399	0.418
P00367	Glutamate dehydrogenase 1, mitochondrial (GDH 1) (EC 1.4.1.3)	GLUD1 GLUD	0.338	0.397	0.420
P35527	Keratin, type I cytoskeletal 9 (Cytokeratin-9) (CK-9) (Keratin-9) (K9)	KRT9	0.196	0.393	0.241
Q49MG5	Microtubule-associated protein 9 (Aster-associated protein)	MAP9 ASAP	-2.251	0.392	0.172
P02511	Alpha-crystallin B chain (Alpha(B)-crystallin) (Heat shock protein beta-5) (HspB5) (Renal carcinoma antigen NY-REN-27) (Rosenthal fiber component)	CRYAB CRYA2 HSPB5	0.270	0.386	0.476
Q9BVK6	Transmembrane emp24 domain-containing protein 9 (GMP25) (Glycoprotein 25L2) (p24 family protein alpha-2) (p24alpha2) (p25)	TMED9 GP25L2	0.432	0.385	0.455
Q02818	Nucleobindin-1 (CALNUC)	NUCB1 NUC	0.231	0.382	0.373
P51571	Translocon-associated protein subunit delta (TRAP-delta) (Signal sequence receptor subunit delta) (SSR-delta)	SSR4 TRAPD	0.362	0.378	0.437
Q99878	Histone H2A type 1-J (Histone H2A/e)	HIST1H2AJ H2AFE	0.466	0.365	0.310
P11279	Lysosome-associated membrane glycoprotein 1 (LAMP-1) (Lysosome-associated membrane protein 1) (CD107 antigen-like family member A) (CD antigen CD107a)	LAMP1	0.352	0.364	0.400
P00558	Phosphoglycerate kinase 1 (EC 2.7.2.3) (Cell migration-inducing gene 10 protein) (Primer recognition protein 2) (PRP 2)	PGK1 PGKA MIG10 OK/SW-cl.110	0.260	0.355	0.273
P05534	HLA class I histocompatibility antigen, A-24 alpha chain (Aw-24) (HLA class I histocompatibility antigen, A-9 alpha chain) (MHC class I antigen A*24)	HLA-A HLAA	0.305	0.353	0.305

P61604	10 kDa heat shock protein, mitochondrial (Hsp10) (10 kDa chaperonin) (Chaperonin 10) (CPN10) (Early-pregnancy factor) (EPF)	HSPE1	0.281	0.351	0.346
P32322	Pyrroline-5-carboxylate reductase 1, mitochondrial (P5C reductase 1) (P5CR 1) (EC 1.5.1.2)	PYCR1	0.307	0.350	0.347
O00487	26S proteasome non-ATPase regulatory subunit 14 (EC 3.4.19.-) (26S proteasome regulatory subunit RPN11) (26S proteasome-associated PAD1 homolog 1)	PSMD14 POH1	0.308	0.348	0.323
Q15233	Non-POU domain-containing octamer-binding protein (NonO protein) (54 kDa nuclear RNA- and DNA-binding protein) (55 kDa nuclear protein) (DNA-binding p52/p100 complex, 52 kDa subunit) (NMT55) (p54(nrb)) (p54nrb)	NONO NRB54	0.287	0.347	0.386
P17096	High mobility group protein HMG-I/HMG-Y (HMG-I(Y)) (High mobility group AT-hook protein 1) (High mobility group protein A1) (High mobility group protein R)	HMGA1 HMGIY	0.192	0.345	0.203
P49755	Transmembrane emp24 domain-containing protein 10 (21 kDa transmembrane-trafficking protein) (S31III125) (S31I125) (Tmp-21-I) (Transmembrane protein Tmp21) (p23) (p24 family protein delta-1) (p24delta1) (p24delta)	TMED10 TMP21	0.410	0.342	0.329
Q12884	Prolyl endopeptidase FAP (EC 3.4.21.26) (170 kDa melanoma membrane-bound gelatinase) (Dipeptidyl peptidase FAP) (EC 3.4.14.5) (Fibroblast activation protein alpha) (FAPalpha) (Gelatine degradation protease FAP) (EC 3.4.21.-) (Integral membrane serine protease) (Post-proline cleaving enzyme) (Serine integral membrane protease) (SIMP) (Surface-expressed protease) (Seprase) [Cleaved into: Antiplasmin-cleaving enzyme FAP, soluble form (APCE) (EC 3.4.14.5) (EC 3.4.21.-) (EC 3.4.21.26)]	FAP	0.384	0.336	0.307
P13674	Prolyl 4-hydroxylase subunit alpha-1 (4-PH alpha-1) (EC 1.14.11.2) (Procollagen-proline,2-oxoglutarate-4-dioxygenase subunit alpha-1)	P4HA1 P4HA	0.329	0.334	0.352
Q07021	Complement component 1 Q subcomponent-binding protein, mitochondrial (ASF/SF2-associated protein p32) (Glycoprotein gC1qBP) (C1qBP) (Hyaluronan-binding protein 1) (Mitochondrial matrix protein p32) (gC1q-R protein) (p33)	C1QBP GC1QBP HABP1 SF2P32	0.201	0.331	0.337
O94905	Erlin-2 (Endoplasmic reticulum lipid raft-associated protein 2) (Stomatin-prohibitin-flotillin-HflC/K domain-containing protein 2) (SPFH domain-containing protein 2)	ERLIN2 C8orf2 SPFH2 UNQ244 1/PRO50 03/PRO9 924	0.339	0.330	0.403

P43307	Translocon-associated protein subunit alpha (TRAP-alpha) (Signal sequence receptor subunit alpha) (SSR-alpha)	SSR1 TRAPA PSEC0262	0.416	0.327	0.369
Q9NYL9	Tropomodulin-3 (Ubiquitous tropomodulin) (U-Tmod)	TMOD3	0.136	0.320	0.281
O00469	Procollagen-lysine,2-oxoglutarate 5-dioxygenase 2 (EC 1.14.11.4) (Lysyl hydroxylase 2) (LH2)	PLOD2	0.372	0.320	0.375
Q14764	Major vault protein (MVP) (Lung resistance-related protein)	MVP LRP	0.273	0.313	0.361
P07996	Thrombospondin-1	THBS1 TSP TSP1	0.342	0.305	0.302
P10809	60 kDa heat shock protein, mitochondrial (60 kDa chaperonin) (Chaperonin 60) (CPN60) (Heat shock protein 60) (HSP-60) (Hsp60) (HuCHA60) (Mitochondrial matrix protein P1) (P60 lymphocyte protein)	HSPD1 HSP60	0.281	0.301	0.334
Q70UQ0	Inhibitor of nuclear factor kappa-B kinase-interacting protein (I kappa-B kinase-interacting protein) (IKBKB-interacting protein) (IKK-interacting protein)	IKBIP IKIP	0.363	0.299	0.321
P25705	ATP synthase subunit alpha, mitochondrial	ATP5A1 ATP5A ATP5AL2 ATPM	0.290	0.290	0.312
P24539	ATP synthase F(0) complex subunit B1, mitochondrial (ATP synthase proton-transporting mitochondrial F(0) complex subunit B1) (ATP synthase subunit b) (ATPase subunit b)	ATP5F1	0.422	0.287	0.337
Q6DD88	Atlastin-3 (EC 3.6.5.-)	ATL3	0.260	0.272	0.321
P35613	Basigin (5F7) (Collagenase stimulatory factor) (Extracellular matrix metalloproteinase inducer) (EMMPRIN) (Leukocyte activation antigen M6) (OK blood group antigen) (Tumor cell-derived collagenase stimulatory factor) (TCSF) (CD antigen CD147)	BSG UNQ6505/PRO21383	0.286	0.266	0.302
Q9HDC9	Adipocyte plasma membrane-associated protein (Protein BSCv)	APMAP C20orf3 UNQ1869/PRO4305	0.293	0.264	0.333
O75367	Core histone macro-H2A.1 (Histone macroH2A1) (mH2A1) (Histone H2A.y) (H2A/y) (Medulloblastoma antigen MU-MB-50.205)	H2AFY MACRO H2A1	0.363	0.263	0.307
Q02809	Procollagen-lysine,2-oxoglutarate 5-dioxygenase 1 (EC 1.14.11.4) (Lysyl hydroxylase 1) (LH1)	PLOD1 LLH PLOD	0.304	0.260	0.324
P13073	Cytochrome c oxidase subunit 4 isoform 1, mitochondrial (Cytochrome c oxidase polypeptide IV) (Cytochrome c oxidase subunit IV isoform 1) (COX IV-1)	COX4I1 COX4	0.309	0.246	0.339

P14868	Aspartate--tRNA ligase, cytoplasmic (EC 6.1.1.12) (Aspartyl-tRNA synthetase) (AspRS) (Cell proliferation-inducing gene 40 protein)	DARS PIG40	0.261	0.205	0.329
P08648	Integrin alpha-5 (CD49 antigen-like family member E) (Fibronectin receptor subunit alpha) (Integrin alpha-F) (VLA-5) (CD antigen CD49e) [Cleaved into: Integrin alpha-5 heavy chain;Integrin alpha-5 light chain]	ITGA5 FNRA	0.316	0.183	0.268
P20042	Eukaryotic translation initiation factor 2 subunit 2 (Eukaryotic translation initiation factor 2 subunit beta) (eIF-2-beta)	EIF2S2 EIF2B	-2.486	-0.119	-7.271
Q13867	Bleomycin hydrolase (BH) (BLM hydrolase) (BMH) (EC 3.4.22.40)	BLMH	-0.338	-0.155	-6.997
P62942	Peptidyl-prolyl cis-trans isomerase FKBP1A (PPIase FKBP1A) (EC 5.2.1.8) (12 kDa FK506-binding protein) (12 kDa FKBP) (FKBP-12) (Calstabin-1) (FK506-binding protein 1A) (FKBP-1A) (Immunophilin FKBP12) (Rotamase)	FKBP1A FKBP1 FKBP12	-2.815	-0.162	-0.324
Q8NC51	Plasminogen activator inhibitor 1 RNA-binding protein (PAI1 RNA-binding protein 1) (PAI-RBP1) (SERPINE1 mRNA-binding protein 1)	SERBP1 PAIRBP1 CGI-55	-0.264	-0.170	-0.324
P16989	Y-box-binding protein 3 (Cold shock domain-containing protein A) (DNA-binding protein A) (Single-strand DNA-binding protein NF-GMB)	YBX3 CSDA DBPA	-0.264	-0.174	-0.385
Q02952	A-kinase anchor protein 12 (AKAP-12) (A-kinase anchor protein 250 kDa) (AKAP 250) (Gravin) (Myasthenia gravis autoantigen)	AKAP12 AKAP250	-0.386	-0.186	-0.426
P62258	14-3-3 protein epsilon (14-3-3E)	YWHAE	-0.346	-0.191	-0.321
P31948	Stress-induced-phosphoprotein 1 (STI1) (Hsc70/Hsp90-organizing protein) (Hop) (Renal carcinoma antigen NY-REN-11) (Transformation-sensitive protein IEF SSP 3521)	STIP1	-0.247	-0.196	-0.307
Q15942	Zyxin (Zyxin-2)	ZYX	-0.285	-0.206	-0.339
P07108	Acyl-CoA-binding protein (ACBP) (Diazepam-binding inhibitor) (DBI) (Endozepine) (EP)	DBI	-0.483	-0.212	-0.445
P24844	Myosin regulatory light polypeptide 9 (20 kDa myosin light chain) (LC20) (MLC-2C) (Myosin RLC) (Myosin regulatory light chain 2, smooth muscle isoform) (Myosin regulatory light chain 9) (Myosin regulatory light chain MRLC1)	MYL9 MLC2 MRLC1 MYRL2	-0.304	-0.216	-0.333
P08729	Keratin, type II cytoskeletal 7 (Cytokeratin-7) (CK-7) (Keratin-7) (K7) (Sarcolectin) (Type-II keratin Kb7)	KRT7 SCL	-0.305	-0.217	-0.307
P17931	Galectin-3 (Gal-3) (35 kDa lectin) (Carbohydrate-binding protein 35) (CBP 35) (Galactose-specific lectin 3) (Galactoside-binding protein) (GALBP) (IgE-binding protein) (L-31) (Laminin-	LGALS3 MAC2	-7.500	-0.218	-7.500

	binding protein) (Lectin L-29) (Mac-2 antigen)				
P62158	Calmodulin (CaM)	CALM1 CALM CAM CAM1;CALM2 CAM2	-0.321	-0.223	-0.342
P58546	Myotrophin (Protein V-1)	MTPN	-7.723	-0.226	-2.731
P67936	Tropomyosin alpha-4 chain (TM30p1) (Tropomyosin-4)	TPM4	-0.329	-0.232	-0.312
P63104	14-3-3 protein zeta/delta (Protein kinase C inhibitor protein 1) (KCIP-1)	YWHAZ	-0.326	-0.235	-0.286
P40925	Malate dehydrogenase, cytoplasmic (EC 1.1.1.37) (Cytosolic malate dehydrogenase) (Diiodophenylpyruvate reductase) (EC 1.1.1.96)	MDH1 MDHA	-0.258	-0.244	-0.320
P27816	Microtubule-associated protein 4 (MAP-4)	MAP4	-0.290	-0.247	-0.418
Q99497	Protein deglycase DJ-1 (DJ-1) (EC 3.1.2.-) (EC 3.5.1.-) (Oncogene DJ1) (Parkinson disease protein 7)	PARK7	-2.791	-0.260	-0.339
P21291	Cysteine and glycine-rich protein 1 (Cysteine-rich protein 1) (CRP) (CRP1) (Epididymis luminal protein 141) (HEL-141)	CSRP1 CSRP CYRP	-0.297	-0.263	-0.319
O43707	Alpha-actinin-4 (Non-muscle alpha-actinin 4)	ACTN4	-0.344	-0.280	-0.321
Q15181	Inorganic pyrophosphatase (EC 3.6.1.1) (Pyrophosphate phospho-hydrolase) (PPase)	PPA1 IOPPP PP	-0.304	-0.290	-0.388
Q3SX28;P07951	Alpha-fetoprotein (Alpha-1-fetoprotein) (Alpha-fetoglobulin)	AFP HPAFP	-0.457	-0.293	-0.395
Q09666	Neuroblast differentiation-associated protein AHNAK (Desmoyokin)	AHNAK PM227	-0.426	-0.299	-0.411
P13797	Plastin-3 (T-plastin)	PLS3	-0.319	-0.300	-0.315
P41250	Glycine--tRNA ligase (EC 3.6.1.17) (EC 6.1.1.14) (Diadenosine tetraphosphate synthetase) (AP-4-A synthetase) (Glycyl-tRNA synthetase) (GlyRS)	GARS	-0.261	-0.301	-0.229
Q14315	Filamin-C (FLN-C) (FLNc) (ABP-280-like protein) (ABP-L) (Actin-binding-like protein) (Filamin-2) (Gamma-filamin)	FLNC ABPL FLN2	-0.269	-0.301	-0.298
P13489	Ribonuclease inhibitor (Placental ribonuclease inhibitor) (Placental RNase inhibitor) (Ribonuclease/angiogenin inhibitor 1) (RAI)	RNH1 PRI RNH	-0.142	-0.304	-0.204
P17655	Calpain-2 catalytic subunit (EC 3.4.22.53) (Calcium-activated neutral proteinase 2) (CANP 2) (Calpain M-type) (Calpain large polypeptide L2) (Calpain-2 large subunit) (Millimolar-calpain) (M-calpain)	CAPN2 CANPL2	-0.183	-0.304	-0.183
Q53GG5	PDZ and LIM domain protein 3 (Actinin-associated LIM protein) (Alpha-actinin-2-associated LIM protein)	PDLIM3 ALP	-0.497	-0.305	-0.712

P62906	60S ribosomal protein L10a (CSA-19) (Neural precursor cell expressed developmentally down-regulated protein 6) (NEDD-6)	RPL10A NEDD6	-0.224	-0.307	-0.247
P08195	4F2 cell-surface antigen heavy chain (4F2hc) (4F2 heavy chain antigen) (Lymphocyte activation antigen 4F2 large subunit) (Solute carrier family 3 member 2) (CD antigen CD98)	SLC3A2 MDU1	-0.119	-0.312	-0.191
Q05682	Caldesmon (CDM)	CALD1 CAD CDM	-0.375	-0.313	-0.488
P50395	Rab GDP dissociation inhibitor beta (Rab GDI beta) (Guanosine diphosphate dissociation inhibitor 2) (GDI-2)	GDI2 RABGDI B	-0.486	-0.315	-0.396
P07195	L-lactate dehydrogenase B chain (LDH-B) (EC 1.1.1.27) (LDH heart subunit) (LDH-H) (Renal carcinoma antigen NY-REN-46)	LDHB	-0.270	-0.316	-0.308
P21333	Filamin-A (FLN-A) (Actin-binding protein 280) (ABP-280) (Alpha-filamin) (Endothelial actin-binding protein) (Filamin-1) (Non-muscle filamin)	FLNA FLN FLN1	-0.300	-0.318	-0.333
P54687	Branched-chain-amino-acid aminotransferase, cytosolic (BCAT(c)) (EC 2.6.1.42) (Protein ECA39)	BCAT1 BCT1 ECA39	-0.232	-0.325	-0.350
P49588	Alanine--tRNA ligase, cytoplasmic (EC 6.1.1.7) (Alanyl-tRNA synthetase) (AlaRS) (Renal carcinoma antigen NY-REN-42)	AARS	-0.173	-0.326	-0.255
P36871	Phosphoglucomutase-1 (PGM 1) (EC 5.4.2.2) (Glucose phosphomutase 1)	PGM1	-0.282	-0.329	-0.299
O75390	Citrate synthase, mitochondrial (EC 2.3.3.1) (Citrate (Si)-synthase)	CS	-0.099	-0.334	-0.181
Q9NQC3	Reticulon-4 (Foocen) (Neurite outgrowth inhibitor) (Nogo protein) (Neuroendocrine-specific protein) (NSP) (Neuroendocrine-specific protein C homolog) (RTN-x) (Reticulon-5)	RTN4 KIAA088 6 NOGO My043 SP1507	-0.120	-0.335	-0.335
O15371	Eukaryotic translation initiation factor 3 subunit D (eIF3d) (Eukaryotic translation initiation factor 3 subunit 7) (eIF-3-zeta) (eIF3 p66)	EIF3D EIF3S7	-0.221	-0.337	-0.218
O00410	Importin-5 (Imp5) (Importin subunit beta-3) (Karyopherin beta-3) (Ran-binding protein 5) (RanBP5)	IPO5 KPNB3 RANBP5	-0.199	-0.337	-0.332
Q96AC1	Fermitin family homolog 2 (Kindlin-2) (Mitogen-inducible gene 2 protein) (MIG-2) (Pleckstrin homology domain-containing family C member 1) (PH domain-containing family C member 1)	FERMT2 KIND2 MIG2 PLEKHC 1	-0.278	-0.338	-0.253
P30041	Peroxiredoxin-6 (EC 1.11.1.15) (1-Cys peroxiredoxin) (1-Cys PRX) (24 kDa protein) (Acidic calcium-independent phospholipase A2) (aiPLA2) (EC 3.1.1.-) (Antioxidant protein 2) (Liver 2D page spot 40) (Non-selenium glutathione peroxidase) (NSGPx) (EC 1.11.1.9) (Red blood cells page spot 12)	PRDX6 AOP2 KIAA010 6	-0.359	-0.343	-0.346

O43776	Asparagine--tRNA ligase, cytoplasmic (EC 6.1.1.22) (Asparaginyl-tRNA synthetase) (AsnRS)	NARS	-0.353	-0.343	-0.309
Q16881	Thioredoxin reductase 1, cytoplasmic (TR) (EC 1.8.1.9) (Gene associated with retinoic and interferon-induced mortality 12 protein) (GRIM-12) (Gene associated with retinoic and IFN-induced mortality 12 protein) (KM-102-derived reductase-like factor) (Thioredoxin reductase TR1)	TXNRD1 GRIM12 KDRF	-0.329	-0.355	-0.288
P15311	Ezrin (Cytovillin) (Villin-2) (p81)	EZR VIL2	-0.300	-0.356	-0.344
P10599	Thioredoxin (Trx) (ATL-derived factor) (ADF) (Surface-associated sulphydryl protein) (SASP)	TXN TRDX TRX TRX1	-0.413	-0.364	-0.407
P49411	Elongation factor Tu, mitochondrial (EF-Tu) (P43)	TUFM	-0.181	-0.364	-0.357
Q16543	Hsp90 co-chaperone Cdc37 (Hsp90 chaperone protein kinase-targeting subunit) (p50Cdc37) [Cleaved into: Hsp90 co-chaperone Cdc37, N-terminally processed]	CDC37 CDC37A	-2.690	-0.365	-5.221
P05787	Keratin, type II cytoskeletal 8 (Cytokeratin-8) (CK-8) (Keratin-8) (K8) (Type-II keratin Kb8)	KRT8 CYK8	-0.434	-0.365	-0.444
P05783	Keratin, type I cytoskeletal 18 (Cell proliferation-inducing gene 46 protein) (Cytokeratin-18) (CK-18) (Keratin-18) (K18)	KRT18 CYK18 PIG46	-0.437	-0.367	-0.399
Q99613	Eukaryotic translation initiation factor 3 subunit C (eIF3c) (Eukaryotic translation initiation factor 3 subunit 8) (eIF3 p110)	EIF3C EIF3S8	-0.314	-0.374	-0.280
P19623	Spermidine synthase (SPDSY) (EC 2.5.1.16) (Putrescine aminopropyltransferase)	SRM SPS1 SRML1	-0.236	-0.375	-0.356
P26022	Pentraxin-related protein PTX3 (Pentaxin-related protein PTX3) (Tumor necrosis factor alpha-induced protein 5) (TNF alpha-induced protein 5) (Tumor necrosis factor-inducible gene 14 protein) (TSG-14)	PTX3 TNFAIP5 TSG14	-0.284	-0.379	-0.224
P02452	Collagen alpha-1(I) chain (Alpha-1 type I collagen)	COL1A1	-0.468	-0.387	-0.441
Q96IZ0	PRKC apoptosis WT1 regulator protein (Prostate apoptosis response 4 protein) (Par-4)	PAWR PAR4	-5.025	-0.400	-5.118
Q9UHB6	LIM domain and actin-binding protein 1 (Epithelial protein lost in neoplasm)	LIMA1 EPLIN SREBP3 PP624	-0.266	-0.400	-0.610
Q01995	Transgelin (22 kDa actin-binding protein) (Protein WS3-10) (Smooth muscle protein 22-alpha) (SM22-alpha)	TAGLN SM22 WS3-10	-0.561	-0.408	-0.553
O14737	Programmed cell death protein 5 (Protein TFAR19)	PDCD5 TFAR19	-0.479	-0.415	-0.564
Q9NZN4	EH domain-containing protein 2 (PAST homolog 2)	EHD2 PAST2	-0.283	-0.422	-2.807

P12081	Histidine--tRNA ligase, cytoplasmic (EC 6.1.1.21) (Histidyl-tRNA synthetase) (HisRS)	HARS HRS	-2.838	-0.444	-2.962
P30086	Phosphatidylethanolamine-binding protein 1 (PEBP-1) (HCNPpp) (Neuropolypeptide h3) (Prostatic-binding protein) (Raf kinase inhibitor protein) (RKIP) [Cleaved into: Hippocampal cholinergic neurostimulating peptide (HCNP)]	PEBP1 PBP PEBP	-0.574	-0.457	-0.595
Q14847	LIM and SH3 domain protein 1 (LASP-1) (Metastatic lymph node gene 50 protein) (MLN 50)	LASP1 MLN50	-0.435	-0.460	-0.606
Q96HC4	PDZ and LIM domain protein 5 (Enigma homolog) (Enigma-like PDZ and LIM domains protein)	PDLIM5 ENH L9	-0.481	-0.460	-0.520
P35221	Catenin alpha-1 (Alpha E-catenin) (Cadherin-associated protein) (Renal carcinoma antigen NY-REN-13)	CTNNA1	-0.325	-0.470	-0.380
O43399	Tumor protein D54 (hD54) (Tumor protein D52-like 2)	TPD52L2	-0.469	-0.481	-0.542
O14558	Heat shock protein beta-6 (HspB6) (Heat shock 20 kDa-like protein p20)	HSPB6	-0.356	-0.486	-0.415
Q04637	Eukaryotic translation initiation factor 4 gamma 1 (eIF-4-gamma 1) (eIF-4G 1) (eIF-4G1) (p220)	EIF4G1 EIF4F EIF4G EIF4GI	-0.411	-0.487	-5.284
Q8WWI1	LIM domain only protein 7 (LMO-7) (F-box only protein 20) (LOMP)	LMO7 FBX20 FBXO20 KIAA0858	-2.858	-0.494	-2.820
Q9P2E9	Ribosome-binding protein 1 (180 kDa ribosome receptor homolog) (RRp) (ES/130-related protein) (Ribosome receptor protein)	RRBP1 KIAA1398	-0.532	-0.498	-0.646
Q9BRA2	Thioredoxin domain-containing protein 17 (14 kDa thioredoxin-related protein) (TRP14) (Protein 42-9-9) (Thioredoxin-like protein 5)	TXNDC17 TXNL5	-5.222	-0.521	-2.910
O75347	Tubulin-specific chaperone A (TCP1-chaperonin cofactor A) (Tubulin-folding cofactor A) (CFA)	TBCA	-2.903	-0.547	-3.005
Q9Y617	Phosphoserine aminotransferase (EC 2.6.1.52) (Phosphohydroxythreonine aminotransferase) (PSAT)	PSAT1 PSA	-0.625	-0.641	-0.430
P08243	Asparagine synthetase [glutamine-hydrolyzing] (EC 6.3.5.4) (Cell cycle control protein TS11) (Glutamine-dependent asparagine synthetase)	ASNS TS11	-0.622	-0.707	-3.032
O94925	Glutaminase kidney isoform, mitochondrial (GLS) (EC 3.5.1.2) (K-glutaminase) (L-glutamine amidohydrolase)	GLS GLS1 KIAA0838	-0.434	-0.722	-0.587
P51911	Calponin-1 (Basic calponin) (Calponin H1, smooth muscle)	CNN1	-1.106	-0.982	-1.022

P12763	Apolipoprotein A-II (Apo-AII) (ApoA-II) (Antimicrobial peptide BAMP-1) (Apolipoprotein A2) [Cleaved into: Proapolipoprotein A-II (ProapoA-II);Truncated apolipoprotein A-II (Apolipoprotein A-II(1-76))]	APOA2	-1.336	-1.176	-1.202
P08727	Keratin, type I cytoskeletal 19 (Cytokeratin-19) (CK-19) (Keratin-19) (K19)	KRT19	-1.214	-1.246	-3.648
ENSEMBL:ENSBTAP00000024146	Hemoglobin subunit alpha (Alpha-globin) (Hemoglobin alpha chain)	HBA	-1.225	-1.325	-1.284
Q9Y3B3	Transmembrane emp24 domain-containing protein 7 (p24 family protein gamma-3) (p24gamma3) (p27)	TMED7 CGI-109	0.451	-2.106	0.533
P31150	Rab GDP dissociation inhibitor alpha (Rab GDI alpha) (Guanosine diphosphate dissociation inhibitor 1) (GDI-1) (Oligophrenin-2) (Protein XAP-4)	GDI1 GDIL OPHN2 RABGDIA XAP4	-7.258	-2.588	-2.571
P54886	Delta-1-pyrroline-5-carboxylate synthase (P5CS) (Aldehyde dehydrogenase family 18 member A1) [Includes: Glutamate 5-kinase (GK) (EC 2.7.2.11) (Gamma-glutamyl kinase);Gamma-glutamyl phosphate reductase (GPR) (EC 1.2.1.41) (Glutamate-5-semialdehyde dehydrogenase) (Glutamyl-gamma-semialdehyde dehydrogenase)]	ALDH18A1 GSAS P5CS PYCS	-0.071	-2.709	-0.350
P04080	Cystatin-B (CPI-B) (Liver thiol proteinase inhibitor) (Stefin-B)	CSTB CST6 STFB	-5.231	-2.752	-7.699
Q3SY69	Mitochondrial 10-formyltetrahydrofolate dehydrogenase (Mitochondrial 10-FTHFDH) (mtFDH) (EC 1.5.1.6) (Aldehyde dehydrogenase family 1 member L2)	ALDH1L2	-2.765	-2.756	-7.416
P31946	14-3-3 protein beta/alpha (Protein 1054) (Protein kinase C inhibitor protein 1) (KCIP-1) [Cleaved into: 14-3-3 protein beta/alpha, N-terminally processed]	YWHAB	-0.441	-2.912	-0.346
P02788	Lactotransferrin (Lactoferrin) (EC 3.4.21.-) (Growth-inhibiting protein 12) (Talalactoferrin) [Cleaved into: Lactoferricin-H (Lfcin-H);Kaliocin-1;Lactoferroxin-A;Lactoferroxin-B;Lactoferroxin-C]	LTF GIG12 LF	-7.269	-2.920	-5.099
P07384	Calpain-1 catalytic subunit (EC 3.4.22.52) (Calcium-activated neutral proteinase 1) (CANP 1) (Calpain mu-type) (Calpain-1 large subunit) (Cell proliferation-inducing gene 30 protein) (Micromolar-calpain) (muCANP)	CAPN1 CANPL1 PIG30	-0.495	-3.025	-0.537
Q9BS40	Latexin (Endogenous carboxypeptidase inhibitor) (ECI) (Protein MUM) (Tissue carboxypeptidase inhibitor) (TCI)	LXN	-5.406	-3.072	-0.706
Q13642	Four and a half LIM domains protein 1 (FHL-1) (Skeletal muscle LIM-protein 1) (SLIM) (SLIM-1)	FHL1 SLIM1	-0.432	-3.091	-0.519

Q0ZGT2	Nexilin (F-actin-binding protein) (Nelin)	NEXN	-7.335	-4.961	-7.335
Q3SZR3	Alpha-1-acid glycoprotein (Orosomucoid) (OMD)	ORM1 AGP	-7.451	-5.123	-7.451
Q13247	Serine/arginine-rich splicing factor 6 (Pre-mRNA-splicing factor SRP55) (Splicing factor, arginine/serine-rich 6)	SRSF6 SFRS6 SRP55	-7.767	-5.182	-2.603
Q86UP2	Kinectin (CG-1 antigen) (Kinesin receptor)	KTN1 CG1 KIAA0004	-4.740	-7.054	-7.054
O95336	6-phosphogluconolactonase (6PGL) (EC 3.1.1.31)	PGLS	-4.769	-7.070	-4.764
P40616	ADP-ribosylation factor-like protein 1	ARL1	-2.251	-7.135	-4.734
O14974	Protein phosphatase 1 regulatory subunit 12A (Myosin phosphatase-targeting subunit 1) (Myosin phosphatase target subunit 1) (Protein phosphatase myosin-binding subunit)	PPP1R12A MBS MYPT1	-7.195	-7.195	-7.195
Q9UMS6	Synaptopodin-2 (Genethonin-2) (Myopodin)	SYNPO2	-7.309	-7.309	-7.309
O76003	Glutaredoxin-3 (PKC-interacting cousin of thioredoxin) (PICOT) (PKC-theta-interacting protein) (PKCq-interacting protein) (Thioredoxin-like protein 2)	GLRX3 PICOT TXNL2 HUSSY-22	-2.467	-7.321	-7.321
Q9UNZ2	NSFL1 cofactor p47 (UBX domain-containing protein 2C) (p97 cofactor p47)	NSFL1C UBXN2C	-7.368	-7.368	-7.368
Q14011	Cold-inducible RNA-binding protein (A18 hnRNP) (Glycine-rich RNA-binding protein CIRP)	CIRBP A18HNRNP CIRP	-7.380	-7.380	-7.380
O14979	Heterogeneous nuclear ribonucleoprotein D-like (hnRNP D-like) (hnRNP DL) (AU-rich element RNA-binding factor) (JKT41-binding protein) (Protein laAUF1)	HNRNPDL HNRPDL JKTBP	-4.913	-7.384	-4.925
Q16822	Phosphoenolpyruvate carboxykinase [GTP], mitochondrial (PEPCK-M) (EC 4.1.1.32)	PCK2 PEPCK2	-7.399	-7.399	-7.399
P17661	Desmin	DES	-7.493	-7.493	-7.493
Q3SZ57	Alpha-fetoprotein (Alpha-1-fetoprotein) (Alpha-fetoglobulin)	AFP	-5.232	-7.537	-2.915
Q8NF91	Nesprin-1 (Enaptin) (Myocyte nuclear envelope protein 1) (Myne-1) (Nuclear envelope spectrin repeat protein 1) (Synaptic nuclear envelope protein 1) (Syne-1)	SYNE1 C6orf98 KIAA0796 KIAA1262 KIAA1756 MYNE1	-7.557	-7.557	-7.557
P06702	Protein S100-A9 (Calgranulin-B) (Calprotectin L1H subunit) (Leukocyte L1 complex heavy chain) (Migration inhibitory factor-related protein 14) (MRP-14) (p14) (S100 calcium-binding protein A9)	S100A9 CAGB CFAG MRP14	-7.590	-7.590	-7.590

P61088	Ubiquitin-conjugating enzyme E2 N (EC 2.3.2.23) (Bendless-like ubiquitin-conjugating enzyme) (E2 ubiquitin-conjugating enzyme N) (Ubc13) (UbcH13) (Ubiquitin carrier protein N) (Ubiquitin-protein ligase N)	UBE2N BLU	-7.783	-7.783	-7.783

Supplementary Table 2. Proteins significantly up-regulated only with Mg-10Gd regarding the other extracts. Data corresponds with the decimal logarithm of the fold change in expression.

Protein name	Mg-10Gd	Mg-2Ag	PMg
Glutaminyl-tRNA synthetase	7.4204	2.4692	2.5008
Fibrilin-1	7.2761	4.8379	4.8020
TAR DNA-binding protein 43	7.2554	4.8655	4.8542

Supplementary Table 3. Proteins significantly up-regulated only with Mg-2Ag regarding the other extracts. Data corresponds with the decimal logarithm of the fold change in expression.

Protein	Mg-10Gd	Mg-2Ag	PMg
Coagulation factor XII	5.0399	7.4859	4.9997
Alpha-1-antichymotrypsin	4.8891	7.3070	4.9758
Membrane-associated progesterone receptor component 1	2.3923	7.1564	4.8293
Microtubule-associated protein 9	-2.2507	0.3915	0.1715

Supplementary Table 4. Proteins significantly up-regulated only with PMg regarding the other extracts. Data corresponds with the decimal logarithm of the fold change in expression.

Protein	Mg-10Gd	Mg-2Ag	PMg
Niban-like protein 1 (Meg-3)	5.0997	5.0344	7.5896
Angiopoietin-related protein 4	4.8626	4.8685	7.3739

13. RISK AND SAFETY STATEMENT

Following is a list of potentially hazardous chemicals with the respective hazard and precautionary statements, as introduced by the Globally Harmonized System of Classification and Labelling of Chemicals (GHS).

Compound	Chemical Abstracts Service No.	Hazard statements	GHS hazard	Precautionary statements
$MgCl_2$	7786-30-3	H319	GHS07	P305 + P351 + P338
$GdCl_3$	10138-52-0	H315; H319	GHS07	P305 + P351 + P338
HCl	7647-01-0	H290; H315; H319; H335	GHS05; GHS07	P305 + P351 + P338
Triton X100	9002-93-1	H318	GHS05	P280; P305 + P351 + P338; P310
Tri-Reagent	T9424	H301 + H311 + H331; H314; H318; H341; H373; H402	GHS05; GHS06; GHS08; GHS09	P201;P261; P280; P301 + P310 + P330; P303 + P361 + P353; P305 + P351 + P338
Bisbenzimide H 33258	23491-45-4	H302; H315; H335; H341	GHS07; GHS08	P280; P301 + P312 + P330
1,9-dimethyl-methylen blue-chloride	931418-92-7	H319	GHS07	P280; P264; P305 + P351 + P338; P337 + P313
B-mercaptoethanol	200-464-6	H301 + H331; H310; H315; H317; H318; H373; H410	GHS05; GHS06; GHS08; GHS09,	P273; P280; P302 + P352; P304 + P340; P305 + P351 + P338; P308 + P310
Papain	A3824	H315; H319; H334; H335	GHS07; GHS08	P260; P305 + P351 + P338; P342 + P311
EDTA	6381-92-6	H332; H373	GHS07;	P314

			GHS08	
Paraformaldehyde	30525-89-4	H228; H302 + H332; H315; H317; H318; H335; H351	GHS02; GHS05; GHS07; GHS08	P210; P261; P280; P301 + P312 + P330; P305 + P351 + P338 + P310-P370 + P378
Glutaraldehyde (2%) in 0.1M Sodium Cacodylate Buffer, pH 7.4	111-30-8 124-65-2	H315; H318; H334	GHS07; GHS08; GHS09	P260; P305 + P351 * P338; P333 + P313

Hazard statements

H228	Flammable solid
H290	May be corrosive to metals
H301	Toxic if swallowed
H302	Harmful if swallowed
H310	Fatal in contact with skin
H311	Toxic in contact with skin
H312	Harmful in contact with skin
H314	Causes severe skin burns and eye damage
H315	Causes skin irritation
H317	May cause an allergic skin reaction
H318	Causes serious eye damage
H319	Causes serious eye irritation
H331	Toxic if inhaled
H332	Harmful if inhaled
H334	May cause allergy or asthma symptoms or breathing difficulties if inhaled
H335	May cause respiratory irritation
H341	Causes severe skin burns and eye damage
H351	Suspected of causing cancer
H373	May cause damage to organs through prolonged or repeated exposure if swallowed
H402	Harmful to aquatic life
H410	Very toxic to aquatic life with long lasting effects

GHS precautionary statements

P202	Do not handle until all safety precautions have been read and understood
P210	Keep away from heat, hot surfaces, sparks, open flames and other ignition sources. No smoking
P260	Do not breathe dust/ fume/ gas/ mist/ vapors/ spray
P261	Avoid breathing dust/fume/gas/mist/vapours/spray
P262	Do not get in eyes, on skin, or on clothing
P264	Wash hands thoroughly after handling
P270	Do not eat, drink or smoke when using this product
P273	Avoid release to the environment
P280	Wear protective gloves/protective clothing/eye protection/face protection
P281	Use of personal protective equipment is required
P301	IF SWALLOWED
P302	IF ON SKIN
P303	IF ON SKIN (or hair)
P304	IF INHALED
P305	IF IN EYES
P308	IF EXPOSED OR CONCERNED
P310	Immediately call a POISON CENTER or doctor/physician
P311	Call a POISON CENTER or doctor/physician
P312	Call a POISON CENTER or doctor/physician if you feel unwell
P313	Get medical advice/attention
P330	Rinse mouth
P332	IF SKIN IRRITATION OCCURS
P333	IF SKIN IRRITATION OR RASH OCCURS
P337	IF EYE IRRITATION PERSISTS
P338	Remove contact lenses, if present and easy to do. Continue rinsing
P342	IF EXPERIENCING RESPIRATORY SYMPTOMS
P340	Remove victim to fresh air and keep at rest in a position comfortable for breathing
P351	Rinse cautiously with water for several minutes
P352	Wash with plenty of soap and water
P361	Take off immediately all contaminated clothing
P362	Take off contaminated clothing

P370 IN CASE OF FIRE

P378 Use … to extinguish

14. ACKNOWLEDGEMENT

I would like to thank all the people who made this thesis possible and the way more pleasant.

I acknowledge my gratitude to my supervisors Prof. Regine Willumeit-Römer, Frank Feyerabend and Beregere Luthringer at HZG for the continuous encouragement and advice during this thesis. Also for the efforts put into training me in the scientific field.

I would like to express my gratitude to Prof. Annelie Weinberg from the Medical University of Graz, who provided me the opportunity to join her team and performing part of this work under her supervision, and who gave access to the research facilities.

I am thankful to Asklepios Klinik Altona for providing the umbilical cord samples, and to all the donors for their altruistic collaboration.

I am thankful to Dr. Danniel Laipple for the assistance with the SEM, EDX and FIB analysis.

My sincere thanks to Maryam Omidi from UKE Hamburg, for the productive collaborations, especially for the mass spectrometry measurements and data generation. Also for your friendship and all the moments shared.

I would also like to thank to Gábor Szakács, because of the big effort made to produce the materials for our projects, and because of being always a good friend.

A special thanks to my fellow labmates of "Metallic Biomaterials" at HZG, because somehow all of you contributed to this work:

Maria Costantino and Nezha Agha, I may thank you for all the interesting conversations, scientific related or not, and for helping each other to solve the numerous problems found during this long way. Also for all the adventures lived together going to conferences or workshops. All of them will be unforgettable for me.

Dorothee Scharfenberg, meine Freundin, thanks for accepting me as I am and always trying to understand me.

Thanks to Gabriele Salomon, for all the unconditional technical and moral support during the whole time. Your advices and opinions have been essential for me.

I wish to thank to all my Geesthacht-friends, for being with me part or the whole last 4 years, specially to Igor, Alberto, Goncalo, Rubén, Maria, Jorge, Alexandra, Antonio, Giovani and Mónica. It is hard to thank you for everything. You have been my family and have become this experience a marvellous time. I also thank to my truly friends spread all over the world: Alba, Vero, Paula, Adri, Bea y Laura thank you because I have felt each of you as if we were together all the time. Without your support it would have not been possible. You are the best!

My very sincere thanks to Francesco, for standing me in my worst moments and encouraging me to give the best of me.

Finally, I take this opportunity to express my gratitude to my parents, even though there are not words enough to do it, thanks for EVERYTHING.

Papá y Mamá, quiero intentar expresar con palabras mi agradecimiento por haberme dado la oportunidad de convertirme en la persona que soy. Me habéis transmitido los mejores valores que una persona puede tener y me habéis animado siempre a continuar formándome y a plantearme nuevos objetivos. Gracias, porque os debo todo lo que soy personal y profesionalmente. Ha sido, es y siempre será mi mayor orgullo teneros como padres. Os quiero.

15. DECLARATION UPON OATH

I hereby declare that I have written the present thesis titled “” independently, and without use of other resources than those indicated. The ideas taken directly or indirectly from external sources (including electronic sources) and well as collaborative research are duly acknowledged in the text. The material, either in full or in part, has not been previously submitted for grading at this or any other academic institution.

Signed:

12.01.2017, Geesthacht